



**CALIFORNIA  
ENERGY COMMISSION**



Energy Research and Development Division

## **FINAL PROJECT REPORT**

# **Performance-Based Earthquake Engineering Assessment Tool for Natural Gas Storage and Pipeline Systems**

Task B - Enhanced Liquefaction and Ground Deformation Report

**Gavin Newsom, Governor  
July 2022**



**PREPARED BY:**

**Primary Authors:**

Chris Bain, Daniel Hutabarat, Jonathan D. Bray, Norman Abrahamson

University of California, Berkeley  
453 Davis Hall, MC-1710  
Berkeley, California 94720-1710

Thomas D. O'Rourke

Cornell University  
422 Hollister Hall  
Ithaca, New York 14853

Scott Lindvall

Lettis Consultants International, Inc.  
27441 Tourney Road, Suite 220  
Valencia, CA 91355

**Contract Number:** PIR-18-003

**PREPARED FOR:**

California Energy Commission

Yahui Yang

**Project Manager**

Laurie ten Hope

**Deputy Director**

**ENERGY RESEARCH AND DEVELOPMENT DIVISION**

Drew Bohan

**Executive Director**

**DISCLAIMER**

This report was prepared as the result of work sponsored by the California Energy Commission. It does not necessarily represent the views of the Energy Commission, its employees or the State of California. The Energy Commission, the State of California, its employees, contractors and subcontractors make no warranty, express or implied, and assume no legal liability for the information in this report; nor does any party represent that the uses of this information will not infringe upon privately owned rights. This report has not been approved or disapproved by the California Energy Commission nor has the California Energy Commission passed upon the accuracy or adequacy of the information in this report.

# ACKNOWLEDGEMENTS

The authors want to recognize the California Energy Commission and thank the Commission for recognizing how vital this research is to the industry. We would like to thank them for funding this project and giving us the opportunity to refine current practice with more in-depth research. Specifically, we would like to thank Yahui Yang, the project manager from the California Energy Commission, for providing guidance throughout the process of developing these interim reports.

Prof. Jonathan Bray of University of California, Berkeley is the PI of the project and Dr. Jennie Watson-Lamprey of Slate Geotechnical Consultants is the Project Manager. Dr. Watson-Lamprey with Micaela Largent and Dr. Barry Zheng of Slate Geotechnical Consultants helped us organize our collaborations with the different research teams. These included Task A (Dr. Norm Abrahamson, Dr. Maxime Lacour, and Dr. Steve Thompson), Task E members (Dr. Kenichi Soga, Dr. James Wang, Peter Hubbard, and Tiachen Xu), Task D members (Prof. Tara Hutchinson, Prof. David McCallen, Prof. Sherif Elfass, Dr. Elide Pantoli and Dr. Suiwen Wu), and Task C members (Dr. Jonny Rutqvist, Dr. Keurfon Luu, Preston Jordan, Dr. Tsubasa Sasaki, Dr. William Foxall and Dr. Yingqi Zhang). Dr. Watson-Lamprey also provided guidance on the development of probabilistic models. Dr. Stevan Gavrilovic, Dr. Sanjay Govindjee, Dr. Frank McKenna, Dr. Matthew Schoettler of the NEHRI SimCenter at UC Berkeley provided software development support. Grace Kang, Dr. Amarnath Kasalanati, and Dr. Arpit Nema of the Pacific Earthquake Engineering Research Center (PEER) provided outreach, administrative, and technical support of the project. Shakhzod Takhirov, Llyr Griffiths, and Matt Cataleta of UC Berkeley's Civil Engineering laboratories also supported the demonstration testing. Pacific Gas and Electric Company and the East Bay Municipal Utility District donated testing samples. Dr. Sjoerd van Ballegooy and his staff at Tonkin & Taylor, Ltd. of New Zealand shared data and insights on the ground characterization (e.g., CPT) and ground performance data (e.g., LiDAR) of the Canterbury Earthquake Sequence. Tim McCrink and Dr. Erik Frost from the California Geological Survey provided a database of rock strength test results and insights into regional slope stability and displacement analyses in California. Dr. Christina Argyrou and Dr. Dilan Roberts shared their experience with Abaqus and the O'Rourke (2016) coupled model. Amy Frithsen managed the grant and contracts through ERSO at UC Berkeley.

The authors thank the project partners of Pacific Gas and Electric Company (PG&E) and Southern California Gas Company (SoCalGas) for sharing data, insights, and technical advice throughout the project, with particular thanks to Chris Madugo, Albert Kottke, Masoud Poul, Nozar Jahangir, Jeremy Dong, Masoud Mogtarder-Zadeh, Jeffrey Bachhuber, and the technical staff at PG&E.

This research study was funded by the California Energy Commission, under Contract No. PIR 18-003. The opinions, findings, conclusions, and recommendations expressed in this publication are those of the authors and do not necessarily reflect the view of California Energy Commission and its employees, the State of California, the Pacific Earthquake Engineering Research (PEER) Center, and the Regents of the University of California.

## PREFACE

The California Energy Commission's (CEC) Energy Research and Development Division manages the Natural Gas Research and Development Program, which supports energy-related research, development, and demonstration not adequately provided by competitive and regulated markets. These natural gas research investments spur innovation in energy efficiency, renewable energy and advanced clean generation, energy-related environmental protection, energy transmission and distribution and transportation.

The Energy Research and Development Division conducts this public interest natural gas-related energy research by partnering with RD&D entities, including individuals, businesses, utilities and public and private research institutions. This program promotes greater natural gas reliability, lower costs and increases safety for Californians and is focused in these areas:

- Buildings End-Use Energy Efficiency.
- Industrial, Agriculture and Water Efficiency
- Renewable Energy and Advanced Generation
- Natural Gas Infrastructure Safety and Integrity.
- Energy-Related Environmental Research
- Natural Gas-Related Transportation.

The *Enhanced Liquefaction and Ground Deformation Report* is an interim report for the Performance-Based Earthquake Engineering Assessment Tool for Natural Gas Storage and Pipeline Systems project (PIR-18-003) conducted by the University of California, Berkeley. The information from this project contributes to the Energy Research and Development Division's Natural Gas Research and Development Program.

For more information about the Energy Research and Development Division, please visit the [CEC's research website](http://www.energy.ca.gov/research/) (www.energy.ca.gov/research/) or contact the CEC at 916-327-1551.

# ABSTRACT

This report is one of a series of reports documenting the methods and findings of a multi-year, multi-disciplinary project conducted by the Pacific Earthquake Engineering Research Center (PEER) with the Lawrence Berkeley National Laboratory (LBNL) and funded by the California Energy Commission (CEC). The overall project is titled *Performance-based Earthquake Engineering Assessment Tool for Natural Gas Storage and Pipeline Systems* henceforth referred to as the *OpenSRA* Project.

The overall goal of the *OpenSRA* Project is to create an open-source research-based seismic risk assessment tool for natural gas infrastructure that can be used by utility stakeholders to better understand state-wide risks, prioritize mitigation, plan new gas infrastructure, and help focus post-earthquake repair work.

The project team includes researchers from UC Berkeley, LBNL, UC San Diego, University of Nevada Reno, the NHERI SimCenter at UC Berkeley, and Slate Geotechnical Consultants and its subcontractors Lettis Consultants International (LCI) and Thomas O'Rourke of Cornell University. Focused research to advance the seismic risk assessment tool was conducted by Task Groups, each addressing a particular area of study and expertise, and collaborating with the other Task Groups.

This report is the product of Task Group B: Liquefaction-Induced Deformation and Seismically Induced Slope Displacement. The scope of this report is to summarize the procedures and data available in California for assessing liquefaction triggering, liquefaction-induced lateral spreading and vertical settlement, and seismic slope instability and displacement at statewide, regional, and site-specific scales. A new procedure for probabilistically assessing liquefaction triggering and lateral spread displacement at regional scales is introduced.

Additionally, this report summarizes the results of existing pipeline test data and the findings from physical testing studies of buried pipelines that explore soil-structure interaction effects. The finite element computer program Abaqus was used to assess underground pipeline response to four modes of permanent ground deformation: 1) strike-slip tension, 2) strike-slip compression, 3) normal-slip, and 4) reverse-slip. The Abaqus results are the basis for deriving fragility functions to estimate tensile and compressive pipe strain to buried pipelines subjected to permanent ground deformations from fault rupture, landslide displacement, or liquefaction-induced lateral spreading or vertical settlement. A fifth mode of ground deformation where the ground deforms in a direction parallel to the longitudinal pipeline axis resulting in tension at the scarp and compression at the toe was evaluated using an analytical model.

**Keywords:** Case history, experiments, fragilities, landslide, liquefaction, risk, seismic

Please use the following citation for this report:

Bain, Chris; Hutabarat, Daniel; Bray, Jonathan D.; Abrahamson, Norman; O'Rourke, Thomas D.; Lindvall, Scott. 2022. *Performance-Based Earthquake Engineering Assessment Tool for Natural Gas Storage and Pipeline Systems, Task B - Enhanced Liquefaction and Ground Deformation Report*. California Energy Commission.

# TABLE OF CONTENTS

ACKNOWLEDGEMENTS.....	III
PREFACE .....	IV
ABSTRACT.....	V
TABLE OF CONTENTS .....	VI
LIST OF FIGURES .....	VII
LIST OF TABLES .....	VIII
EXECUTIVE SUMMARY .....	IX
CHAPTER 1: INTRODUCTION .....	1
CHAPTER 2: EXISTING PIPELINE TEST DATA .....	1
2.1 Laboratory Test Data Literature Review.....	1
2.2 Pipeline Fragility Models .....	2
2.2.1 Tensile Strain Fragility Models .....	2
2.2.2 Compressive Strain Fragility Models .....	4
CHAPTER 3: PROJECT APPROACH.....	6
3.1 Liquefaction Triggering Models and Data.....	7
3.1.1 Level 1 Liquefaction Triggering Models and Data .....	7
3.1.2 Level 2 Liquefaction Triggering Models and Data .....	8
3.1.3 Level 3 Liquefaction Triggering Models and Data .....	9
3.2 Liquefaction-Induced Lateral Spread Displacement and Vertical Settlement Models and Data .....	10
3.2.1 Level 1 Liquefaction-Induced Lateral Spread Displacement and Vertical Settlement Procedures and Data.....	10
3.2.2 Level 2 Liquefaction-Induced Lateral Spread Displacement and Vertical Settlement Models and Data.....	11
3.2.3 Level 3 Liquefaction-Induced Lateral Spread Displacement and Vertical Settlement Models and Data.....	16
3.3 Seismic Slope Stability and Slope Displacement Models and Data.....	17
3.3.1 Level 1 Seismic Slope Stability and Slope Displacement Models and Data .....	17
3.3.2 Level 2 Seismic Slope Stability and Slope Displacement Models and Data .....	18
3.3.3 Level 3 Seismic Slope Stability and Slope Displacement Models and Data .....	20
3.4 Numerical Modeling of Soil-Pipeline Interaction.....	20
3.4.1 Ground Deformation Modes.....	20
3.4.2 Abaqus Model.....	22
3.4.3 Model Validations.....	22
3.4.4 Sensitivity Study .....	23
3.4.5 Representative Simulation Results .....	25
3.5 Development of Relationships to Estimate Longitudinal Pipe Strain for Pipelines Subjected to Permanent Ground Deformation.....	27
3.5.1 Pipe Strain Estimation Model for Strike-Slip Tension Ground Deformation Mode..	28

3.5.2	Pipe Strain Estimation Model for Strike-Slip Compression Ground Deformation Mode .....	30
3.5.3	Pipe Strain Estimation Model for Permanent Ground Deformation Parallel to Axis of Pipeline .....	31
CHAPTER 4: CONCLUSIONS.....		34
4.1	Summary .....	34
4.2	Implementation into <i>OpenSRA</i> .....	35
4.3	Recommendations for Future Research .....	36
GLOSSARY AND LIST OF ACRONYMS .....		37
REFERENCES .....		42
APPENDIX A: <i>OPENSRA</i> DATA MATRIX.....		47
APPENDIX B: <i>OPENSRA</i> LIQUEFACTION AND SLOPE STABILITY DISPLACEMENT MODELS ....		57
APPENDIX C: <i>OPENSRA</i> GEOSPATIAL DATASETS .....		71
APPENDIX D: FRAGILITY MODELS .....		75

## **LIST OF FIGURES**

Figure 1:	Diagram of Cornell University Test Box.....	1
Figure 2:	Lifelines Geotechnical Large-Scale Testing Facility Experimental Results .....	2
Figure 3:	Tensile Damage State Fragility Functions .....	3
Figure 4:	Critical Compressive Pipe Strain Data .....	4
Figure 5:	Probability of Compressive Rupture for Select D/t Ratios .....	5
Figure 6:	Mapping of Relative Liquefaction Susceptibility in San Francisco Bay Area .....	8
Figure 7:	Comparison of Median Liquefaction Triggering Relationships .....	10
Figure 8:	Liquefaction Probability Curves for the Sandy Artificial Fill over Bay Mud (afem) Deposits in the San Francisco Bay Area .....	12
Figure 9:	Locations of USGS CPTs in San Francisco Bay Area with Geology .....	13
Figure 10:	Prob(LDI="0") vs. PGA/MSF Data for afem Deposits .....	14
Figure 11:	Mean, Non-Zero LN(LDI) Data for afem Deposits .....	14
Figure 12:	Comparison of Continuous and Mixed Random Distributions .....	15
Figure 13:	USGS CoSMoS Depth to Groundwater Model in the San Francisco Bay Area .....	16
Figure 14:	Comparison of Level 1 and Level 2 Geologic Maps in Northern San Fernando Valley .....	19
Figure 15:	Assessed Ground Deformation Modes.....	21
Figure 16:	Abaqus Beam-Spring Models.....	22
Figure 17:	Comparison of Modeled and Experimentally Measured Axial Pipe Strain .....	23
Figure 18:	Tornado Diagrams from Sensitivity Study .....	25
Figure 19:	Longitudinal Pipe Strain versus Ground Deformation Simulation Results .....	26
Figure 20:	Modeled Pipeline Response to Tensile and Compressive Pipe Strain .....	28
Figure 22:	Example Calculation for Old Line 120 at the Balboa Boulevard Demonstration Site	33

# LIST OF TABLES

Table 1: List of Parameters Used in Sensitivity Analysis .....	24
Table 2: Range of Parameters Used in Numerical Simulations .....	27
Table 3: Recommended Default $\epsilon_{ult}$ (%) Values Based on Steel Grade .....	29
Table 4: Model Regression Coefficients to Estimate $\Delta_u$ .....	29
Table 5: Model Regression Coefficients to Estimate $\epsilon_{long}$ .....	30

# EXECUTIVE SUMMARY

## Introduction

This report is one of a series of reports documenting the methods and findings of a multi-year, multi-disciplinary project conducted by the Pacific Earthquake Engineering Research Center (PEER) with the Lawrence Berkeley National Laboratory (LBNL) and funded by the California Energy Commission (CEC). The overall project is titled *Performance-based Earthquake Engineering Assessment Tool for Natural Gas Storage and Pipeline Systems*, henceforth referred to as the *OpenSRA* Project.

The overall goal of the *OpenSRA* Project is to create an open-source research-based seismic risk assessment tool for natural gas infrastructure that can be used by utility stakeholders to better understand state-wide risks, prioritize mitigation, plan new gas infrastructure, and help focus post-earthquake repair work.

The project team includes researchers from UC Berkeley, LBNL, UC San Diego, University of Nevada Reno, the NHERI SimCenter at UC Berkeley, and Slate Geotechnical Consultants and its subcontractors Lettis Consultants International (LCI) and Thomas O'Rourke of Cornell University. Focused research to advance the seismic risk assessment tool was conducted by Task Groups, each addressing a particular area of study and expertise, and collaborating with the other Task Groups.

The scope of this report is to summarize the procedures and data available in California for assessing liquefaction triggering, liquefaction-induced lateral spreading and vertical settlement, and seismic slope instability and displacement at statewide, regional, and site-specific scales. A new procedure for probabilistically assessing liquefaction triggering and lateral spread displacement at regional scales is introduced.

Additionally, this report summarizes the results of existing pipeline test data and the findings from physical testing studies of buried pipelines that explore soil-structure interaction effects. The finite element computer program Abaqus was used to assess generic cases of underground pipeline response to four modes of permanent ground deformation: 1) strike-slip tension, 2) strike-slip compression, 3) normal-slip, and 4) reverse-slip. The Abaqus results are the basis for deriving fragility functions to estimate tensile and compressive pipe strain to buried pipelines subjected to permanent ground deformations from fault rupture, landslide displacement, or liquefaction-induced lateral spreading or vertical settlement. A fifth mode of ground deformation where the ground deforms in a direction parallel to the longitudinal pipeline axis resulting in tension at the scarp and compression at the toe was evaluated using an analytical model.

## Project Purpose

The purpose of this report is to summarize the procedures and data available in California for assessing liquefaction triggering, liquefaction-induced lateral spreading and vertical settlement, and seismic slope instability and displacement at statewide, regional, and site-specific scales. Gaps in the literature are identified and targeted research is performed to develop new

analytical methods. This report describes the procedures implemented in *OpenSRA* for assessing earthquake-induced ground deformation. Estimates of ground deformation resulting from liquefaction-induced lateral spreading and settlement or earthquake-induced landslides, or both, are required to assess the seismic vulnerability of buried natural gas pipelines.

Additionally, this report summarizes the experimental data and analytical methods used to derive fragilities to estimate a distribution of pipe strain for pipes subjected to five modes of ground deformation. Examples of the fragility models that can be developed are shared. A separate report discusses their use within the *OpenSRA* software at the demonstration sites utilized in the *OpenSRA* project (i.e., Bain et al. 2022b).

## **Project Approach**

There is a requirement in this project to assess natural gas systems at the statewide, regional, and site-specific scales. Because there is variation in the resolution of the data as well as the uncertainty of the ground deformation estimates, four levels of available data are identified, and different analytical methods are utilized for each level.

Level 1 analyses utilize data that are geospatially continuous at a uniform resolution over the entire state of California. These analyses have lower data resolution and are not informed by detailed site data, which leads to very high uncertainty of earthquake effects.

Level 2 analyses utilize data produced at regional scales collected at higher resolution than Level 1 data but are not necessarily geospatially continuous over the entire state of California. These analyses may be informed by subsurface data or estimated engineering properties. Level 2 analyses have high uncertainty, but less than that at Level 1.

Level 3 analyses utilize site-specific data such as Cone Penetration Test (CPT) data or 1:24,000 scale or larger geologic maps to evaluate geohazards or the response of natural gas infrastructure to ground shaking or ground deformation. Level 3 data enable assessment with medium uncertainty, which is less than possible with Level 2 data.

Level 4 analyses utilize high-quality geotechnical laboratory test data such as strength tests on “undisturbed” soil samples to enable the performance of advanced numerical analyses. They will have the least uncertainty in evaluating the response of natural gas infrastructure to ground shaking or ground deformation. Level 4 analyses are beyond the current scope of the *OpenSRA* Project.

The data and methods available at each of the first three levels are delineated in Appendix A.

Additionally, the results of existing pipeline test data and the findings from physical testing studies of buried pipelines are discussed. The finite element computer software Abaqus is used to numerically model the soil-pipeline interaction for pipelines subjected to permanent ground deformation from fault rupture, landslides, or liquefaction-induced deformations. The results of the simulations are used to derive models to estimate longitudinal pipe strain (including the epistemic uncertainty of the model) given system parameters such as pipe diameter and wall thickness, pipeline-ground offset interaction angle, and pipeline length.

## **Project Results**

This study delineates procedures and data for assessing liquefaction and seismic slope stability hazards at statewide, regional, and site-specific scales in California. A new procedure is developed to assess probabilistically liquefaction triggering and lateral spread displacement at regional scales.

Existing experimental data and numerical models for examining soil-structure interaction of buried pipelines are summarized. The results of the numerical modeling using the Abaqus finite element analysis software support the development of fragility functions for estimating longitudinal pipe strain for buried pipes subjected to the strike-slip tension, strike-slip compression, normal-slip, and reverse-slip modes of permanent ground deformation. Fragility functions for a fifth mode of permanent ground deformation are derived using the results calculated by an analytical model.

# CHAPTER 1:

## Introduction

---

This report is one of a series of reports documenting the methods and findings of a multi-year, multi-disciplinary project conducted by the Pacific Earthquake Engineering Research Center (PEER) with the Lawrence Berkeley National Laboratory (LBNL) and funded by the California Energy Commission (CEC). The overall project is titled *Performance-based Earthquake Engineering Assessment Tool for Natural Gas Storage and Pipeline Systems*, henceforth referred to as the *OpenSRA* Project.

The overall goal of the *OpenSRA* Project is to create an open-source research-based seismic risk assessment tool for natural gas infrastructure that can be used by utility stakeholders to better understand state-wide risks, prioritize mitigation, plan new gas infrastructure, and help focus post-earthquake repair work.

The probabilistic seismic risk tool developed in this project follows the widely accepted risk methodology of Cornell (1968). A seismic source characterization is used to develop a suite of earthquake scenarios with associated rates of occurrence to represent the seismic hazard. Fault ruptures and the resulting ground shaking are generated for each earthquake scenario to represent the seismic loading, which includes a map of ground motion parameters. This scenario-based seismic parameter map is overlaid on the infrastructure system, and the seismic loading is related to the capacities of the infrastructure to calculate the seismic performance of the natural gas system for the scenario. By repeating the process for all the scenarios in the suite, the tool can evaluate the seismic risk to the system.

A user-driven research approach was used to develop *OpenSRA* to be applied easily by regulators and utilities, and to include updated models and methods for the seismic demands and capacities that control the seismic risk for natural gas systems. The project includes several innovative approaches that improve the basic methodology and distinguish this project's approach from standard approaches currently used. Current risk studies developed by the utilities use risk scoring approaches that are highly subjective and qualitative. They do not incorporate properly the uncertainties in the seismic demand and in the fragility of the system and its components. Targeted research was conducted in this project to improve the characterization of uncertainty of key inputs to the seismic risk assessment tool. The seismic risk methodology employed in this project provides quantitative estimates of the probabilistic seismic risk. For risk-informed decision-making processes, the reliability of the risk estimates needs to be considered because this can be significant, particularly for large, rare earthquakes.

The project team includes researchers from UC Berkeley, LBNL, UC San Diego, University of Nevada Reno, the PEER Center, the NHERI SimCenter, and Slate Geotechnical Consultants and its subcontractors Lettis Consultants International (LCI) and Thomas O'Rourke of Cornell University. Focused research to advance the seismic risk assessment tool was conducted by Task Groups, each addressing a particular area of study and expertise, and collaborating with the other Task Groups. The Task Groups are as follows:

Task A: Fault displacement

Task B: Liquefaction-induced deformation and seismically induced slope displacement

Task C: Performance of natural gas storage well casings and caprock

Task D: Performance of gas storage and pipeline system surface infrastructure

Task E: Smart gas infrastructure sensing of wells and pipeline connections performance

Task F: Synthesis of component fragilities into a system performance model

This report is the product of Task Group B: Liquefaction-Induced Deformation and Seismically Induced Slope Displacement. The scope of this report is to assess the ground deformation hazards posed to natural gas infrastructure in California from liquefaction-induced lateral spreading and vertical settlements and from earthquake-induced landslides. The analytical methods and data available in the literature are summarized and their implementation into *OpenSRA* is described. Methods developed during this research effort will be introduced with emphasis on how these methods improve the state-of-practice for hazard analyses.

Additionally, this report summarizes the results of existing pipeline test data and the findings from physical testing studies of buried pipelines that explore soil-structure interaction effects. The finite element computer program Abaqus was used to assess four generic cases of underground pipeline response to permanent ground deformation: 1) strike-slip tension, 2) strike-slip compression, 3) normal-slip, and 4) reverse-slip ground deformation. The Abaqus results are the basis for deriving fragility functions to estimate longitudinal strain to underground pipelines subjected to permanent ground deformation from fault rupture, landslide displacement, or liquefaction-induced lateral spreading or vertical settlement. A fifth mode of ground deformation was evaluated using an analytical model where the ground deforms in a direction parallel to the pipeline axis resulting in tension at the scarp and compression at the toe of the unstable ground mass.

# CHAPTER 2: Existing Pipeline Test Data

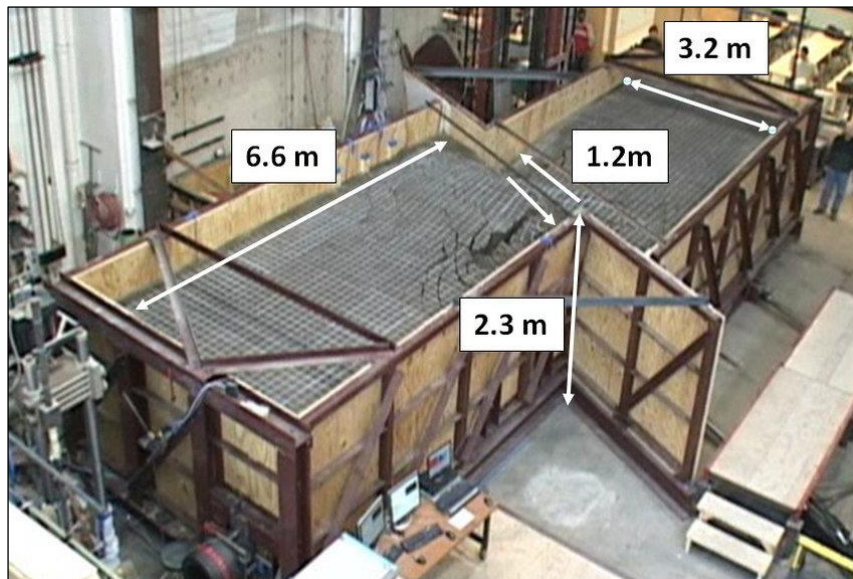
---

## 2.1 Laboratory Test Data Literature Review

A comprehensive literature review was performed to identify physical test data that can be used to describe how natural gas pipelines respond to ground deformation. Illustrative examples of the test data available in the literature are shared in this chapter. Additional information is provided in the more detailed reports by Bain et al. (2022a) and Hutabarat et al. (2022).

There are many significant papers in the literature that describe the tests and document the performance of pipelines subjected to permanent ground deformations with Cornell University and Rensselaer Polytechnic Institute (RPI) making many important contributions. Led by Prof. Thomas D. O'Rourke, the Geotechnical Lifelines Large-Scale Testing Facility at Cornell University has performed extensive testing of soil-pipeline systems subjected to permanent ground deformation using their large-scale split-box. The results of many of these tests have been used to validate the results of the Abaqus modeling, which was performed for the purpose of deriving new pipe strain fragility models for buried steel pipelines subjected to permanent ground deformation. A photograph of the Cornell University Large-Scale Testing Facility split-box test is shown in Figure 1 (O'Rourke et al., 2008) during an experiment in which a buried pipeline is subject to abrupt strike-slip displacement.

**Figure 1: Diagram of Cornell University Test Box**

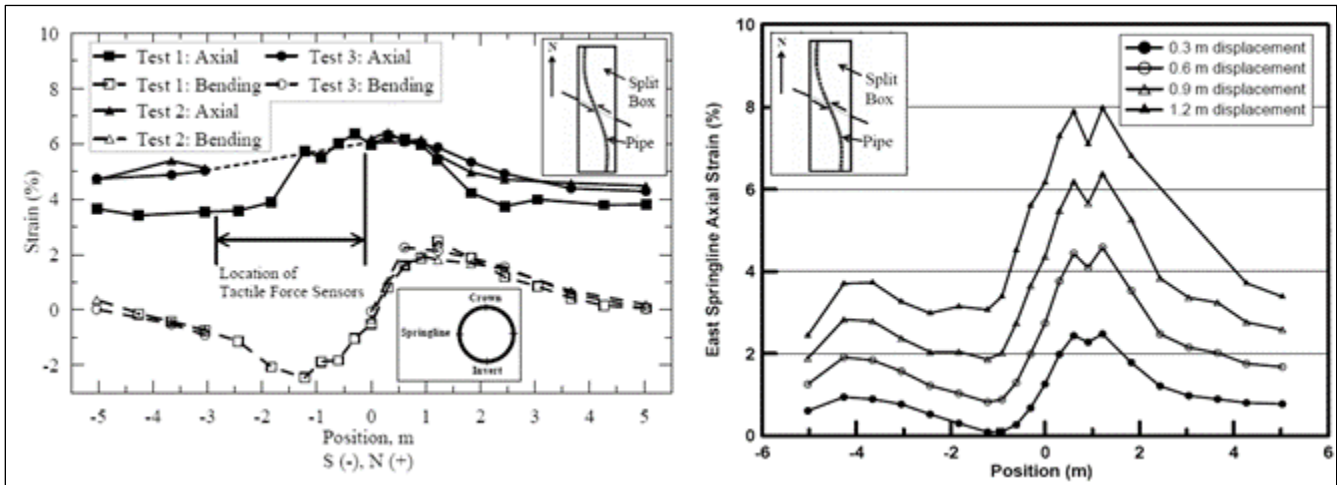


Split-box test apparatus with a pipeline buried in soil at the end of experiment after 1.2 m of strike-slip ground deformation was imposed (from O'Rourke et al., 2008)

Figure 2 shows a comparison of the measured axial and bending strains along a nominal 400 mm-diameter (outside diameter = 407 mm, wall thickness = 24 mm) high-density

polyethylene (HDPE) pipeline at 1.22 m of strike-slip displacement for three large-scale tests (O'Rourke et al., 2012). The inset diagram in Figure 2 shows a schematic of the deformed shape of the test pipe within the test basin. Axial strains are the average of the pipe crown and invert strains, and bending strains were determined as one half the difference between the springline strains. The calculated bending strain is the incremental strain caused by pipeline flexure relative to the axial strain. Plotting the strain in this way allows one to see the axial strains caused by pipeline extension relative to the additional strains generated by bending. The axial pipe strains are maximum at the location of ground rupture and decrease with increasing distance from this location. Pipe flexural strains are zero at the location of abrupt ground deformation, consistent with double curvature bending and a point of counterflexure at the plane of strike-slip displacement.

**Figure 2: Lifelines Geotechnical Large-Scale Testing Facility Experimental Results**



Geotechnical Large-Scale Testing Facility split-box basin experimental test results from O'Rourke et al. (2012)

## 2.2 Pipeline Fragility Models

Section 2.2 addresses pipeline damage state fragility models that estimate the probability of nuisance leakage that does not interfere with pipeline operability, or the probability of pipeline rupture given longitudinal pipe strain caused by permanent ground deformations from fault offset or landslide or liquefaction-induced ground deformation. These models are for continuous steel pipelines with high-quality, overmatched girth welds and are applicable to underground and aboveground pipelines. These models are discussed further in Appendix D.

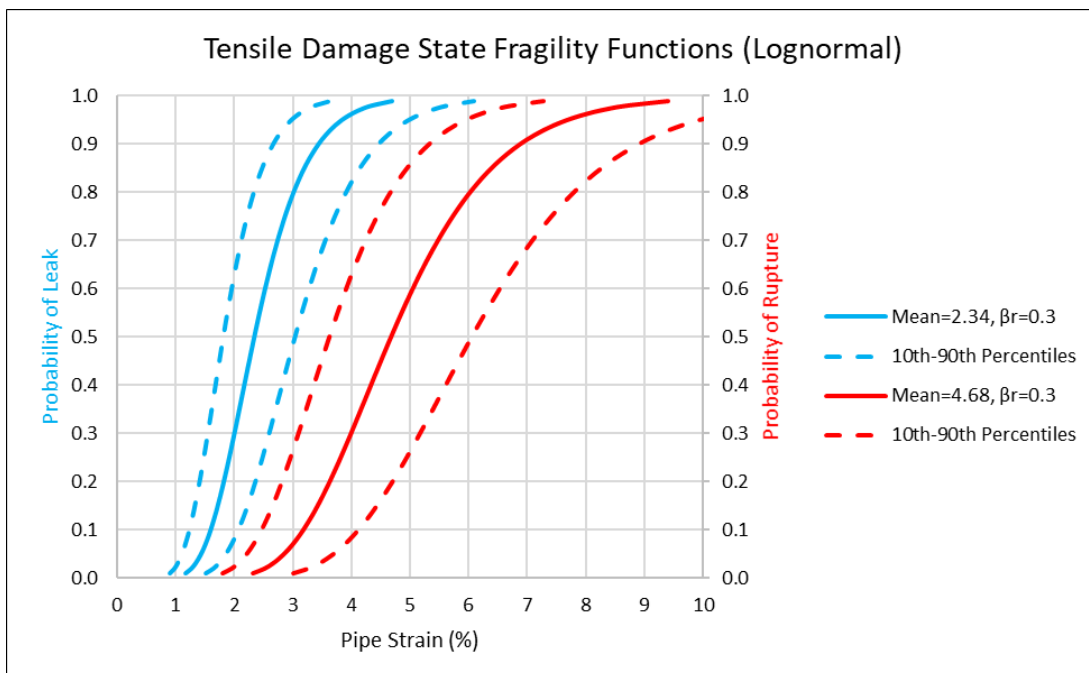
### 2.2.1 Tensile Strain Fragility Models

For continuous steel pipelines with high-quality, overmatched girth welds subjected to tensile strain caused by permanent ground deformation (PGD), the 1984 ASCE *Guidelines for the Seismic Design of Oil and Gas Pipeline Systems* permit longitudinal strains in the 3–5% range while the 2001 ALA *Guidelines for the Design of Buried Steel Pipe* recommend a tensile strain limit of 2% to maintain normal operability of the pipeline and 4% to maintain pressure

integrity. Similarly, the 2004 PRCI *Guidelines for Gas and Liquid Hydrocarbon Pipelines* (Honegger & Nyman, 2004) suggest tensile strain limits of 1–2% for normal operability and 2–4% to maintain pressure integrity. For a natural gas pipeline risk assessment project in British Columbia, Canada, Wijewickreme et al. (2005) use 7% tensile strain as the median value to maintain pressure integrity, with the 90–10% probability of exceedance tensile strains assumed to be 3% and 10%, respectively. Wijewickreme et al. (2005) developed these values with the goal of not being overly conservative after a review of pipeline rupture criterion available at the time, including the ASCE (1984) guidelines.

To develop realistic (and not overly conservative) tensile damage state fragility functions, this study assumes that the 2% pipe strain criterion suggested by ALA (2001) and Honegger & Nyman (2004) to maintain normal operability corresponds to a 30% probability of minor, nuisance leakage and the 4% pipe strain criterion to maintain pressure integrity corresponds to a 30% probability of pipeline rupture. These values are used as anchor points to develop a full distribution of damage state fragility functions. Figure 3 presents suggested lognormal cumulative distribution functions (CDFs) for these damage state fragility functions assuming the aleatory variability,  $\beta_r=0.30$ , which was estimated using expert opinion (Abrahamson, 2022). 10<sup>th</sup> and 90<sup>th</sup> percentiles are presented for the fragility functions assuming the epistemic uncertainty,  $\beta_u=0.20$ , a common assumption for structural systems.  $\beta_r$  represents the aleatory variability in the fragility models due to inherent randomness in the loading conditions (e.g., eccentricities in the pipe alignment, nonuniform backfill soil conditions) and pipe properties (e.g., post-yield stress-strain behavior, weld quality, corrosion).  $\beta_u$  represents the epistemic uncertainty in the mean or median value (i.e., uncertainty resulting from whether the suggested models are the correct models).

**Figure 3: Tensile Damage State Fragility Functions**

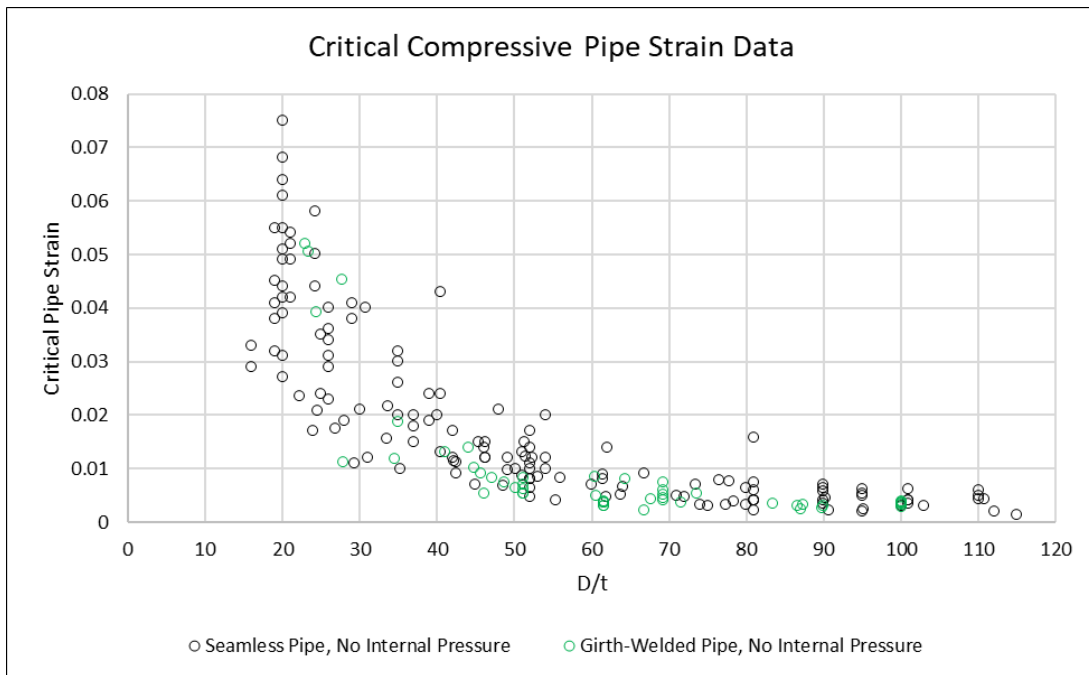


**Lognormal damage state fragility functions corresponding to the probability of leakage or rupture given pipe strain for steel pipelines with high-quality girth welds (arithmetic scale)**

## 2.2.2 Compressive Strain Fragility Models

For continuous steel pipelines with high-quality, overmatched girth welds subjected to compressive strain caused by permanent ground deformation, leakage and rupture are often not differentiated. As stated in Wijewickreme et al. (2005), "*The pipe wall response following the onset of compressive wrinkling is complex and it is not well understood in terms of specifying pressure integrity strain limits.*" Buckling itself is therefore taken as the critical damage state because tearing of the pipe wall can occur during buckling and any further straining in the pipe that occurs from permanent ground deformation tends to concentrate at the buckle, dramatically increasing the likelihood of pipe wall tearing or rupture. Mohr (2003) collected the results of published laboratory compressive pipe tests. These are the same data used in pipeline performance studies (e.g., O'Rourke & Liu, 2012). The results of the tests, which are plotted as the critical compressive pipe strain versus the diameter to pipe wall thickness (D/t) ratio, are presented in Figure 4. These data correspond to the longitudinal pipe strain at the maximum compressive stress. According to Harris et al. (1957), buckling occurs at or just before the maximum load the pipe can resist.

**Figure 4: Critical Compressive Pipe Strain Data**



**Critical compressive pipe strain developed in steel pipe without internal pressure as a function of the pipe diameter (D) to pipe wall thickness (t) ratio (after Mohr, 2003)**

The data in Figure 4 were used to derive a compressive pipe strain fragility function that estimates the probability of compressive buckling or pipe wall wrinkling given the D/t ratio and the estimated axial pipe strain. Details regarding the derivation of the compressive pipe strain damage state fragility function are provided in Appendix D. Furthermore, the data presented in Figure 4 are for pipes without internal pressure. In tension, the effects of internal pressure on the performance of the pipeline are small and it is reasonable to ignore it; however, in compression, the stabilizing effect of internal pressure should be considered. Mohr (2003)

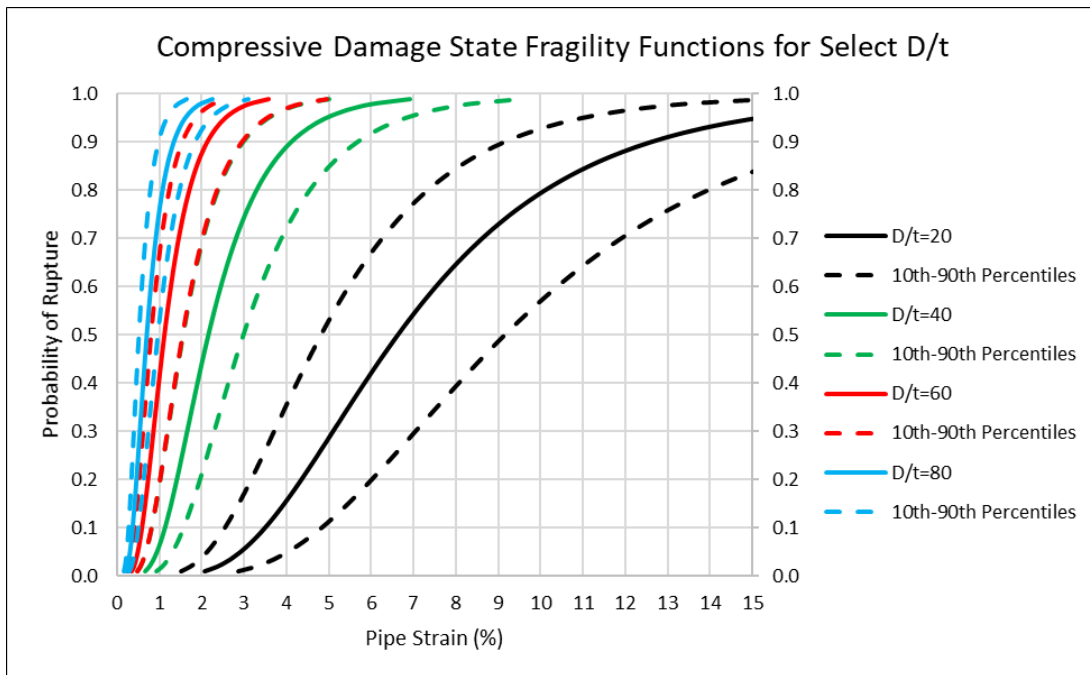
recommends a correction factor to convert a pipe strain estimate to a zero-pressure-equivalent pipe strain.

The data presented in Figure 4 come from controlled laboratory experiments that should have less uncertainty than that of field conditions. To account for greater uncertainty associated with field conditions,  $\beta_r$  is increased from 0.407 to 0.50, as explained in Appendix D.

Pipelines can often sustain more axial strain after the initiation of buckling or pipe wall wrinkling before pipe wall tearing or rupturing occurs. The probability of compressive rupture (due to buckling or pipe wall wrinkling) fragility function accounts for this additional capacity by shifting the 50% probability of exceedance values in the original fragility function up to the 20% probability of exceedance level in the final function, as explained in Appendix D.

Figure 5 displays the probability of compressive rupture CDFs for pipes with D/t ratios of 20, 40, 60, and 80 along with the 10<sup>th</sup> and 90<sup>th</sup> percentiles assuming  $\beta_u=0.25$ .

**Figure 5: Probability of Compressive Rupture for Select D/t Ratios**



**Compressive rupture fragility functions for select D/t ratios**

Additional details of the pipeline fragility models are provided in Appendix D.

# CHAPTER 3:

## Project Approach

---

This report assesses the earthquake-induced ground deformation hazard to natural gas infrastructure in California from liquefaction-induced lateral spreading and vertical settlement and from seismic slope instability and slope displacement. A review of the procedures and data available in the literature is presented and gaps in the literature are identified. New procedures and existing procedures, including updates or modifications, resulting from targeted research are presented.

The *OpenSRA* Project requires the analysis of seismic risk at statewide to site-specific scales. To do this, data and procedures to evaluate geohazards are categorized into four levels (see Appendix A):

1. Level 1 analyses utilize data that are continuous at a uniform resolution over the entire state of California. With its lower level of resolution and without site-specific or subsurface data, the statewide data lead to very high uncertainty.
2. Level 2 analyses utilize data produced at regional scales collected at higher resolution than Level 1 data. Level 2 data are not necessarily geospatially continuous over the entire state of California. There is minimal, generic subsurface data or estimated engineering properties. Use of Level 2 data leads to high uncertainty, but less uncertainty than with Level 1 data.
3. Level 3 analyses utilize site-specific geologic and topographic mapping and includes subsurface data through CPTs, borings with SPT, and soil/rock index tests. Subsurface data can be used in performance-based liquefaction, lateral spreading, slope displacement, and settlement procedures. Level 3 data enable assessment with medium uncertainty, less than with Level 2 data.
4. Level 4 analyses utilize high-quality laboratory test data with the Level 3 site-specific geologic, topographic, and geotechnical data. Use of Level 4 data support the performance of advanced numerical analyses. Level 4 analyses will have the least uncertainty in estimating the effects of earthquake-induced ground deformation on buried pipes. Due to the high level of data required they will not be employed commonly in making systemwide seismic risk assessments. Instead, they will be used on project-specific efforts. Level 4 analyses are beyond the current scope of the *OpenSRA* Project.

The qualitative descriptions of uncertainty at each data and analysis level (i.e., very high, high, and medium) are intended to communicate the decreasing amount of uncertainty possible as more robust data and analytical methods are employed. The uncertainties associated with these data and analyses levels for a liquefaction triggering assessment illustrates the ranges of uncertainty typically associated with these descriptions. Liquefaction triggering models are assumed to be lognormally distributed with aleatory variability on the order of  $\beta_r \approx 0.8 - 1.0$  at Level 1,  $\beta_r \approx 0.7 - 0.9$  at Level 2, and  $\beta_r \approx 0.5 - 0.7$  at Level 3.

This report recommends data and procedures available in the literature for performing analyses at levels 1 – 3 and introduces new procedures developed during this project. This report also describes the derivation of fragility functions for assessing pipe strain for pipelines subjected to permanent ground deformation. Pipelines subjected to the strike-slip tension, strike-slip compression, normal-slip, and reverse-slip modes of ground deformation were numerically analyzed using the finite element program Abaqus. More than one million realistic combinations of relevant system parameters were assessed, and the results used to develop relationships to estimate the distribution of longitudinal pipe strain for each mode of ground deformation. The developed relationships capture the mechanics of soil-pipeline systems undergoing permanent ground deformation. A fifth mode of ground deformation where the ground deforms in a direction parallel to the longitudinal pipeline axis causing tension at the scarp and compression at the toe of the ground deformation zone was assessed using an analytical model.

## **3.1 Liquefaction Triggering Models and Data**

### **3.1.1 Level 1 Liquefaction Triggering Models and Data**

To enable Level 1 assessments of liquefaction triggering, the only models that can be applied at a uniform data resolution across the entire state of California come from Zhu et al. (2015) and Zhu et al. (2017). These regional-scale methods use inputs that are proxies for geotechnical, geologic, and groundwater conditions to quantitatively assess the probability of liquefaction triggering at the statewide scale. Zhu et al. (2015, 2017) claim their models capture general trends observed at the regional scale for a few earthquakes. They do not provide quantitative assessments of the performance of their models. As no subsurface data are used to inform the models, Level 1 liquefaction triggering assessments are judged to have very high uncertainty.

The inputs for the Zhu et al. (2015) model include peak ground acceleration (PGA), compound topographic index (CTI), and the time-averaged shear wave velocity in the upper 30-meters of the subsurface ( $V_{S30}$ ). The inputs for the Zhu et al. (2017) models include the peak ground velocity (PGV),  $V_{S30}$ , the average annual precipitation (precip), nearest distance to the coast ( $d_c$ ), nearest distance to a river ( $d_r$ ), nearest distance to any water ( $d_w$ ), and a depth to groundwater model (wtd). Statewide datasets of the model inputs are presented in Appendix C. The statewide Zhu et al. (2015) and Zhu et al. (2017) datasets shown in Appendix C are included in *OpenSRA* enabling Level 1 liquefaction triggering assessments to be performed across the entire state of California without additional inputs required from the user.

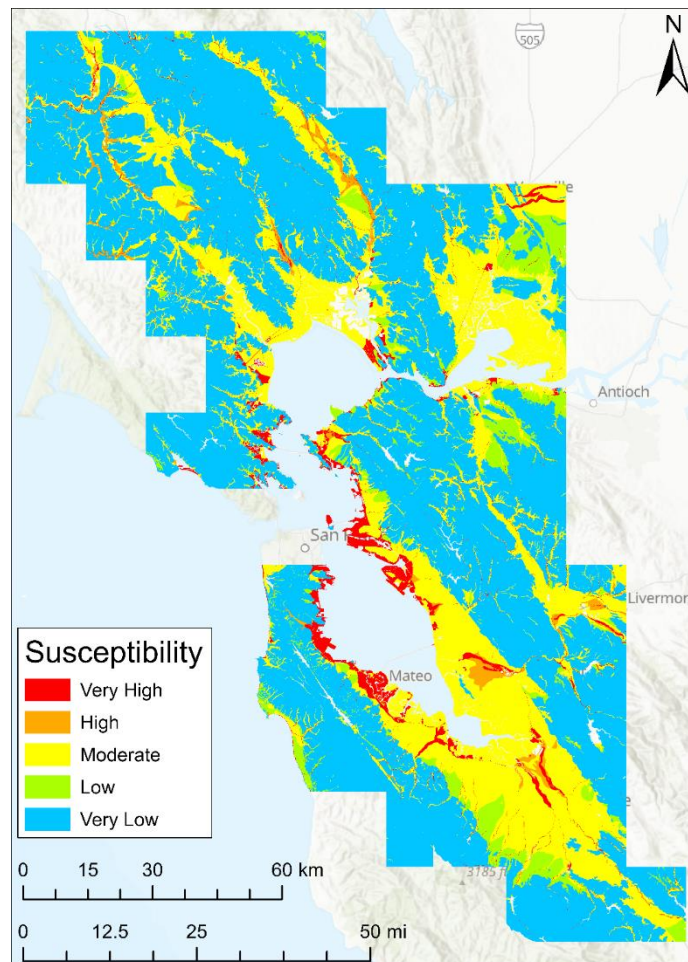
Neither Zhu et al. (2015) nor Zhu et al. (2017) provide estimates for the aleatory variability (due to inherent randomness of data which is denoted as  $\beta_r$ ) or epistemic uncertainty (due to incomplete scientific knowledge leading to modeling uncertainty which is denoted as  $\beta_u$ ) associated with their models. For implementation into *OpenSRA*, the aleatory variability in the intermediate parameter (see model equations in Appendix B) is assumed to be lognormally distributed with  $\beta_r=0.90$  and the epistemic uncertainty is assumed to be lognormally distributed with  $\beta_u=0.50$ .

### 3.1.2 Level 2 Liquefaction Triggering Models and Data

At Level 2, liquefaction triggering can be analyzed using Youd & Perkins (1978)-type geologic based assessments in conjunction with the Hazus (FEMA, 2020) methodology. Youd & Perkins (1978)-type geologic based assessments characterize the relative liquefaction susceptibility (i.e., none, very low, low, moderate, high, very high) of mapped surficial geologic deposits based on the depositional environment and age of the deposits (see Table B.7 in Appendix B). This is a significant improvement over the  $V_{S30}$  proxy for geotechnical conditions employed in the Zhu et al. (2015, 2017) methods. Although  $V_{S30}$  is correlated to the depositional environment and age of the deposits, large-scale geologic mapping that differentiates quaternary units is a better indicator of where liquefiable soils are likely to exist in the subsurface. The Hazus (FEMA, 2020) liquefaction triggering methodology, presented in Appendix B, uses a site's relative liquefaction susceptibility classification, the depth to groundwater, PGA, and  $M_w$  to estimate the probability of liquefaction triggering.

An example of applying the Youd & Perkins (1978) methodology at a regional scale is the mapping in the San Francisco Bay Area by Witter et al. (2006), which is presented in Figure 6.

**Figure 6: Mapping of Relative Liquefaction Susceptibility in San Francisco Bay Area**



Liquefaction susceptibility mapping of the San Francisco Bay Area based on mapped geologic units (from Witter et al., 2006)

The Level 2 liquefaction triggering model from Hazus (FEMA, 2020) is applied across selected regions such as the San Francisco Bay area or the Los Angeles Basin where both large-scale geologic and liquefaction susceptibility mapping have been performed. Liquefaction susceptibility mapping based on large-scale geologic mapping is a significant improvement over Level 1 liquefaction triggering assessments performed using the Zhu et al. (2015) or Zhu et al. (2017) models. Such models do not directly consider the geomorphic environment or the age of the deposits.

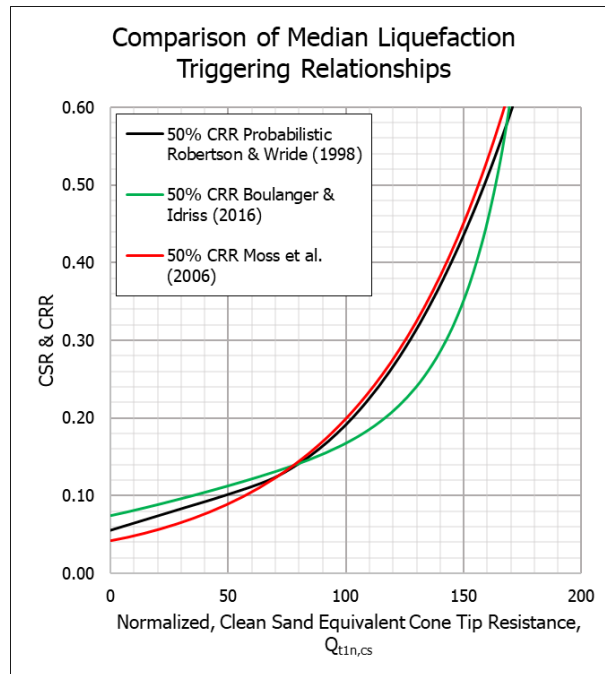
As subsurface conditions still do not directly inform Level 2 liquefaction triggering assessments, uncertainty remains high. Hazus (FEMA, 2020) does not specify the aleatory variability or epistemic uncertainty for the liquefaction triggering model. To implement the Hazus (FEMA, 2020) liquefaction triggering model into *OpenSRA*, the aleatory variability is assumed to be lognormally distributed with  $\beta_r=0.80$  (compared to  $\beta_r=0.90$  at Level 1) and the epistemic uncertainty is assumed to be lognormally distributed with  $\beta_u=0.40$  (compared to  $\beta_u=0.50$  at Level 1).

### **3.1.3 Level 3 Liquefaction Triggering Models and Data**

At Level 3, liquefaction triggering is analyzed using Cone Penetration Test (CPT) or Standard Penetration Test (SPT) based procedures, with CPT procedures being preferred due to the improved repeatability and reliability of CPT data compared to SPT data.

Three probabilistic liquefaction triggering methods are available for the CPT: the Moss et al. (2006) method, the Ku et al. (2012) probabilistic modification to the Robertson & Wride (1998) as updated by Robertson (2009) procedure, and the Boulanger & Idriss (2016) procedure. Each method follows a simplified process for evaluating soil liquefaction triggering originally outlined by Seed & Idriss (1971), which defines the factor of safety against liquefaction triggering ( $FS_L$ ) as the ratio of the cyclic resistance ratio (CRR) to the cyclic stress ratio (CSR). These procedures differ in the calculation of both CRR and CSR and all evaluate liquefaction triggering probabilistically. A comparison of the median liquefaction triggering curves associated with these methods is shown in **Error! Reference source not found..**

**Figure 7: Comparison of Median Liquefaction Triggering Relationships**



**Median liquefaction triggering curves from the Ku et al. (2012) probabilistic modification to the Robertson & Wride (1998) as updated by Robertson (2009) procedure, the Boulanger & Idriss (2016) procedure, and the Moss et al. (2006) procedure**

For the SPT data, three procedures are again recommended to evaluate liquefaction triggering: the NCEER procedure described by Youd et al. (2001), the Idriss & Boulanger (2008) approach as updated by Boulanger & Idriss (2014), and the Cetin et al. (2018) method. Of these methods, only Cetin et al. (2018) assesses liquefaction triggering probabilistically. These procedures were selected because they are most commonly used in professional engineering practice.

These procedures are coded into *OpenSRA*, and the user will be able to specify the weighting given to each procedure. Level 3 liquefaction triggering evaluations require the user to provide either CPT or SPT data in the assessment area.

## **3.2 Liquefaction-Induced Lateral Spread Displacement and Vertical Settlement Models and Data**

### **3.2.1 Level 1 Liquefaction-Induced Lateral Spread Displacement and Vertical Settlement Procedures and Data**

At Level 1, the Hazus (FEMA, 2020) lateral spread displacement and vertical settlement models, presented in Appendix B, can be used to estimate liquefaction-induced lateral spread displacement and ground settlement. The Hazus (FEMA, 2020) models are the only models currently available that are capable of estimating lateral spread displacements and vertical settlements at the statewide scale.

To use these models, the relative liquefaction susceptibility must first be mapped. At the statewide level, relative liquefaction susceptibility can be mapped using the Zhu et al. (2017) procedure by excluding the magnitude-scaled-PGV term from the calculation. The resulting dimensionless value is referred to as the susceptibility quantity and its value correlates to a liquefaction susceptibility class, presented as Table B.10 in Appendix B.

After mapping liquefaction susceptibility, only PGA and  $M_w$  are required to estimate liquefaction-induced lateral spread displacement, while only the liquefaction susceptibility class is necessary to estimate vertical settlement. Given that the Hazus (FEMA, 2020) lateral spread displacement and vertical settlement models do not require knowledge of subsurface or topographic conditions, the uncertainty must necessarily be very high.

Hazus (FEMA, 2020) does not specify the aleatory variability or epistemic uncertainty for the lateral spread displacement model. Uncertainty in the estimated liquefaction-induced vertical settlement is assumed in Hazus (FEMA, 2020) to take the form of a uniform distribution with bounds of one-half to two times the mean values. To implement the Hazus (FEMA, 2020) liquefaction-induced lateral spread displacement and vertical settlement models in *OpenSRA*, the aleatory variability is assumed to be lognormally distributed with  $\beta_r=0.90$ . The epistemic uncertainty is assumed to be lognormally distributed with  $\beta_u=0.50$ .

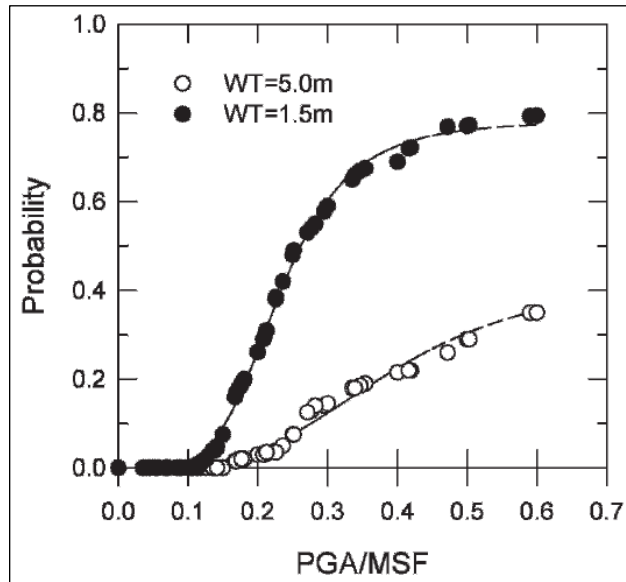
As statewide datasets of the Zhu et al. (2017) model inputs are built into *OpenSRA*, Level 1 liquefaction-induced lateral spreading and vertical settlement assessments can be performed without additional inputs from the user in the state of California.

### **3.2.2 Level 2 Liquefaction-Induced Lateral Spread Displacement and Vertical Settlement Models and Data**

At Level 2, the Hazus (FEMA, 2020) methodology can again be applied to estimate potential lateral spread displacement and vertical settlement due to liquefaction. However, because enhanced data are available at Level 2 compared to Level 1 and because it is desired to estimate lateral spread displacement probabilistically, research has been performed to develop a new Level 2 procedure for assessing lateral spread displacement.

The proposed procedure is based on liquefaction probability curves for surficial geologic units, described in Holzer et al. (2011). The curves presented in Holzer et al. (2011) estimate the probability of liquefaction triggering versus magnitude-scaled-PGA for two discrete groundwater depths. An example of liquefaction probability curves for the sandy artificial fill over Bay Mud (afem) deposits in the San Francisco Bay area is presented in Figure 8.

**Figure 8: Liquefaction Probability Curves for the Sandy Artificial Fill over Bay Mud (afem) Deposits in the San Francisco Bay Area**



**Probability of liquefaction in sandy artificial fill over young bay mud deposits for water table depths of 1.5 m and 5.0 m as a function of magnitude-scaled PGA (from Holzer et al., 2011)**

There are several issues related to the liquefaction probability curves. Relationships are presented for only two discrete groundwater depths rather than presenting relationships that are continuous with groundwater depth, no estimates of aleatory variability or epistemic uncertainty are provided, and the consequences of liquefaction, such as potential lateral spread displacements, are not evaluated.

Research has modified and expanded the framework of the Holzer et al. (2011) procedure to include assessments for the probability of liquefaction triggering, potential lateral spread displacements, and estimates of their uncertainties.

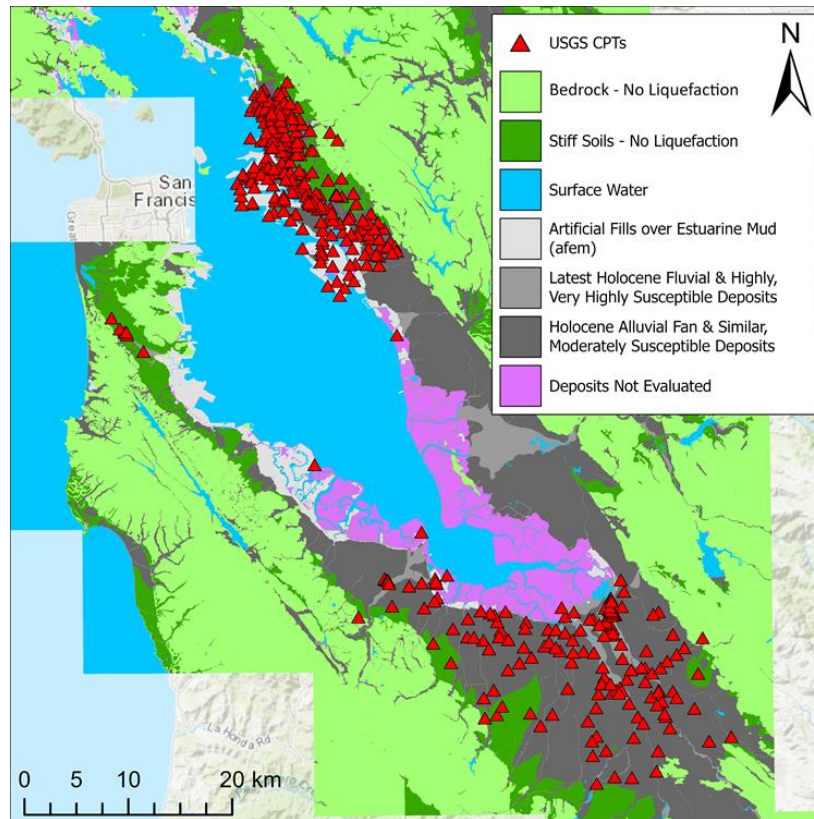
For this new procedure, CPTs are collected in a study region and classified by surficial geology. Lateral displacement index (LDI) is calculated for 225 combinations of PGA,  $M_w$ , and GWT and a relationship to assess the probability of LDI="0", where  $LDI < 3$  is assumed to essentially equal zero, is developed. Additionally, a relationship is developed to estimate the mean, non-zero LDI, and their uncertainty. These two relationships are combined assuming a mixed-random variable model whereby there is a mass probability that LDI="0" and a distribution of non-zero LDI.

LDI is calculated using the 50% probability of liquefaction cyclic resistance ratio (CRR) relationships from Boulanger & Idriss (2016) and the Ku et al. (2012) probabilistic modification to the Robertson & Wride (1998) as updated by Robertson (2009) procedure. Equal weights are given to the two procedures. Three procedures are used to estimate the soil's relative density ( $D_r$ ): Idriss & Boulanger (2008), Jamiolkowski et al. (2001), and Kulhawy & Mayne (1990), with weightings of 0.4, 0.3, and 0.3, respectively. Finally, to estimate the maximum shear strain potential induced by the liquefaction ( $\gamma_{max}$ ), which is an index of the amount of

lateral ground deformation, the procedures from Zhang et al. (2004) and Idriss & Boulanger (2008) are used, with equal weights given to the two procedures.

The CPTs used to develop the procedure in the San Francisco Bay Area come from the USGS and are presented in Figure 9, overlaid on a simplified version of the 1:24,000 scale Witter et al. (2006) geologic map.

**Figure 9: Locations of USGS CPTs in San Francisco Bay Area with Geology**



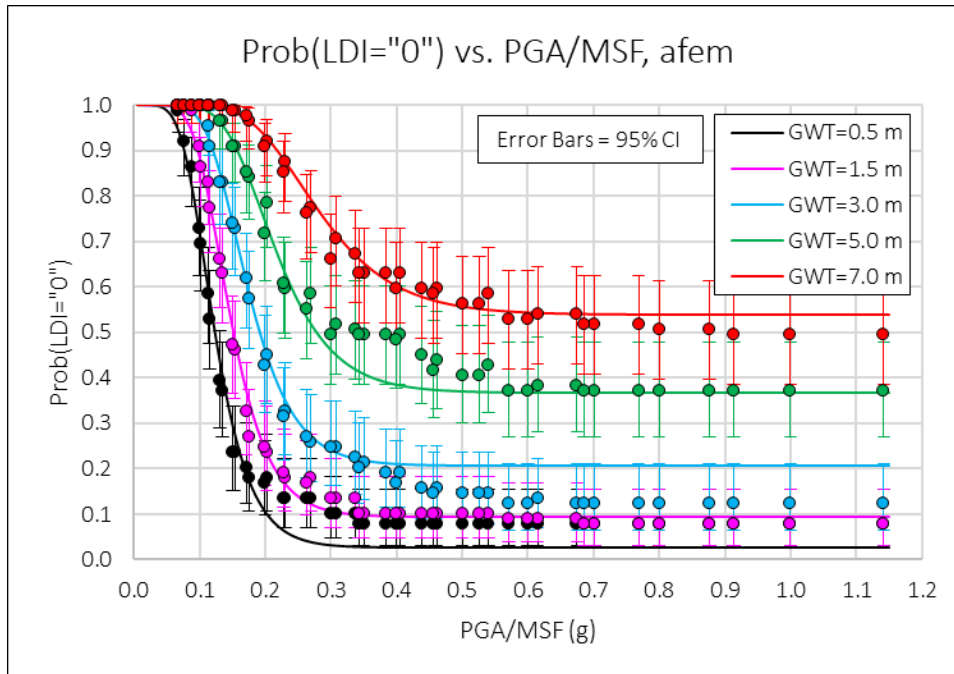
**CPTs in the USGS Database in the San Francisco Bay Area Overlaid on a Simplified Version of Geologic Mapping from Witter et al. (2006)**

In total, there are 89 CPTs located in the afem deposits, 41 CPTs located in latest Holocene fluvial and similar highly, very highly susceptible deposits, and 177 CPTs located in Holocene alluvial fan and similar, moderately susceptible deposits.

Equations are presented in Appendix B to estimate the probability of  $LDI=“0”$ . Equations are also provided for the mean, non-zero  $LN(LDI)$ , along with the model regression coefficients.

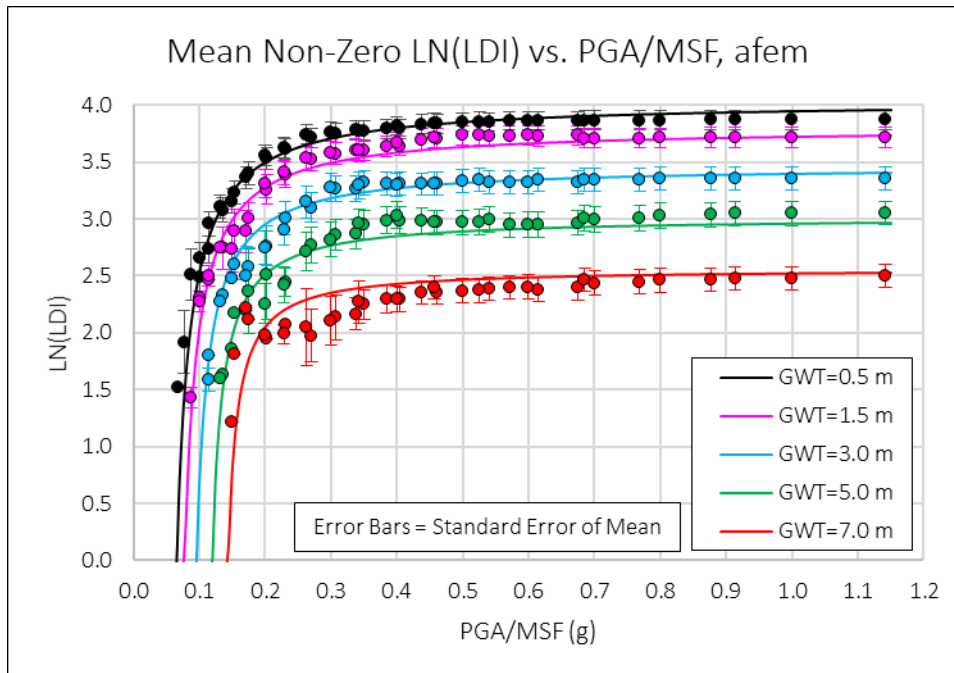
An example of the probability of  $LDI=“0”$  data for the sandy artificial fill over Bay Mud deposits is presented in Figure 10. The mean, non-zero  $LN(LDI)$  data for these deposits are presented in Figure 11.

**Figure 10: Prob(LDI="0") vs. PGA/MSF Data for afem Deposits**



Fit of Prob(LDI="0") regression model to data calculated for sandy artificial fill over Bay Mud deposits

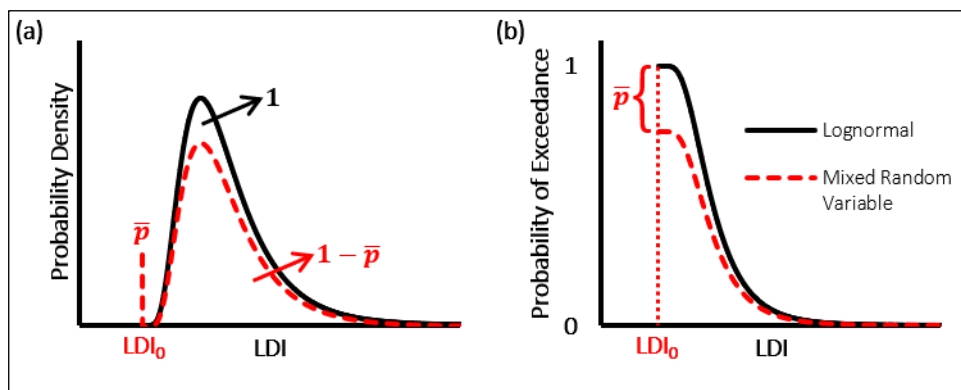
**Figure 11: Mean, Non-Zero LN(LDI) Data for afem Deposits**



Fit of Mean, Non-Zero LN(LDI) regression model to data calculated for sandy artificial fill over Bay Mud deposits

Similar to the Bray & Macedo (2019) model for assessing the seismic slope displacement, the Prob(LDI="0") and non-zero LN(LDI) data (examples shown in Figure 10 and Figure 11, respectively) are combined using a mixed-random variable model, as illustrated in Figure 12.

**Figure 12: Comparison of Continuous and Mixed Random Distributions**



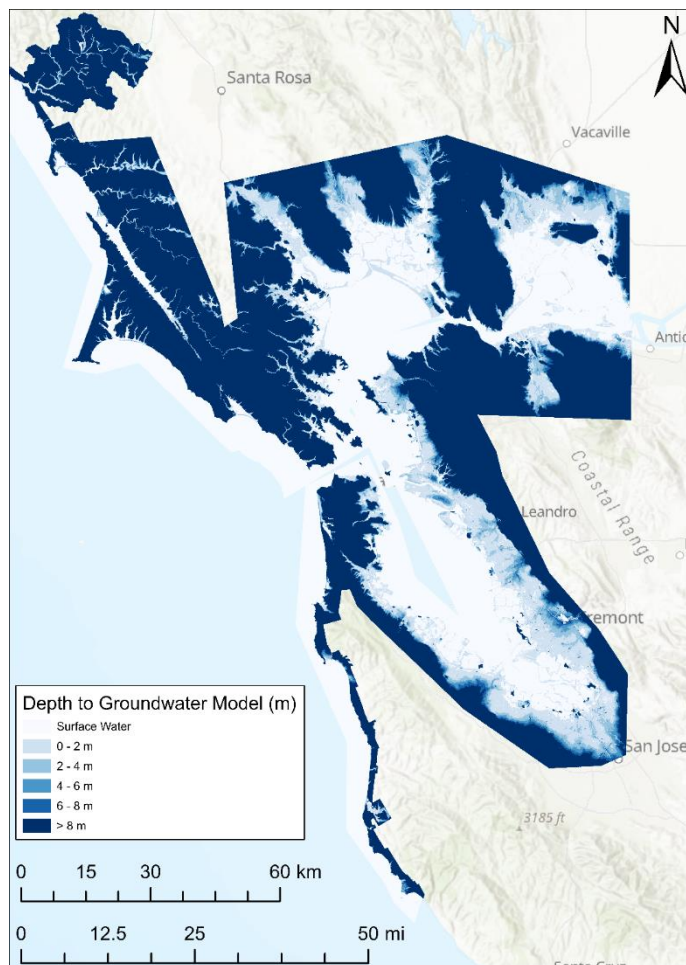
**(a) PDF for a Mixed and Continuous Random Variable and (b) Probability of Exceedance for a Mixed and Continuous Random Variable**

These models estimate only a distribution of LDI. The estimated LDI distribution is converted to a distribution of lateral spread displacement using topographic correlations of LDI to lateral spread displacement (i.e., Zhang et al., 2004). The Zhang et al. (2004) models are presented in Appendix B.

Using maps of surficial geology, depth to groundwater, and topography, the lateral spread displacement can be estimated probabilistically at regional scales using this newly developed procedure. Although this method has been shown to provide reasonable results in the San Francisco Bay Area and in Christchurch, New Zealand, it requires sufficient CPT data over an area to implement it in *OpenSRA*. At present this new procedure is only implemented in *OpenSRA* in the San Francisco Bay area.

An example of Level 2 groundwater data comes from the USGS, who used the program MODFLOW to create depth to groundwater models in coastal areas as part of the Coastal Storm Modeling System (CoSMoS) project (USGS, 2021). The USGS CoSMoS mean higher high water (MHHW) model is presented in Figure 13 for the San Francisco Bay area.

**Figure 13: USGS CoSMoS Depth to Groundwater Model in the San Francisco Bay Area**



**Mean higher high water groundwater (MHHW) model developed by USGS CoSMoS project (USGS, 2021)**

The proposed new model is an improvement over the Hazus (FEMA, 2020) lateral spread displacement model because subsurface conditions are used to derive the geologic deposit specific models, the lateral spread displacement assessment utilizes topography, and lateral spread displacement is assessed probabilistically. The procedure, however, has currently only been developed for the Bay area and future development is limited to regions with a significant number of CPTs available.

### **3.2.3 Level 3 Liquefaction-Induced Lateral Spread Displacement and Vertical Settlement Models and Data**

At Level 3, liquefaction-induced lateral spreading and vertical settlement are assessed using the CPT following the procedures provided by Zhang et al. (2004) and Zhang et al. (2002), respectively. These procedures were selected because they are the CPT-based methods used most often in professional engineering practice to assess liquefaction-induced lateral spreading and settlement.

The Zhang et al. (2004) procedure computes LDI, which is related to lateral spread displacement through topographic correlations. The Zhang et al. (2002) procedure estimates the post-liquefaction volumetric strain at level sites far from a free-face slope. Both the Zhang et al. (2004) and Zhang et al. (2002) procedures can be applied with any of the CPT-based liquefaction triggering procedures discussed previously.

At Level 3, the Youd et al. (2002) and Cetin et al. (2009) procedures can be used to estimate liquefaction-induced lateral spread displacements and vertical settlements using SPT data. Youd et al. (2002) provides two multilinear regression equations to estimate lateral spread displacement for gently sloping sites and for sites near a free face, as presented in Appendix B. The Youd et al. (2002) procedure has two important limitations. Firstly, the multilinear regression they employed is a statistical fitting to field case history data without an underlying mechanistic model; hence, the mechanics of lateral spreading may not be entirely captured. Secondly, earthquake shaking intensity is characterized by the horizontal distance to the seismic source. Characterizing shaking intensity by only the horizontal distance to the seismic source does not capture the many variables that affect the intensity of ground shaking at a given site. Such variables can be captured by sophisticated ground motion models (GMMs). For example, using the PGA estimated with a GMM would provide a more statistically robust estimate of ground shaking. Moreover, local site condition effects as well as the aleatory and epistemic uncertainties could be considered. The Cetin et al. (2009) procedure probabilistically assesses the volumetric strain potential of saturated, cohesionless soil using a closed form solution. Volumetric strain is correlated to settlement at the ground surface using a case history database.

The Level 3 liquefaction-induced lateral spread displacement and vertical settlement models are compatible with the Level 3 CPT and SPT based liquefaction triggering models and require *OpenSRA* users to input Level 3 data.

### **3.3 Seismic Slope Stability and Slope Displacement Models and Data**

#### **3.3.1 Level 1 Seismic Slope Stability and Slope Displacement Models and Data**

The procedures available to assess seismic slope stability and potential slope displacement are robust and include Bray & Macedo (2019), Grant et al. (2016), and Jibson (2007); however, the data available to assess slope stability and potential slope displacement at the statewide level (i.e., Level 1) have very high uncertainty. The slope stability and displacement models are presented in Appendix B.

Several distinct modes of seismic slope failures exist, such as infinite slope type failures, rotational slides and slumps, and rockslides and rockfalls. Many seismically induced landslides, including during California earthquakes, can be analyzed reasonably well as infinite slope failures with Level 1 data.

Given the simplicity and appropriateness of infinite slope models, they represent the only style of landsliding considered at Level 1. Such seismic slope stability assessments require estimates for distributions of the friction angle and cohesion strength parameters, which are roughly correlated to surficial geology.

For Level 1 statewide analyses, geology is assessed using the geologic map from Wills et al. (2015) which is a compilation of published geologic maps ranging in scale from 1:250,000 to 1:24,000, with the population centers of the San Francisco Bay area and the Los Angeles basin covered by the larger scale mapping. This map contains 17 units including surface water, artificial dam fill, eight rock units, and seven alluvial units. The younger alluvial units are subdivided based on topographic slope. In areas mapped as young alluvium and sloping greater than 2%, the deposits are likely to be coarser-grained, slopes between 0.5% and 2% are likely to be composed of a mixture of sand, silty sand, and gravels, and slopes less than 0.5% are likely to be composed of finer sands, silts, and clays. The GIS mapping includes a single large polygon for the entire extent of the Sierra Nevada granite. Due to the significantly higher strength of the granite in the Sierras compared to crystalline rocks in some other parts of the state, such as the Bay Area, the map is altered to differentiate this unit. The Wills et al. (2015) geologic map is presented in Appendix C. A description of the geologic units is provided in Table B.14 in Appendix B.

At Level 1, the estimated distributions for the friction angle and cohesion for each of the mapped units, which defines the shear strength of each unit using the Mohr-Coulomb criteria) comes from the California Geological Survey database of shear strength tests assembled for the USGS HayWired project (USGS, 2018) and provided by Tim McCrink and Erik Frost (McCrink & Frost, 2021). Table B.15 in Appendix B summarizes the estimated mean, median, and standard deviation for each of the mapped units.

The cohesion data are approximately lognormally distributed for each of the units. For the friction angle, it is not clear if the data are best represented by a normal or lognormal distribution. Using the Lilliefors test, some geologic units (i.e., Qi, Qoa, QT, Tsh/Tss, Tv, and crystalline rocks; see Appendix B for descriptions) are found to be best represented using the normal distribution, while other geologic units (i.e., Qal, Qs, sp, Kss, and KJf; see Appendix B) are found to be better represented using the lognormal distribution.

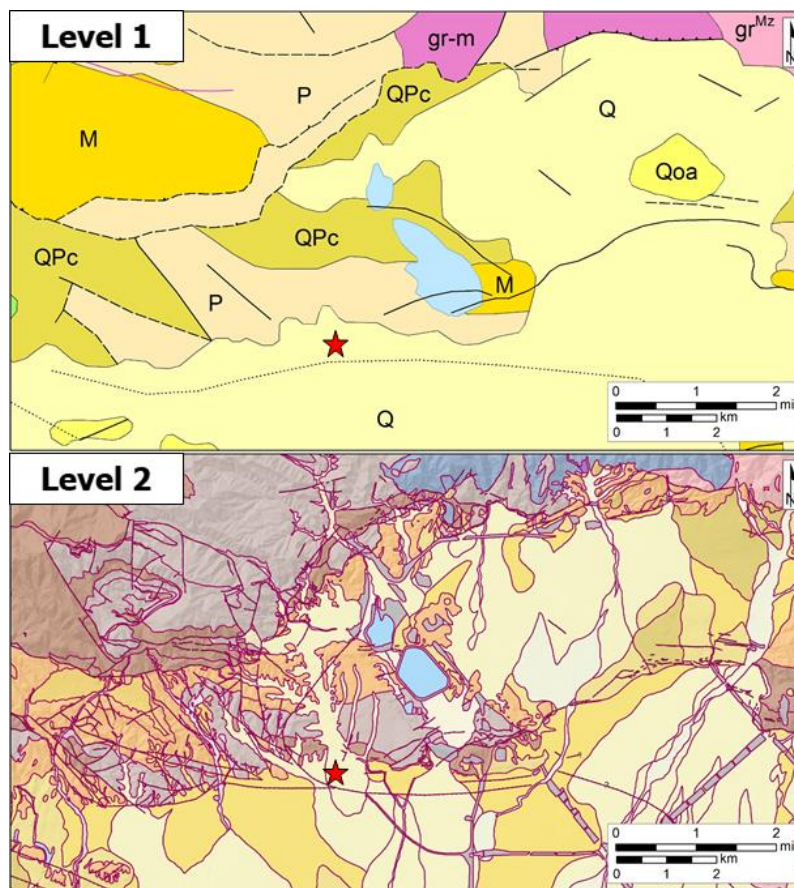
The Wills et al. (2015) geologic map is coded into *OpenSRA* and Level 1 seismic slope stability and slope displacement assessments can be performed in *OpenSRA* without additional input from the user.

### **3.3.2 Level 2 Seismic Slope Stability and Slope Displacement Models and Data**

At Level 2, the analytical procedures used to evaluate potential seismic slope displacement are the same as those used at Level 1; the difference between Level 1 and Level 2 analyses are the resolution and quality of the input geological data used to define the shear strength of the geologic material.

At Level 2, it is expected that the user will have collected geologic data at higher resolution than the statewide geologic map used for Level 1 analyses and may include GIS-based geologic mapping at larger scale than the statewide map with estimates for engineering parameters from seismic hazard zone reports (SHZR) from the California Geological Survey (CGS) or other subsurface data collected at regional scales. The difference in resolution between Level 1 and Level 2 geologic maps is illustrated in Figure 14, which shows the significant detail gained moving from the small-scale statewide geologic map to the larger-scale geologic map from Bedrossian et al. (2012). The red star denotes the location of the Balboa Boulevard demonstration site that is examined in a separate task of the *OpenSRA* project, which is discussed in the Bain et al. (2022b) report.

**Figure 14: Comparison of Level 1 and Level 2 Geologic Maps in Northern San Fernando Valley**



**Comparison of geologic maps from CGS (2010) and Bredrossian et al. (2012) in the northern San Fernando Valley**

For implementing Level 2 seismic slope stability and slope displacement assessments in *OpenSRA*, the user is required to input larger scale geologic mapping and strength parameter distributions for the mapped units. However, by doing so, the uncertainty in the seismic slope displacement estimates is reduced significantly.

### **3.3.3 Level 3 Seismic Slope Stability and Slope Displacement Models and Data**

Many natural gas transmission pipelines are installed in geologic materials that can be explored with the CPT. Using correlations of CPT tip resistance and sleeve friction to soil strength parameters, a distribution of the undrained shear strength or effective friction angle can be estimated from a profile of CPT measurements to characterize the soil shear strength of clay and sand, respectively. After developing a distribution for the undrained shear strength or effective friction angle, a distribution for the yield coefficient can be estimated and potential earthquake-induced landslide displacements can be assessed using the previously presented models, such as Bray & Macedo (2019) or Jibson (2007). The yield coefficient ( $k_y$ ) describes the dynamic resistance of the slope to ground deformation. It is the seismic coefficient required to bring the static slope stability factor of safety down to unity. The uncertainty in the estimate of seismic slope displacement is reduced further from that in Level 2 by CPT data for additional site characterization.

## **3.4 Numerical Modeling of Soil-Pipeline Interaction**

This study numerically modeled the soil-pipeline interaction and pipe response to permanent ground deformation for the purpose of deriving relationships to estimate a distribution of longitudinal pipe strain given various soil-pipeline system parameters. More than one million realistic combinations of system parameters including pipe diameter, wall thickness, pipe steel grade, burial depth, soil type and strength, pipeline-ground deformation zone intersection angle, internal pressure, anchorage length, and magnitude of ground deformation were assessed using the finite element software Abaqus Version 6.1 (a computer program used extensively in the natural gas industry). Details of the selected scenarios and numerical modeling techniques (e.g., finite element mesh, beam element type, springs, boundary conditions, integration points) are provided in the Hutabarat et al. (2022) report.

### **3.4.1 Ground Deformation Modes**

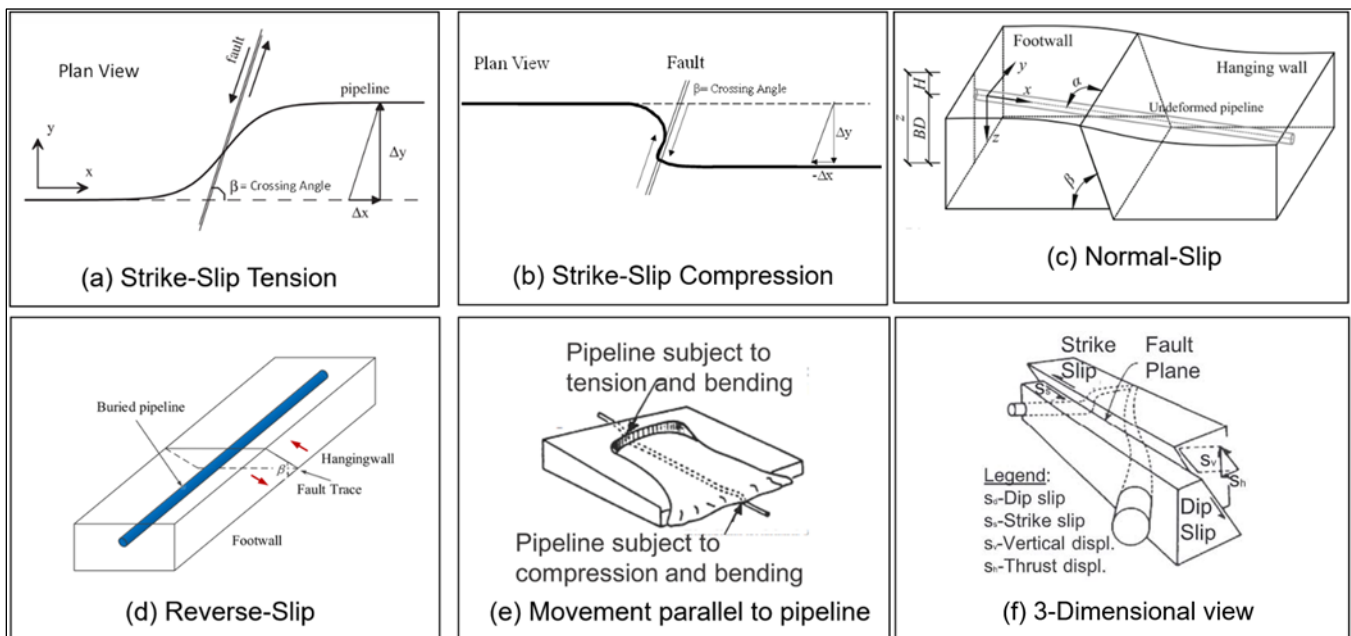
Abrupt permanent ground deformations that pull, compress, or bend pipelines are caused by surface fault rupture or creep, rainfall or seismically induced landslides, liquefaction-induced lateral spreading or vertical settlement, or ground subsidence caused by mining, groundwater extraction, or other reasons. The first step in deriving models for assessing pipe strain for pipelines subjected to permanent ground deformation is to determine the modes of ground deformation to be analyzed. The numerical modeling in this study analyzed only abrupt ground movements. Abrupt (“knife-edge”) ground movements result in locally higher strain concentrations compared to distributed ground movements, which were not studied. The assumption of knife-edge ground movements is appropriate for many practical cases, and it introduces a moderately conservative bias to the pipe strain fragility models for the cases involving distributed ground movements.

Pure strike-slip tension, pure strike-slip compression, pure normal-slip, and pure reverse-slip modes of ground deformation were analyzed using Abaqus for the *OpenSRA* Project. Although

each of these modes of ground deformation can have an oblique component of movement, such deformation was not evaluated. Sensitivity analyses indicated that the key aspects of soil-pipeline interaction for a seismic risk assessment are captured with the primary modes of ground deformation employed in this study. A fifth mode of ground deformation where a pipeline crosses a ground deformation zone that displaces parallel to the longitudinal pipeline axis and places the pipeline in pure tension at the landslide or lateral spread scarp and pure compression at the landslide or lateral spread toe without induced bending strains was analyzed using an analytical model presented by O'Rourke & Liu (2012).

Figure 15 summarizes the ground deformation modes assessed for the *OpenSRA* Project. The strike-slip tension (Figure 15a), strike-slip compression, (Figure 15b), normal-slip (Figure 15c), and reverse-slip (Figure 15d) modes of ground deformation were assessed using Abaqus with input parameters provided by Jung et al. (2016) and O'Rourke et al. (2014, 2016). An intermediate "bending" model for the strike-slip and normal-slip modes of ground deformation was employed to transition from ground deformation that induces tension to deformation that induces compression. Movement parallel to the pipeline axis without induced bending strains (similar to Figure 15e) was assessed using an analytical model presented in O'Rourke & Liu (2012). Two-dimensional views of abrupt soil deformation are shown in Figure 15a and Figure 15b, whereas three-dimensional views of same are shown in Figure 15c through Figure 15f.

**Figure 15: Assessed Ground Deformation Modes**



**Ground deformation modes assessed to derive pipe strain fragility models**

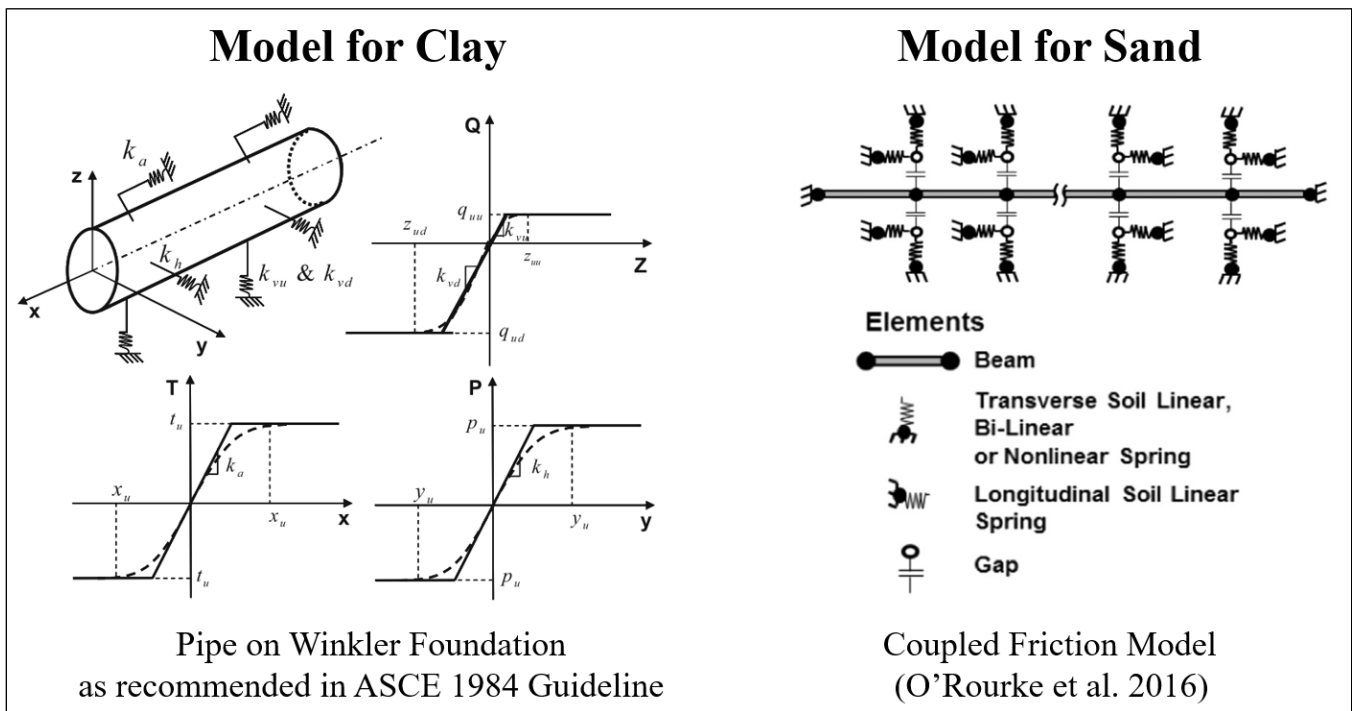
Pipelines that cross landslides or lateral spreads parallel to the direction of displacement can be reasonably modeled using the normal-slip mode at the scarp and reverse-slip mode at the toe or as the fifth case of ground deformation where no bending strains are induced. Pipelines that cross landslides or lateral spreads perpendicular or at an oblique angle can be modeled as the strike-slip tension or strike-slip compression ground deformation mode where the pipe

transitions from moving, unstable soil to stationary, stable soil. Ground settlement can be modeled as vertical normal-slip deformation.

### 3.4.2 Abaqus Model

All numerical simulations performed in this study are based on the two-dimensional (2D) beam-spring model as typically employed in engineering practice. The analyses performed in this study employed two different models for assessing the different frictional behavior of sandy and clayey soils as illustrated in Figure 16. For clayey soils, the analyses used the model recommended in the ASCE (1984) guidelines. For sandy soils, the analyses used the O'Rourke et al. (2016) and Jung et al. (2016) beam-spring model to account for the coupled normal and frictional forces on the pipe through the Coulomb frictional law. This model is used to account for the increase in frictional forces from sandy soils when the pipe experiences an increase in normal force due to relative lateral or vertical ground deformation. Enhanced frictional forces are negligible for clayey soils, where the soil undrained shear strength affects shear transfer from the soil to the pipe. These models are described in greater detail in Hutabarat et al. (2022).

**Figure 16: Abaqus Beam-Spring Models**



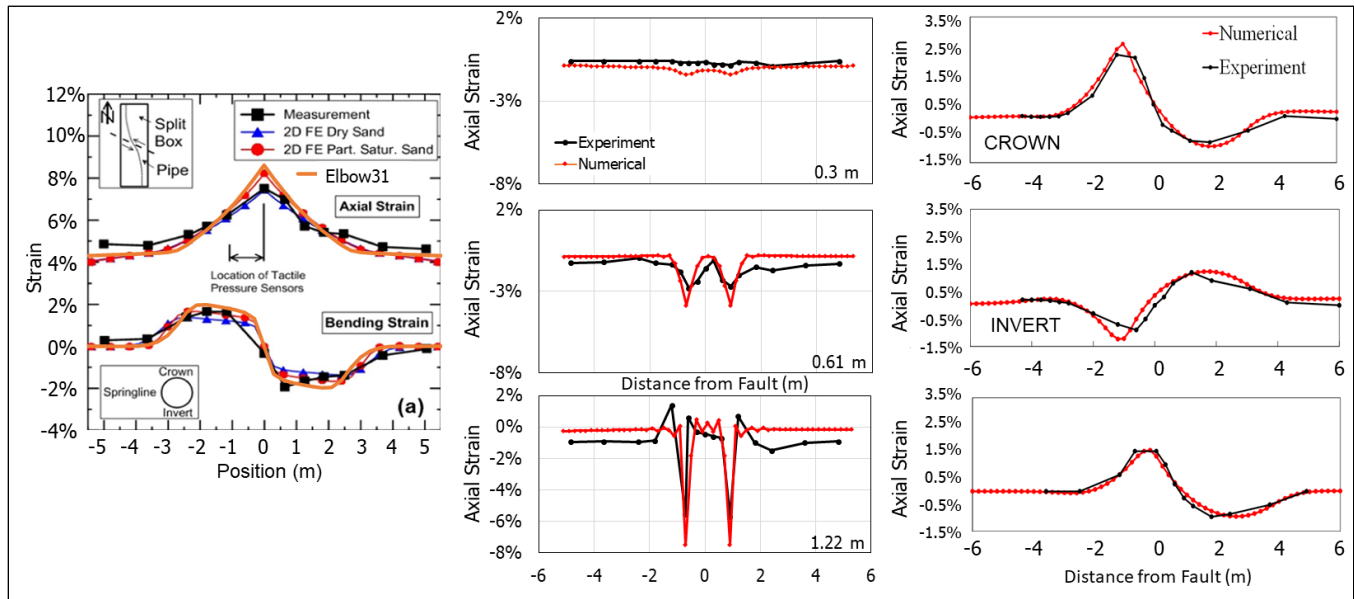
**Abaqus beam-spring models for clayey and sandy backfills**

### 3.4.3 Model Validations

The Abaqus soil-pipeline models were validated using the results of experiments performed by researchers at the Cornell University Geotechnical Lifelines Large-Scale Testing Facility (O'Rourke et al., 2008), RPI, and elsewhere. Details of the validation studies are presented in the Hutabarat et al. (2022) report. Figure 17 shows illustrative comparisons of Abaqus numerical simulation results and experimental results for strike-slip tension, strike-slip

compression, and normal-slip modes of ground deformation. The results of the Abaqus simulations were first compared with full-scale experiments performed at the Geotechnical Lifelines Large-Scale Testing Facility at Cornell University, which investigated the tensile and compressive pipeline response to strike-slip ground deformation, and with centrifuge experiments performed at RPI, which investigated the tensile pipeline response to normal-slip ground deformation. Only after favorable comparisons between numerical simulation results and experimental results were achieved, were additional analyses performed to evaluate natural gas pipeline response to strike-slip, normal-slip, and reverse-slip permanent ground deformation.

**Figure 17: Comparison of Modeled and Experimentally Measured Axial Pipe Strain**



**Abaqus Simulation Results for Strike-Slip Tension, 250 mm HDPE Pipe Cornell Box Large-Scale Testing**

**Abaqus Simulation Results for Strike-Slip Compression, 400 mm HDPE Pipe Cornell Box Large-Scale Testing**

**Abaqus Simulation Results for Normal-Slip Tension 250 mm HDPE Pipe RPI Centrifuge Testing**

### 3.4.4 Sensitivity Study

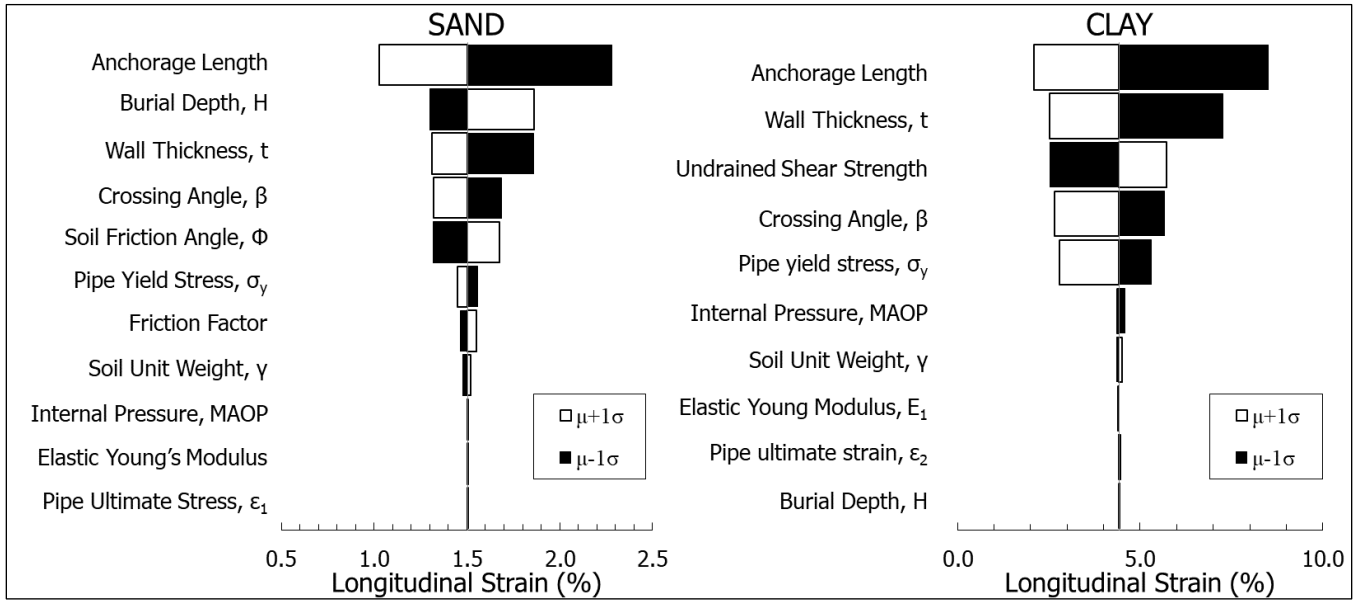
A sensitivity study was performed to identify the system parameters that most greatly affect the estimated longitudinal pipe strain for each ground deformation mode. A baseline scenario was selected which consists of a 61 cm outside diameter X-52 pipe, buried 1.3 m deep, subjected to 1.0 m of strike-slip tension permanent ground deformation with the assumption that the pipeline-ground deformation zone interaction angle was 50 degrees. Each system parameter was varied by plus- and minus-one standard deviation ( $\sigma$ ) from their respective mean ( $\mu$ ) value to assess the sensitivity of the results to reasonable variations of that parameter, as shown in Table 1. The coefficient of variation ( $CoV = \sigma/\mu$ ) of a parameter is used to characterize its uncertainty.

**Table 1: List of Parameters Used in Sensitivity Analysis**

Parameters	Sand			Clay		
	Base ( $\mu$ )	CoV	$\mu \pm \sigma$	Base ( $\mu$ )	CoV	$\mu \pm \sigma$
<b>Pipeline Properties</b>						
Outside Diameter, D (cm)	61.0	-	-	61.0	-	-
Wall Thickness, t (mm)	9.2	30%	6.4 to 12.7	9.2	30%	6.4 to 12.7
Steel Specified Minimum Yield Stress, SMYS (MPa)	358	10%	322 to 394	358	10%	322 to 294
<b>Site &amp; Soil Properties</b>						
Soil Cover, $H_c$ (m)	1.2	30%	0.9 to 1.5	1.2	30%	0.9 to 1.5
Effective Unit Weight, $\gamma$ (kN/m <sup>3</sup> )	18.5	10%	18 to 19	18.5	10%	18 to 19
Soil Friction Angle, $\Phi$ (°)	40	8%	37 to 43	N/A	N/A	N/A
Soil-Pipeline Interface Friction Factor, k	0.9	25%	0.8 to 1.0	N/A	N/A	N/A
Backfill Relative Density	Dense	-	Medium Dense to Very Dense	Firm	-	Soft to Stiff
Undrained Shear Strength, $s_u$ (kPa)	N/A	N/A	N/A	50	50%	25 to 75
<b>Fault Properties</b>						
Permanent Ground Deformation, $\Delta_f$ (m)	1.0	40%	0.6 to 1.4	1.0	40%	0.6 to 1.4
Pipeline-Ground Deformation Zone Intersection Angle	50	20%	40 to 60	45	22%	35 to 55

Figure 18 shows tornado diagrams for the described pipeline buried in sand and clay and subjected to the described strike-slip tension mode of ground deformation. Tornado diagrams show the sensitivity of the analysis to each variable. The larger the box on the diagram, the greater the sensitivity to that variable.

**Figure 18: Tornado Diagrams from Sensitivity Study**



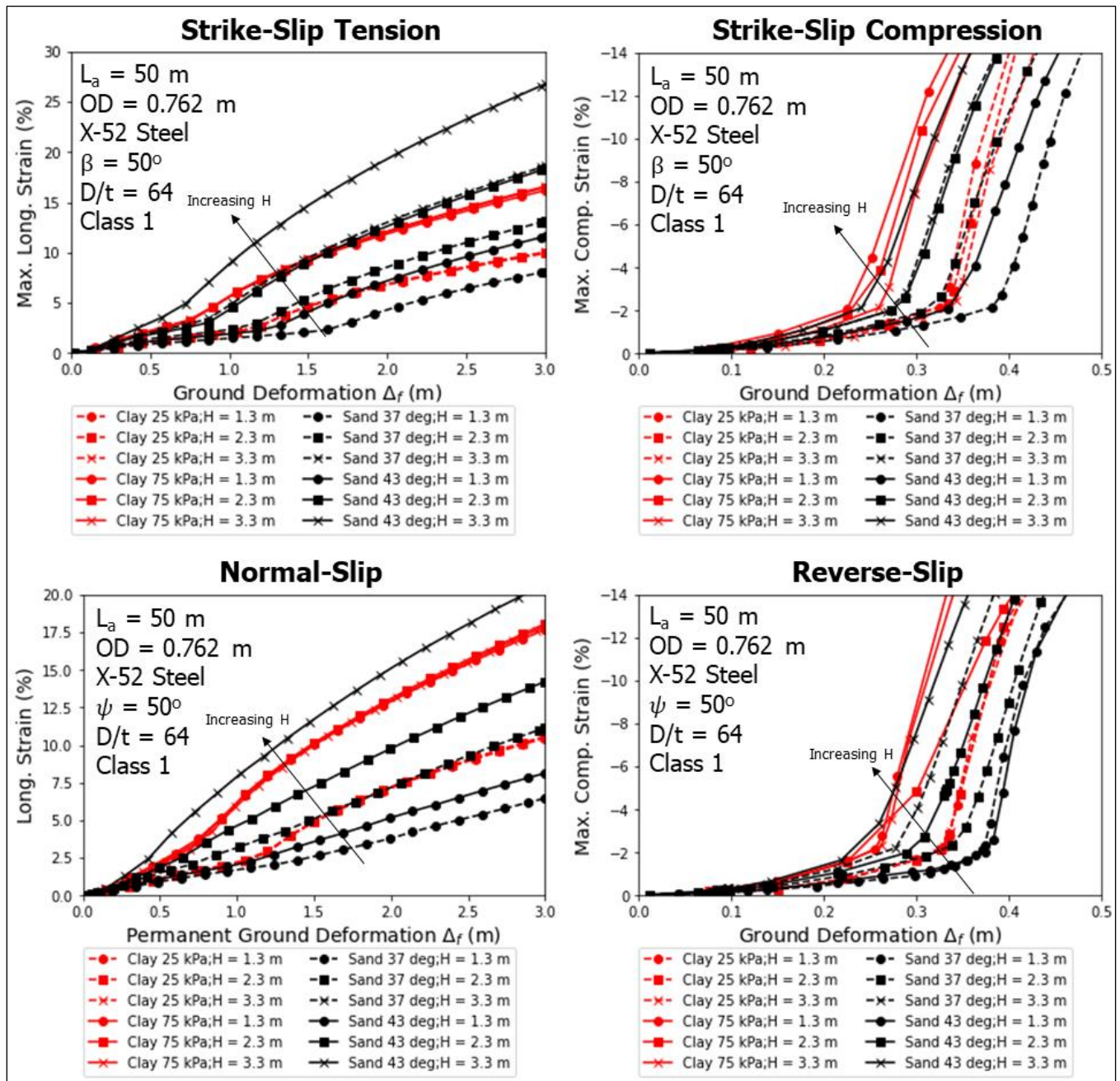
**Tornado diagrams for soil-pipeline systems subjected to strike-slip tension ground movement where the results are most sensitive to those input parameters that have the widest boxes on the diagram. Results for pipelines buried in sandy soils are shown on the left and results for pipelines buried in clayey soils are shown on the right.**

Based on the results of this study, soil-pipeline systems subjected to permanent ground deformation are typically most sensitive to the anchorage length, soil type and strength (i.e., burial depth and friction angle for pipelines buried in sand and undrained shear strength for pipelines buried in clay), pipe wall thickness, yield stress, the magnitude of permanent ground deformation, and the pipeline-ground deformation zone intersection or dip angle (which is termed the crossing angle).

### 3.4.5 Representative Simulation Results

To ensure that the Abaqus models properly represented the complex mechanics of soil-pipeline systems subjected to permanent ground deformation, a representative soil-pipeline system consisting of an X-52 steel pipe with 61 cm outside diameter, 9.5 mm wall thickness, and buried at depths ranging from 1.3 to 3.3 m was assessed for the primary ground deformation modes. Ground displacements up to 3 m were assessed. As the amount of ground displacement increases, the potential error in the pipe strain calculated in these simulations increases. The use of the O'Rourke et al. (2016) method for estimating this error is described in Hutabarat et al. (2022). The complete results of the buried natural gas pipeline system modeling are provided in Hutabarat et al. (2022). Select plots of longitudinal pipe strain versus permanent ground deformation are displayed in Figure 19.

**Figure 19: Longitudinal Pipe Strain versus Ground Deformation Simulation Results**



**Longitudinal pipe strain versus ground deformation simulation results for soil-pipeline systems subjected to strike-slip tension, strike-slip compression, normal-slip, and reverse-slip ground deformation**

The results of the simulations show that key aspects of the soil-pipeline system mechanics are captured. They include, for example, that the coupled normal and frictional forces acting on the pipeline lead to increased pipe strain, when compared with a constant transfer of shear force per distance along the pipeline.

### 3.5 Development of Relationships to Estimate Longitudinal Pipe Strain for Pipelines Subjected to Permanent Ground Deformation

Using the parameters listed in Table 2, more than one million numerical simulations of pipelines subjected to permanent ground deformation were performed. The simulation results are used to develop relationships that estimate a distribution of longitudinal pipe strain as a function of the soil-pipeline system parameters.

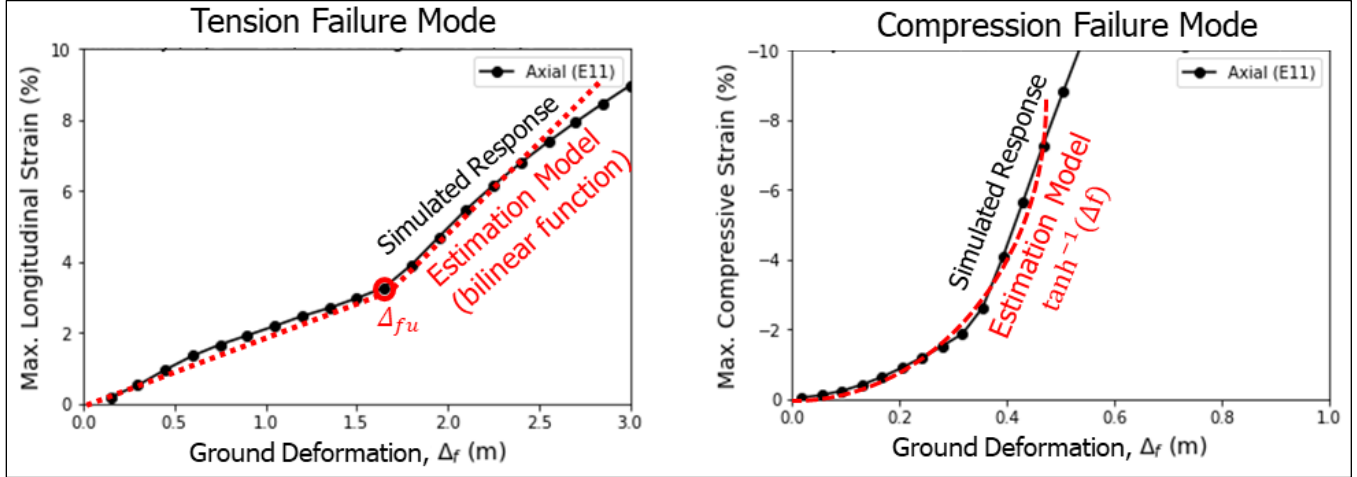
**Table 2: Range of Parameters Used in Numerical Simulations**

Parameter	Range
Outside Diameter (cm)	10.2, 20.3, 30.5, 40.6, 50.8, 61.0, 76.2, 86.4, 106.7
Wall Thickness (mm)	2 to 22 (realistically paired with pipe diameter)
Burial Depth (m)	0.3 to 4.5
Soil Friction Angle (°)	37 to 43
Undrained Shear Strength (kPa)	25 to 75
Strike-Slip Crossing Angle (°)	15, 45, 75, 90
Normal-Slip Dip Angle (°)	15, 45, 75, 90
Reverse-Slip Dip Angle (°)	15, 45, 75, 90
Pipe Material	Grade-A, Grade-B, X-42, X-52, X-60, X-70
Class Location	0, 1, 4
Sand Relative Density	Medium Dense to Very Dense
Clay Undrained Shear Strength	Soft to Stiff

The pipe strain estimation models have been developed to capture the strain response of pipelines responding to the modes of ground deformation illustrated in Figure 15. The slope of pipe strain versus the ground deformation changes significantly at up to two locations for pipeline responding to tensile ground deformation (depending on the strike-slip crossing angle) and at one location for pipelines responding to compressive ground deformation.

Figure 20 presents numerical results in terms of the longitudinal strain for representative tensile and compressive failure mode cases. Pipe strain estimation models for the strike-slip tension and strike-slip compression ground deformation modes, which are based on the Abaqus finite element analyses, and the case with ground deformation parallel to the longitudinal axis of the pipeline, which is based on the results of an analytical model, are provided in this report to illustrate the form of these models. The complete suite of pipe strain estimation models for all cases will be provided in the fragility report being prepared for this project.

**Figure 20: Modeled Pipeline Response to Tensile and Compressive Pipe Strain**



Modeled pipeline response to tensile pipe strain (strike-slip tension or normal-slip mode) and compressive pipe strain (strike-slip compression or reverse-slip mode) with examples of bi-linear and inverse hyperbolic tangent regression models used to capture the simulated responses

### 3.5.1 Pipe Strain Estimation Model for Strike-Slip Tension Ground Deformation Mode

The model to estimate pipe strain for pipes subjected to strike-slip tension ground deformation with ground deformation interaction angle,  $\beta$ , ranging from  $5^\circ$  to  $85^\circ$  (using only one break point) is presented as Equation (3.1) through Equation (3.3). Equation (3.1) estimates the ultimate soil frictional resistance along the pipeline, Equation (3.2) estimates the ground deformation at the pipe ultimate stress, and Equation (3.3) estimates the longitudinal tensile pipe strain. Equation (3.1) applies to uncoupled friction and normal forces to the pipeline.

$$t_{ult} = \begin{cases} \pi * D * H * \gamma_{soil} * 0.5 * (1 + K_0) * \tan(k\phi) & - \text{Sand} \\ \pi * D * \alpha * s_u & - \text{Clay} \end{cases} \quad (3.1)$$

where:

$t_{ult}$  is the ultimate  $K_0$  condition soil frictional resistance (kN/m);

$D$  is the outside pipe diameter (m);

$H$  is the burial depth to the pipe centerline (m);

$s_u$  is the undrained shear strength of clayey soil (kPa);

$\gamma_{soil}$  is the soil effective unit weight ( $\text{kN/m}^3$ );

$\alpha$  is the soil-pipeline adhesion factor (unitless);

$\phi$  is the friction angle of sandy soil ( $^\circ$ );

$K_0$  is the coefficient of Earth pressure at rest, estimated as  $(1 - \sin \phi)$ ;

$k = 0.9$  is the friction factor for peak cohesionless soil and rough steel pipe (unitless)

$$\ln(\Delta_u) = a_0 + a_1 \ln(\varepsilon_{ult}) + a_2 \ln(L_a) \quad (3.2)$$

where:

$\Delta_u$  is the estimated ground deformation at the pipe ultimate stress (m);

$a_0, a_1, a_2$  are model regression coefficients;

$L_a$  is the pipeline anchorage length (m);

$E$  is the Young's Modulus of steel =  $2.1 \times 10^8$  kPa;

$\sigma_y$  is the pipe steel yield stress (MPa);

$\varepsilon_{ult}$  is the estimated pipe strain at the ultimate tensile stress estimated with the Ramberg-Osgood model using  $\varepsilon_{ult} = 100 \frac{\sigma_{ult}}{E} \left[ 1 + \frac{n}{1+r} \left( \frac{\sigma_{ult}}{\sigma_y} \right)^r \right]$  (%)

Recommended default values for  $\varepsilon_{ult}$  are provided in Table 5.

**Table 3: Recommended Default  $\varepsilon_{ult}$  (%) Values Based on Steel Grade**

Steel Grade	$\sigma_y$ (MPa)	n	r	$\sigma_{ult}$ (MPa)	$\varepsilon_{ult}$ (%)
Grade-B	241	3	8	344	1.09
X-42	290	3	9	414	1.64
X-52	359	8	10	455	1.90
X-60	414	8	12	517	2.43
X-70	483	14	15	565	2.77
X-80	552	15	20	625	2.85

In Equation (3.2):

$$a_1 = c_3 \ln(L_a) + c_{41} F_{t_{ult}} + c_{42} (1 - F_{t_{ult}}) + c_{51} F_{D/t} \left( \frac{D}{t} - 100 \right) + c_{52} - (1 - F_{D/t})$$

where:

$a_0, a_2, c_3, c_{41}, c_{42}, c_{51}, c_{52}$  are model regression coefficient given in Table 4;

$t$  is the pipe wall thickness (m);

$\beta$  is the pipe – ground deformation interaction angle (°);

$$F_{t_{ult}} = \begin{cases} 1; & t_{ult} < 70 \text{ kN/m} \\ 0; & \text{otherwise} \end{cases}, \quad F_{D/t} = \begin{cases} 1; & \text{for } D/t < 100 \\ 0; & \text{otherwise} \end{cases}$$

**Table 4: Model Regression Coefficients to Estimate  $\Delta_u$**

Coefficient	$5^\circ < \beta \leq 45^\circ$	$45^\circ < \beta \leq 85^\circ$
$a_0$	$-0.05402 * (\beta - 45^\circ) - 1.82829$	$0.00735 * (\beta - 75^\circ) - 1.60779$
$a_2$	$0.01347 * (\beta - 45^\circ) + 0.37664$	$0.00484 * (\beta - 75^\circ) + 0.52187$
$c_3$	$-0.00301 * (\beta - 45^\circ) - 0.01591$	$-0.02185 * (\beta - 75^\circ) - 0.67156$
$c_{41}$	$0.02182 * (\beta - 45^\circ) + 0.49488$	$0.05619 * (\beta - 75^\circ) + 2.18087$
$c_{42}$	$0.02436 * (\beta - 45^\circ) + 0.47831$	$0.06430 * (\beta - 75^\circ) + 2.40733$
$c_{51}$	$-0.00001 * (\beta - 45^\circ) - 0.00165$	$-0.00153$
$c_{52}$	$0.00228 * (\beta - 45^\circ) + 0.10021$	$0.00144 * (\beta - 75^\circ) + 0.14358$

$$\ln(\varepsilon_{long}) = b_0 + b_1 \ln\left(\frac{\Delta_f}{\Delta_u}\right) + b_2 \ln\left(\frac{D}{t}\right) + F_{soil} b_3 \ln t_{ult} \pm \sigma_{\ln \varepsilon} \quad (3.3)$$

where:

$\varepsilon_{long}$  is the estimated pipe longitudinal (tensile) strain (%);

$b_0, b_1, b_2, b_3$  are model regression coefficients given in Table 5;

$\Delta_f$  is the input permanent ground deformation (m);

$\sigma_{\ln \varepsilon}$  is the model standard deviation (natural log units);

$\beta_u = 0.3$  is the estimated model epistemic uncertainty;

$$F_{\Delta_f} = \begin{cases} 1, & \text{for } \Delta_f < \Delta_u \\ 0, & \text{otherwise} \end{cases}, \quad F_{L_a} = \begin{cases} 1, & \text{for } L_a < 50 \\ 0, & \text{otherwise} \end{cases}, \quad F_{soil} = \begin{cases} 1, & \text{Sand} \\ 0, & \text{Clay} \end{cases}$$

$$b_1 = \left[ F_{\Delta_f} \left( d_2 + d_3 t_{ult} + d_{41} F_{L_a} (L_a - 50) + d_{42} (1 - F_{L_a}) + d_5 \left( \frac{D}{t} \right) \right) \right] + \left[ (1 - F_{\Delta_f}) (d_6 + d_{71} F_{L_a} (L_a - 50) + d_{72} (1 - F_{L_a}) + d_8 (\ln \varepsilon_{ult})) \right]$$

**Table 5: Model Regression Coefficients to Estimate  $\varepsilon_{long}$**

Coefficient	$5^\circ < \beta \leq 45^\circ$	$45^\circ < \beta \leq 85^\circ$
$b_0$	$-0.02174 * (\beta - 45^\circ) + 0.16235$	$-0.02787 * (\beta - 75^\circ) - 0.67388$
$b_2$	$0.00203 * (\beta - 45^\circ) + 0.24407$	$0.00361 * (\beta - 75^\circ) + 0.35249$
$b_3$	$-0.02801 * (\beta - 45^\circ) + 1.64437$	$0.00794 * (\beta - 75^\circ) + 1.88270$
$d_2$	$-0.00010 * (\beta - 45^\circ) - 0.00387$	$-0.00002 * (\beta - 75^\circ) - 0.00456$
$d_3$	$-0.00114 * (\beta - 45^\circ) + 0.00514$	$0.00057 * (\beta - 75^\circ) + 0.02215$
$d_{41}$	$0.01436 * (\beta - 45^\circ) - 0.12124$	$-0.00844 * (\beta - 75^\circ) - 0.37439$
$d_{42}$	$0.00002 * (\beta - 45^\circ) + 0.0092$	$0.00002 * (\beta - 75^\circ) + 0.00156$
$d_5$	$0.01326 * (\beta - 45^\circ) + 0.97745$	$-0.00799 * (\beta - 75^\circ) + 0.73788$
$d_6$	$0.00061 * (\beta - 45^\circ) + 0.00602$	$-0.00081 * (\beta - 75^\circ) - 0.01826$
$d_{71}$	$-0.00728 * (\beta - 45^\circ) - 0.06927$	$0.00522 * (\beta - 75^\circ) + 0.08748$
$d_{72}$	$0.01480 * (\beta - 45^\circ) + 0.46008$	$-0.00924 * (\beta - 75^\circ) + 0.18293$
$d_8$	$0.00272 * (\beta - 45^\circ) + 0.11565$	$0.00122 * (\beta - 75^\circ) + 0.15234$
$\sigma_{\ln \varepsilon}$	$0.00302 * (\beta - 45^\circ) + 0.53947$	$0.00428 * (\beta - 75^\circ) + 0.66796$

### 3.5.2 Pipe Strain Estimation Model for Strike-Slip Compression Ground Deformation Mode

The model to estimate pipe strain for pipes subjected to strike-slip compression ground deformation with ground deformation interaction angle,  $\beta$ , ranging from  $95^\circ$  to  $175^\circ$  is presented as Equation (3.4).

$$\ln(\varepsilon_{comp}) = \frac{\tanh^{-1}\left(\frac{\ln \Delta_f - b_0}{b_1}\right)}{b_2} - 4 \pm \sigma_{\ln \varepsilon} \quad (3.4)$$

where:

$\varepsilon_{comp}$  is the pipe longitudinal compressive strain (%);

$\Delta_f$  is the input ground deformation (m);

$\sigma_{ln \varepsilon}$  is the standard deviation of the model (natural log units);

$b_0 = -6.50785 + 0.98692 D + 0.01601 L_a + (-0.04575 F_\beta)$  ;

$b_1 = 4.54097 - 0.01093 L_a$ ;

$b_2 = 0.34262 + (-0.10918 OD) + 0.00197 L_a + 0.0027 F_\beta$ ;

$$F_\beta = \begin{cases} 0, & \text{for } 120 < \beta < 175. \\ 0 - 120, & \text{for } 95 < \beta < 120' \end{cases}$$

$\sigma_{ln \varepsilon} = 0.571$ ;

$\beta_u = 0.3$  is the estimated model epistemic uncertainty

### 3.5.3 Pipe Strain Estimation Model for Permanent Ground Deformation Parallel to Axis of Pipeline

Models were also developed to estimate pipe strain for the case of permanent ground deformation parallel to the pipe where no bending strains are induced. Further explanation of this mode of ground deformation and of the fragility model development can be found in Bain et al. (2022b) and Hutabarat et al. (2022). For the case of pipelines buried in sand, Equation (3.5) is used to estimate an intermediate parameter called the embedment length,  $L_e$ , and for the case of pipelines buried in clay, Equation (3.6) is used to estimate the embedment length.

$$\ln(L_e) = 0.188 + 0.853 * \ln(t) - 0.018 * \ln(D) + 0.751 * \ln(\sigma_y) - 0.862 * \ln(H) - 0.863 * \ln(\gamma_t) - 1.005 * \ln(\Phi') - \ln(\delta) + 0.136 * \ln(PGD) + \varepsilon\sigma \quad (3.5)$$

$$\ln(L_e) = -4.019 + 0.876 * \ln(t) + 0.787 * \ln(\sigma_y) - 0.886 * \ln(s_u) - 0.889 * \ln(\alpha) + 0.114 * \ln(PGD) + \varepsilon\sigma \quad (3.6)$$

where:

$L_e$  is an intermediate parameter to estimate the pipe strain termed the embedment length;

$t$  is the pipe wall thickness;

$D$  is the pipe diameter;

$\sigma_y$  is the pipe steel yield stress;

$H$  is the soil cover to the pipe centerline;

$\gamma_t$  is the soil total unit weight;

$\Phi'$  is the sand friction angle;

$\delta$  is the sand-pipeline interface friction angle ratio (sand-pipeline interface friction angle divided by sand friction angle);

$s_u$  is the undrained shear strength of clay;

$\alpha$  is the clay-pipeline adhesion factor;

$\varepsilon$  is the number of standard deviations from the mean;

$\sigma$  is the model standard deviation

From regression, Equation (3.5) and Equation (3.6) have small uncertainty with  $\beta_r=0.06$  and  $\beta_r=0.03$ , respectively. After evaluating Equation (3.5) or Equation (3.6) to estimate the value of  $L_e$ , longitudinal pipe strain is calculated using Equation (3.7).

$$\varepsilon_p = \frac{\beta_p * L^*}{E} * \left[ 1 + \frac{n}{1+r} * \left( \frac{\beta_p * L^*}{\sigma_y} \right)^r \right] \quad (3.7)$$

where:

$$L^* = \min \left\{ \begin{array}{l} L_e \\ L/2 \end{array} \right.$$

$$\beta_p = t_u / A$$

$$\left\{ \begin{array}{ll} t_u = \gamma * \left( H_c + \frac{D}{2} \right) * \tan(\Phi' * \delta) * \pi * D & - \text{Sand} \\ t_u = \alpha * S_u * \pi * D & - \text{Clay} \end{array} \right.$$

where:

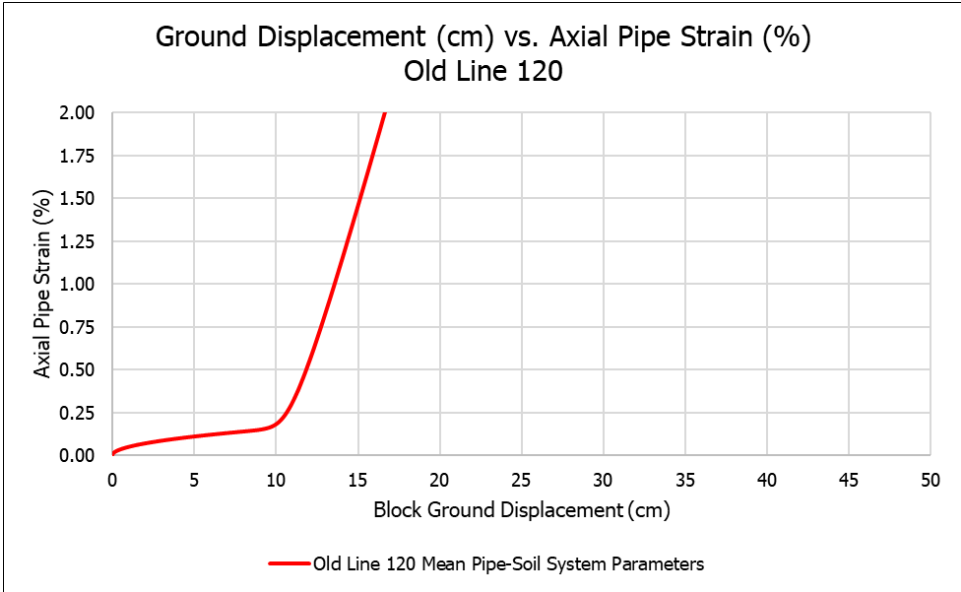
$\beta_p$  is termed the pipe burial parameter;

$E$  is the Young's Modulus of the pipe steel;

$n$  and  $r$  are Ramberg-Osgood parameters.

Epistemic uncertainty for Equation (3.7) is estimated as  $\beta_u=0.3$ . An example calculation for Old Line 120 at the Balboa Boulevard demonstration site (which is described in detail in Bain et al., 2022b) is shown in Figure 21. Old Line 120 was constructed in 1930 out of Grade B steel with an early shielded electric arc welding technique. It was buried in low-plasticity clay (mean  $s_u \approx 48$  kPa), the outside diameter is 56 cm, the wall thickness is approximately 7.1 mm, the assumed adhesion factor is 0.7, the estimated mean yield stress is 308,000 kPa, and the Ramberg-Osgood  $n$  and  $r$  parameters are estimated to be 8 and 50, respectively. The length of the ground deformation zone,  $L$ , is approximately 280 m.

**Figure 21: Example Calculation for Old Line 120 at the Balboa Boulevard Demonstration Site**



**Example calculation for Old Line 120 at the Balboa Boulevard demonstration site**

# CHAPTER 4:

## Conclusions

---

### 4.1 Summary

This report summarizes the procedures implemented in the *OpenSRA* software for assessing the effects of earthquake-induced ground movements on buried natural gas pipelines. The ground movements are produced by surface fault rupture, liquefaction-induced lateral spreading and ground settlement, and seismic slope displacement. In support of this effort, existing and new models are employed to estimate the ground deformation resulting from liquefaction-induced lateral spreading and settlement and from earthquake-induced landslides. Fragility models are then utilized to estimate the longitudinal strain developed in the buried pipelines as a function of the imposed earthquake-induced ground deformation. These models are required in *OpenSRA* to assess the seismic vulnerability of buried natural gas pipelines in the state of California.

To address the requirement by the CEC to assess natural gas systems at the statewide, regional, and site-specific scales, three levels of available data and analytical methods were employed. The resolution of the data and the uncertainty of the estimate of ground deformation possible at each of these scales vary. These levels, therefore, enable regulators and owners to evaluate the seismic risk to the natural gas pipeline system according to the available data.

Level 1 analyses utilize data that are geospatially continuous at a uniform resolution over the entire state of California. As a result, these data are at low resolution, so the uncertainty of the estimates made at Level 1 are very high. Level 2 analyses utilize data produced at regional scales collected at higher resolution than Level 1 data. These analyses may be informed by subsurface data or estimated engineering properties, so the uncertainty of the Level 2 estimates is reduced relative to Level 1 estimates, but Level 2 analyses are still considered to have high uncertainty. Level 3 analyses utilize site-specific data such as Cone Penetration Test data or 1:24,000 scale or larger geologic maps to evaluate geohazards or the response of natural gas infrastructure to ground shaking or ground deformation. Level 3 data enable assessment with medium uncertainty. Level 4 analyses utilize high-quality geotechnical laboratory test data to support the performance of advanced numerical analyses of project-specific components and systems. Level 4 analyses are beyond the current scope of the *OpenSRA* Project. The data and methods available at each of the first three levels are described in Appendix A. When appropriate, limitations and reservations with some of the procedures and the evaluation of uncertainty are discussed.

The results of this study establish procedures and data to be incorporated in the *OpenSRA* software to assess liquefaction and seismic slope stability hazards at statewide, regional, and site-specific scales in California (i.e., levels 1 - 3). A new procedure is developed for probabilistically assessing lateral spread displacement at the regional scale to fill a gap that

existed at Level 2. Methods and models to estimate permanent ground deformation due to liquefaction or earthquake-induced landslides with characterization of the uncertainty of the estimate enable more robust seismic risk assessments of natural gas pipelines to be performed.

This study employed the calibrated numerical models of soil-pipeline systems and the resulting buried pipe strain response to four generic modes of permanent ground deformation: strike-slip tension, strike-slip compression, normal-slip, and reverse-slip to form the basis for developing fragility models to assess buried pipeline performance. Fragility models for these modes of ground deformation that estimate longitudinal pipe strain can be derived from the results of the more than one million soil-pipeline numerical analyses using the finite element software Abaqus. Additionally, an existing analytical procedure was employed to develop a fragility model to assess pipe strain for ground deformation oriented parallel to the longitudinal axis of the pipeline. The developed relationships capture the mechanics of soil-pipeline systems undergoing permanent ground deformation. The models can be used to estimate longitudinal pipe strain for buried natural gas pipelines subjected to fault rupture, liquefaction-induced ground deformation, and earthquake-induced landslide displacement.

## **4.2 Implementation into *OpenSRA***

The purpose of the research presented in this report is to develop models and procedures for implementation into *OpenSRA* to estimate the demands to buried natural gas pipelines from ground deformation hazards. The models and procedures are then used to produce results that can be used in support of the development of fragility functions that assess the performance of buried pipeline systems undergoing permanent ground deformation. Post-earthquake reconnaissance surveys show that the primary cause of damage to buried natural gas pipeline systems is from seismically induced permanent ground deformation. The response of those systems to permanent ground deformation varies significantly with the amount and mode of ground deformation, the properties and geometry of the pipelines, and the properties of the soil adjacent to the buried pipeline.

The ground deformation models presented in this paper and implemented in *OpenSRA* estimate the probability and distribution of potential permanent ground deformations at statewide to site-specific scales. The pipeline fragility models estimate the maximum longitudinal strain induced in the buried pipeline as a function of key variables. The magnitude of the maximum longitudinal pipe strain is a primary indicator of the probability of leakage or rupture for pipelines subjected to permanent ground deformations. Hence, models estimating longitudinal pipe strain are required to support the development of the fragility functions in *OpenSRA* to characterize seismic risk due to geo-hazards.

### 4.3 Recommendations for Future Research

Sensitivity studies performed with the ground deformation hazard models and soil-pipeline interaction models required in *OpenSRA* identified several future research needs to advance the capabilities and reliability of *OpenSRA*. Firstly, liquefaction and liquefaction-induced displacement hazard assessments at regional to site-specific scales are highly sensitive to the depth to groundwater. Lowering or raising the groundwater table can “turn off” or “turn on” liquefaction triggering. Estimating the depth to groundwater with currently available data and methods is difficult, especially at regional scales, and therefore, the uncertainty of the depth of groundwater produces significant uncertainty in the estimation of liquefaction effects on natural gas infrastructure. However, as outlined in the Task E report of this study (Wang et al. 2022), techniques for measuring the depth to groundwater, including Distributed Acoustic Sensing (DAS), could be employed to reduce the uncertainty in the estimate of groundwater depth. Collecting these data would reduce the uncertainty in liquefaction hazard assessments. As there can be significant temporal variations in the groundwater level, additional measurements over several years would further reduce uncertainty and enhance the estimates of risk generated by *OpenSRA*.

Regional scale liquefaction and landslide deformation models that represent better the spatial heterogeneity of ground deformation observed after major earthquakes are required to reduce the tendency of regional scale models to overestimate the pervasiveness of permanent ground deformation. These enhancements would enable more robust, mean-centered, less uncertain, estimates of ground deformations and their resulting effects on buried natural gas pipelines for scenario earthquake assessments.

Additional physical testing of the stress-strain-strength response of steel pipelines and the response of natural gas infrastructure to imposed permanent ground deformation would improve soil-pipeline models and pipeline fragility models. There is little published data detailing the stress-strain response of grades A, B, C, and D steels as well as the X-grade steels used in the State’s natural gas transmission and distribution pipelines. Reducing the uncertainty in the yield stress and post-yield behavior of these pipe steels would be of great benefit. There are few studies that assess the response of buried pipelines to normal-slip and reverse-slip ground movements. It would be advantageous to perform additional large-scale lab and centrifuge tests of underground pipeline response to normal-slip and especially reverse-slip ground displacement.

Furthermore, this study did not evaluate the pipe strain response to oblique ground deformation modes. While key aspects of the pipe strain response can be captured by evaluating the strike-slip tension, strike-slip compression, normal-slip, and reverse-slip ground deformation modes, future numerical modeling efforts should incorporate oblique components of movement.

## GLOSSARY AND LIST OF ACRONYMS

<b>A</b>	Cross-Sectional Area of Pipe
<b>Abaqus</b>	Finite Element Software
<b>afem</b>	Artificial Fill over Bay Mud Deposits
<b>ALA</b>	American Lifelines Alliance
<b>Anchorage Length</b>	Distance to location where pipeline is fixed in location such as a significant bend ( $L_a$ )
<b>ASCE</b>	American Society of Civil Engineers
<b>CDF</b>	Cumulative Distribution Function
<b>CEC</b>	California Energy Commission
<b>CGS</b>	California Geological Survey
<b>CoSMoS</b>	Coastal Storm Modeling System
<b>CoV</b>	Coefficient of Variation
<b>CPT</b>	Cone Penetrometer Test
<b>CRR</b>	Cyclic Resistance Ratio
<b>CSR</b>	Cyclic Stress Ratio
<b>CTI</b>	Compound Topographic Index
<b>D</b>	Pipe Outside Diameter
<b><math>d_c</math></b>	Nearest Distance to the Coast (km)
<b><math>d_r</math></b>	Nearest Distance to a River (km)
<b><math>d_w</math></b>	Nearest Distance to Either a River or the Coast (km)
<b>E</b>	Young's Modulus

<b>FS<sub>L</sub></b>	Factor of Safety Against Liquefaction Triggering
<b>GMM</b>	Ground Motion Model
<b>GWT</b>	Depth to Groundwater
<b>H</b>	Burial Depth of Midpoint of Pipeline Diameter from Ground Surface
<b>Hazus</b>	Natural Hazard Risk Assessment Tool Distributed by the Federal Emergency Management Agency
<b>KJf</b>	Franciscan Complex rocks, Including Mélange, Sandstone, Shale, Chert, and Greenstone
<b>Kss</b>	Cretaceous Sandstone of the Great Valley Sequence in the Central Coast Ranges
<b>k<sub>y</sub></b>	Yield Coefficient
<b>LBNL</b>	Lawrence Berkeley National Laboratory
<b>LCI</b>	Lettis Consultants International
<b>LDI</b>	Lateral Displacement Index
<b>L<sub>e</sub></b>	Pipeline Embedment Length in Sliding Block
<b>MAOP</b>	Maximum Allowable Operating Pressure
<b>MHHW</b>	Mean Higher High Water
<b>MODFLOW</b>	Modular Finite-Difference Flow Model Software Distributed by the United States Geological Survey
<b>MSF</b>	Magnitude Scaling Factor
<b>M<sub>w</sub></b>	Moment Magnitude
<b>n</b>	Ramberg-Osgood <i>n</i> Parameter
<b>NCEER</b>	National Center for Earthquake Engineering Research
<b>NHERI</b>	Natural Hazards Engineering Research Infrastructure
<b><i>OpenSRA</i></b>	Open Seismic Risk Assessment Tool

<b>PAGER</b>	USGS Prompt Assessment of Global Earthquakes for Response
<b>PEER</b>	Pacific Earthquake Engineering Research Center
<b>PGA</b>	Peak Ground Acceleration (g)
<b>PGD</b>	Permanent Ground Deformation
<b>PGV</b>	Peak Ground Velocity (g)
<b>PG&amp;E</b>	Pacific Gas and Electric Company
<b>PRCI</b>	Pipeline Research Council International
<b>precip</b>	Average Annual Precipitation (mm)
<b>Qal</b>	Quaternary (Holocene) Alluvium
<b>Qhly</b>	Latest Holocene Alluvial Fan Levee Deposits
<b>Qi</b>	Intertidal Mud, Including Mud Around the San Francisco Bay and Similar Mud Around the Sacramento/San Joaquin Delta and Humboldt Bay (Quaternary)
<b>Qoa</b>	Quaternary (Pleistocene) alluvium
<b>Qs</b>	Quaternary (Pleistocene) Sand Deposits, such as the Merritt Sand in the Oakland Area
<b>QT</b>	Quaternary to Tertiary (Pleistocene to Pliocene) Alluvial Deposits, such as the Saugus Formation of Southern California, the Paso Robles Formation of the Central Coast Ranges, and the Santa Clara Formation of the San Francisco Bay Area
<b>r</b>	Ramberg-Osgood r Parameter
<b>RPI</b>	Rensselaer Polytechnic Institute
<b>SoCalGas</b>	Southern California Gas Company
<b>sp</b>	Serpentinite
<b>SPT</b>	Standard Penetration Test

<b><math>s_u</math></b>	Clay Undrained Shear Strength
<b>SYMS</b>	Specified Minimum Yield Stress
<b>t</b>	Pipe Wall Thickness
<b>Tsh</b>	Tertiary Shale and Siltstone Units, such as the Repetto, Fernando, Puente, and Modelo Formations of the Los Angeles Area
<b>Tss</b>	Tertiary Shale and Siltstone Units, such as the Topanga Formation in the Los Angeles Area and the Butano Formation in the San Francisco Area
<b><math>t_{ult}</math></b>	Shear Force per Unit Length of Pipeline
<b>Tv</b>	Tertiary Volcanic Units Including the Conejo Volcanics in the Santa Monica Mountains and the Leona Rhyolite in the East Bay Hills
<b>UC</b>	University of California
<b>USGS</b>	United States Geological Survey
<b><math>V_{s30}</math></b>	Time-averaged shear wave velocity in the upper 30-meters of the subsurface (m/s)
<b>wtd</b>	Depth to Groundwater (m)
<b><math>\beta</math></b>	Pipeline-Ground Deformation Zone Interaction Angle (i.e., Crossing Angle)
<b><math>\beta_p</math></b>	Pipe Burial Parameter Defined as Shear Force per Unit Length of Pipeline Divided by the Cross-Section Area of the Pipe
<b><math>\beta_r</math></b>	Aleatory Variability
<b><math>\beta_u</math></b>	Epistemic Uncertainty
<b><math>\epsilon</math></b>	Longitudinal Pipe Strain
<b><math>\gamma</math></b>	Soil Total Unit Weight
<b><math>\gamma_{max}</math></b>	Maximum Potential Shear Strain
<b><math>\sigma_{ult}</math></b>	Pipe Ultimate Stress
<b><math>\sigma_y</math></b>	Pipe Yield Stress
<b><math>\sigma</math></b>	Standard Deviation

$\mu$	Mean
$\Phi'$	Sand Friction Angle
<b>2D</b>	Two-Dimensional

## REFERENCES

- Abrahamson, N. (2022). Personal Communication.
- ALA (2001). Guidelines for the Design of Buried Steel Pipe. American Lifelines Alliance. Retrieved March 16, 2022, from <https://www.americanlifelinesalliance.com/pdf/Update061305.pdf>
- ASCE (1984). Guidelines for the Seismic Design of Oil and Gas Pipeline Systems. Committee on Gas and Liquid Fuel Lifelines, American Society of Civil Engineers.
- Bain, Chris, Hutabarat, Daniel, Bray, Jonathan, Abrahamson, Norman, O'Rourke, Thomas, Lindvall, Scott. (2022a). *Performance-Based Earthquake Engineering Assessment Tool for Natural Gas Storage and Pipeline Systems, Task B - Enhanced Liquefaction and Ground Deformation*. Pacific Earthquake Engineering Research (PEER) Center Report, in preparation.
- Bain, Chris, O'Rourke, Thomas, Bray, Jonathan, Lindvall, Scott, Hutabarat, Daniel. (2022b). *Performance-Based Earthquake Engineering Assessment Tool for Natural Gas Storage and Pipeline Systems, Validation Report*. Pacific Earthquake Engineering Research (PEER) Center Report, in preparation.
- Bedrossian, T.L., Roffers, P., Hayhurst, C.A., Lancaster, J.T. & Short, W.R. (2012) Geologic Compilation of Quaternary Surficial Deposits in Southern California (Special Report 217). Department of Conservation, California Geological Survey, Sacramento
- Boulanger, R. W., & Idriss, I. M. (2016). CPT-Based Liquefaction Triggering Procedure. *Journal of Geotechnical and Geoenvironmental Engineering*, 142(2), 04015065. [https://doi.org/10.1061/\(asce\)gt.1943-5606.0001388](https://doi.org/10.1061/(asce)gt.1943-5606.0001388)
- Bray, J.D., & Macedo, J. (2019). Procedure for Estimating Shear-Induced Seismic Slope Displacement for Shallow Crustal Earthquakes. *J. of Geotechnical and Geoenvironmental Engineering*, ASCE, V. 145(12), doi: 10.1061/(ASCE)GT.1943-5606.0002143
- Cetin, K. O., Bilge, H. T., Wu, J., Kammerer, A. M., & Seed, R. B. (2009). Probabilistic Model for the Assessment of Cyclically Induced Reconsolidation (Volumetric) Settlements. *Journal of Geotechnical and Geoenvironmental Engineering*, 135(3), 387–398. [https://doi.org/10.1061/\(asce\)1090-0241\(2009\)135:3\(387\)](https://doi.org/10.1061/(asce)1090-0241(2009)135:3(387))
- Cetin, K. O., Seed, R. B., Kayen, R. E., Moss, R. E. S., Bilge, H. T., Ilgac, M., & Chowdhury, K. (2018). SPT-Based Probabilistic and Deterministic Assessment of Seismic Soil Liquefaction Triggering Hazard. *Soil Dynamics and Earthquake Engineering*, 115, 698–709. <https://doi.org/10.1016/j.soildyn.2018.09.012>
- CGS (2010). Geologic Map of California. California Geological Survey, Retrieved June 1, 2020, from <https://maps.conservation.ca.gov/cgs/gmc/>
- Cornell, C.A. (1968), Engineering Seismic Risk Analysis, *Bulletin of the Seismological Society of America*, V58(5), 1583-1606, doi: 10.1785/BSSA0580051583

- Deep Seated Landslide Susceptibility (CGS Map Sheet 58). (n.d.). Retrieved April 2, 2022, from <https://gis.data.ca.gov/maps/3cdc744bec6b45c28206e472e8ad0f89/explore>
- ESRI (2019). USA Detailed Streams. Retrieved June 15, 2020, from <https://www.arcgis.com/home/item.html?id=1e29e33360c8441bbb018663273a046e>
- FEMA (2020). Hazus 4.2 SP3 Technical Manual. Federal Emergency Management Agency. [https://www.fema.gov/sites/default/files/2020-10/fema\\_hazus\\_earthquake\\_technical\\_manual\\_4-2.pdf](https://www.fema.gov/sites/default/files/2020-10/fema_hazus_earthquake_technical_manual_4-2.pdf)
- Grant, A., Wartman, J., & Abou-Jaoude, G. (2016). Multimodal Method for Coseismic Landslide Hazard Assessment. *Engineering Geology*, 212, 146–160. doi: 10.1016/j.enggeo.2016.08.005
- Harris, L. A., Suer, H. S., Skene, W. T., & Benjamin, R. J. (1957). The Stability of Thin-Walled Unstiffened Circular Cylinders Under Axial Compression Including the Effects of Internal Pressure. *Journal of the Aeronautical Sciences*, 24(8), 587–596. <https://doi.org/10.2514/8.3911>
- Holzer, T. L., Noce, T. E., & Bennett, M. J. (2011). Liquefaction Probability Curves for Surficial Geologic Deposits. *Environmental and Engineering Geoscience*, 17(1), 1–21. <https://doi.org/10.2113/gseegeosci.17.1.1>
- Honegger, D. G., & Nyman, D. J. (2004). Guidelines for the Seismic Design and Assessment of Natural Gas and Liquid Hydrocarbon Pipelines. Pipelines Research Council International
- Hutabarat, D., O'Rourke, T.D., Bray, J.D., Bain, C., Lindvall, S. (2022). *Performance-Based Earthquake Engineering Assessment Tool for Natural Gas Storage and Pipeline Systems, Task B - Underground Pipeline Fragilities*. Pacific Earthquake Engineering Research (PEER) Center Report, in preparation.
- Idriss, I.M., & Boulanger, R.W. (2008). Soil Liquefaction During Earthquakes. EERI Publication, Monograph MNO-12, Earthquake Engineering Research Institute, Oakland. <https://www.eeri.org/>
- Jamiolkowski, M., Lo Presti, D.C.F., & Manassero, M. (2001). Evaluation of Relative Density and Shear Strength of Sands from Cone Penetration Test (CPT) and Flat Dilatometer Test (DMT). ASCE Geotechnical Special Publication No. 119: 201–238
- Jefferies, M., & Been, K. (2006). Soil liquefaction: A Critical State Approach. Taylor and Francis.
- Jibson, R. W. (2007). Regression Models for Estimating Coseismic Landslide Displacement. *Engineering Geology*, 91(2-4), 209-218. doi:10.1016/j.enggeo.2007.01.013
- Jung, J. K., O'Rourke, T. D., & Argyrou, C. (2016). Multi-Directional Force–Displacement Response of Underground Pipe in Sand. *Canadian Geotechnical Journal*, 53(11), 1763–1781. <https://doi.org/10.1139/cgj-2016-0059>

- Ku, C.-S., Juang, C. H., Chang, C.-W., & Ching, J. (2012). Probabilistic Version of the Robertson and Wride Method for Liquefaction Evaluation: Development and Application. *Canadian Geotechnical Journal*, 49(1), 27–44. doi: 10.1139/t11-085
- Kulhawy, F. H., & Mayne, P. W. (1990). *Manual on Estimating Soil Properties for Foundation Design*. Cornell University. Prepared for Electric Power Research Institute.
- Macedo, J., Bray, J., Abrahamson, N., & Travararou, T. (2018). Performance-Based Probabilistic Seismic Slope Displacement Procedure. *Earthquake Spectra*, 34(2), 673–695. doi: 10.1193/122516eqs251m
- McCrink, T., & Frost, E. (2021). Personal Communication.
- Mohr, W. (2003). *Strain-Based Design of Pipelines*. Edison Welding Institute. Retrieved March 16, 2022, from <https://www.bsee.gov/sites/bsee.gov/files/tap-technical-assessment-program/434aa.pdf>
- Moss, R. E., Seed, R. B., Kayen, R. E., Stewart, J. P., Kiureghian, A. D., & Cetin, K. O. (2006). CPT-Based Probabilistic and Deterministic Assessment of In Situ Seismic Soil Liquefaction Potential. *Journal of Geotechnical and Geoenvironmental Engineering*, 132(8), 1032–1051. doi: 10.1061/(asce)1090-0241(2006)132:8(1032)
- Newmark, N. M. (1965). Effects of Earthquakes on Dams and Embankments. *Géotechnique*, 15(2), 139-160. doi:10.1680/geot.1965.15.2.139
- Newmark N. M., (1967). Problems in Wave Propagation in Soil and Rock. *Proceedings on International Symposium on Wave Propagation and Dynamic Properties of Earth Materials*, University of New Mexico, Albuquerque, pp. 7-26
- O'Rourke, M. J., & Hmadi, E. (1988). Analysis of Continuous Buried Pipelines for Seismic Wave Effects. *International Journal of Earthquake Engineering and Structural Dynamics*, Vol. 16, 917-929
- O'Rourke, M. J., & Liu, J. X. (2012). *Seismic Design of Buried and Offshore Pipelines*. Monograph MCEER-12-MN04, Multidisciplinary Center for Earthquake Engineering Research, Buffalo, NY
- O'Rourke, T. D., Jeon, S.-S., Toprak, S., Cubrinovski, M., & Jung, J. K. (2012). Underground Lifeline System Performance During the Canterbury Earthquake Sequence, in *Proceedings, 15th World Conference in Earthquake Engineering*, Lisbon, Portugal.
- O'Rourke, T.D., Jezerski, N.A., Olson, T., Bonneau, A.L., Palmer, M.C., Stewart, H.E., O'Rourke, M.J. & Abdoun, T. (2008). *Geotechnics of Pipeline System Response to Earthquakes*. Keynote Paper, *Proceedings, Geotechnical Earthquake Engineering and Soil Dynamics IV (GEESD)* Sacramento, CA, May
- O'Rourke, T. D., Jeon, S.-S., Toprak, S., Cubrinovski, M., Hughes, M., van Ballegooy, S., & Bouziou, D. (2014). Earthquake Response of Underground Pipeline Networks in Christchurch, NZ. *Earthquake Spectra*, 30(1), 183–204. <https://doi.org/10.1193/030413eqs062m>

- O'Rourke, T. D., Jung, J. K., & Argyrou, C. (2016). Underground Pipeline Response to Earthquake-Induced Ground Deformation. *Soil Dynamics and Earthquake Engineering*, 91, 272–283. <https://doi.org/10.1016/j.soildyn.2016.09.008>
- Robertson, P. (2009). Performance Based Earthquake Design Using the CPT. *Performance-Based Design in Earthquake Geotechnical Engineering*. <https://doi.org/10.1201/noe0415556149.ch1>
- Robertson, P. K., & Cabal, K. L. (2015). *Guide to Cone Penetration Testing for Geotechnical Engineering* (6<sup>th</sup> ed.). Gregg Drilling & Testing Inc.
- Robertson, P. K., & Campanella, R. G. (1983a). Interpretation of Cone Penetration Tests. Part I: Sand. *Canadian Geotechnical Journal*, 20(4), 718–733. <https://doi.org/10.1139/t83-078>
- Robertson, P. K., & Campanella, R. G. (1983b). Interpretation of Cone Penetration Tests. Part II: Clay. *Canadian Geotechnical Journal*, 20(4), 734–745. <https://doi.org/10.1139/t83-079>
- Robertson, P. K., & Wride, C. E. (1998). Evaluating Cyclic Liquefaction Potential using the Cone Penetration Test. *Canadian Geotechnical Journal*, 35(3), 442–459. doi: 10.1139/t98-017
- Seed, H. B., & Idriss, I. M. (1971). Simplified Procedure for Evaluating Soil Liquefaction Potential. *Journal of the Soil Mechanics and Foundations Division*, 97(9), 1249–1273. <https://doi.org/10.1061/jsfeaq.0001662>
- Shinozuka, M., & Koike, T. (1979). Estimation of Structural Strains in Underground Lifeline Pipes. PVP-34, ASME
- USGS (2021). Coastal Storm Modeling System (CoSMoS). U.S. Geological Survey. Retrieved October 1, 2021, from <https://www.usgs.gov/centers/pcmssc/science/cosmos-groundwater#overview>
- USGS (n.d.). Ground Failure Scientific Background. U.S. Geological Survey. Retrieved June 1, 2020, from <https://earthquake.usgs.gov/data/ground-failure/background.php>
- USGS (n.d.). Map of CPT Data: All Regions. U.S. Geological Survey. Retrieved June 1, 2020, from <https://earthquake.usgs.gov/research/cpt/data/>
- USGS (n.d.). PAGER Scientific Background. U.S. Geological Survey. Retrieved June 1, 2020, from <https://earthquake.usgs.gov/data/pager/background.php>
- USGS (2018). The HayWired Earthquake Scenario – Earthquake Hazards. U.S. Geological Survey. Retrieved June 1, 2020, from [https://pubs.usgs.gov/sir/2017/5013/sir20175013ah\\_v1.2.pdf](https://pubs.usgs.gov/sir/2017/5013/sir20175013ah_v1.2.pdf)
- Wijewickreme, D., Honegger, D., Mitchell, A., & Fitzell, T. (2005). Seismic Vulnerability Assessment and Retrofit of a Major Natural Gas Pipeline System: A Case History. *Earthquake Spectra*, 21(2), 539–567. <https://doi.org/10.1193/1.1898273>

- Wang, Chien-Chih; Peter Hubbard; Tianchen Xu; Kenichi Soga. (2022). *Performance-Based Earthquake Engineering Assessment Tool for Natural Gas Storage and Pipeline Systems, Task 4E Final Report – Sensor and Monitoring Technologies*. California Energy Commission. Publication Number: CEC-500-202X-XXX.
- Wills, C. J., Gutierrez, C. I., Perez, F. G., & Branum, D. M. (2015). A Next Generation VS30 Map for California Based on Geology and Topography. *Bulletin of the Seismological Society of America*, 105(6), 3083-3091. doi:10.1785/0120150105
- Witter, R.C., Knudsen, K.L, Sowers, J.M., Wentworth, C.M., Koehler, R.D., Randolph, C. E., Brooks, S.K., & Gans, K.D. (2006). Maps of Quaternary Deposits and Liquefaction Susceptibility in the Central San Francisco Bay Region, California: U.S. Geological Survey Open-File Report 06-1037 (<http://pubs.usgs.gov/of/2006/1037/>)
- Youd, T. L., Hansen, C. M., & Bartlett, S. F. (2002). Revised Multilinear Regression Equations for Prediction of Lateral Spread Displacement. *Journal of Geotechnical and Geoenvironmental Engineering*, 128(12), 1007-1017. doi:10.1061/(asce)1090-0241(2002)128:12(1007)
- Youd, T. L., Idriss, I. M., Andrus, R. D., Arango, I., Castro, G., Christian, J. T., Dobry, R., Finn, W. D., Harder, L. F., Hynes, M. E., Ishihara, K., Koester, J. P., Liao, S. S., Marcuson, W. F., Martin, G. R., Mitchell, J. K., Moriwaki, Y., Power, M. S., Robertson, P. K., ... Stokoe, K. H. (2001). Liquefaction Resistance of Soils: Summary Report from the 1996 NCEER and 1998 NCEER/NSF Workshops on Evaluation of Liquefaction Resistance of Soils. *Journal of Geotechnical and Geoenvironmental Engineering*, 127(10), 817–833. [https://doi.org/10.1061/\(asce\)1090-0241\(2001\)127:10\(817\)](https://doi.org/10.1061/(asce)1090-0241(2001)127:10(817))
- Youd, T. L., & Perkins, D. M. (1978). Mapping Liquefaction-Induced Ground Failure Potential. *Journal of the Geotechnical Engineering Division*, 104(4), 433–446
- Zhang, G., Robertson, P. K., & Brachman, R. W. I. (2002). Estimating Liquefaction-Induced Ground Settlements from CPT for Level Ground. *Canadian Geotechnical Journal*, 39(5), 1168–1180. <https://doi.org/10.1139/t02-047>
- Zhang, G., Robertson, P. K., & Brachman, R. W. I. (2004). Estimating Liquefaction-Induced Lateral Displacements Using the Standard Penetration Test or Cone Penetration Test. *Journal of Geotechnical and Geoenvironmental Engineering*, 130(8), 861–871. doi: 10.1061/(asce)1090-0241(2004)130:8(861)
- Zhu, J., Baise, L. G., & Thompson, E. M. (2017). An Updated Geospatial Liquefaction Model for Global Application. *Bulletin of the Seismological Society of America*, 107(3), 1365–1385. doi: 10.1785/0120160198
- Zhu, J., Daley, D., Baise, L. G., Thompson, E. M., Wald, D. J., Knudsen, K. L. (2015). A geospatial liquefaction model for rapid response and loss estimation. *Earthquake Spectra*, 31(3), 1813–1837. <https://doi.org/10.1193/121912eqs353m>

# Appendix A:

## *OpenSRA* Data Matrix

---

	<b>Level 1</b>	<b>Level 2</b>	<b>Level 3</b>	<b>Level 4</b>
<b>Description</b>	Level 1 analyses utilize data that are geospatially continuous at a uniform resolution over the entire state of California. With its lower level of resolution and without site-specific or subsurface data, the state-wide data lead to very high uncertainty.	Level 2 analyses utilize data produced at regional scales collected at higher resolution than level 1 data. Level 2 data are not necessarily geospatially continuous over the entire state of California. There is minimal, generic subsurface data or estimated engineering properties. Use of level 2 data leads to high uncertainty, but less uncertainty than with level 1 data.	Level 3 analyses utilize site-specific geologic and topographic mapping and includes subsurface data through CPTs, borings with SPT, and soil/rock index tests. Subsurface data can be used in performance-based liquefaction, lateral spreading, slope displacement, and settlement procedures. Level 3 data enable assessment with medium uncertainty.	Level 4 analyses utilize high-quality laboratory test data with the Level 3 site-specific geologic, topographic, and geotechnical data. Use of Level 4 data enable the performance of advanced numerical analyses. Level 4 analyses will have the least uncertainty in estimating the effects of earthquake-induced ground deformation on buried pipes. Due to the high level of data required they will not be employed commonly.
<b>Topographic Data</b>	Statewide 10 m DEM.	Regional 1 m DEM.	Site-specific high-resolution topography from SfM or lidar.	Site-specific high-resolution topography from SfM or lidar.
<b>Geologic Data</b>	Statewide geologic maps generally produced at scales of 1:250,000 or smaller or regulatory maps: <b>A)</b> Wills et al. (2015) 1:250,000 to 1:24,000 statewide compilation of geologic maps. Population centers of the San Francisco Bay area and Los Angeles basin covered by the larger scale mapping. <b>B)</b> Digital Geologic Map of CA (CGS 2010) at 1:750,000. <b>C)</b> CGS Deep-Seated Landslide Susceptibility Map, GIS based.	Geologic maps produced at scales of 1:100,000 to 1:24,000: <b>A)</b> Bedrossian et al. (2012) 1:100,000 GIS based map of Quaternary geologic units in Southern California. <b>B)</b> Yerkes & Campbell (2005) 1:100,000 maps, some digital, incomplete coverage. <b>C)</b> Dibblee maps at 1:24,000, incomplete coverage. <b>D)</b> CGS Regional Geologic Maps at 1:100,000 and 1:24,000, incomplete coverage, some maps preliminary.	<b>A)</b> Detailed geologic maps produced at scales of 1:24,000 or larger. <b>B)</b> Level 2 maps at 1:24,000 scale, when available.	Detailed geologic maps produced at scales of 1:24,000 or larger.
<b>Geotechnical Data</b>	Not available. May use modeled $V_{S30}$ and similar geotechnical data.	Limited subsurface data available (e.g., CGS borehole database). May use estimated soil or rock mass properties (e.g., CGS Seismic Hazard Reports).	CPTs or borings with SPTs. Soil index test data (e.g., Atterberg limits or grain-size distributions).	CPTs or borings utilizing SPTs. Extensive, high-quality, site-specific laboratory test data (e.g., TX, CSS tests).
<b>Groundwater Data</b>	No measurements available. May use statewide depth to groundwater model.	Limited data such as historic high-water table depths, regional maps of depth to groundwater, or regional groundwater models.	Groundwater depth measurements.	Groundwater depth measurements.
<b>Output</b>	Probabilistic analysis of ground failure hazard and effects to infrastructure with very high uncertainty.	Probabilistic analysis of ground failure hazard and effects to infrastructure with less uncertainty than at Level 1, but still high uncertainty.	Probabilistic analysis of ground failure hazard and effects to infrastructure with medium uncertainty.	Probabilistic analysis of ground failure hazard and effects to infrastructure with less uncertainty than at Level 3.

**Liquefaction Triggering**

<p style="text-align: center;"><b>Preferred Liquefaction Triggering Procedures and Model Inputs &amp; Outputs</b></p>	<p><b>A)</b> Zhu et al. (2017) coastal (&lt;20 km to coast and within coastal basin) and non-coastal models  <u>Inputs:</u> PGV, modeled <math>V_{s30}</math>, precip, <math>d_c</math>, <math>d_r</math>, <math>d_w</math>, modeled GWT  <u>Outputs:</u> <math>P_L</math></p>	<p><b>A)</b> Youd &amp; Perkins (1978) and Witter et al. (2006) geologic based assessments used with HAZUS methodology to estimate probability of liquefaction triggering  <u>Inputs:</u> Surficial Quaternary geologic maps, PGA, <math>M_w</math>, GWT  <u>Outputs:</u> Liquefaction susceptibility converted to <math>P_L</math>  <b>B)</b> Proposed Bain &amp; Bray (2022) probabilistic lateral spread displacement procedure  <u>Inputs:</u> Surficial Quaternary geologic maps, PGA, <math>M_w</math>, GWT  <u>Outputs:</u> Probabilistic assessment of liquefaction triggering and lateral spread displacement</p>	<p><b>A)</b> Boulanger &amp; Idriss (2016) probabilistic liquefaction triggering procedure  <u>Inputs:</u> CPT, PGA, <math>M_w</math>, GWT  <u>Outputs:</u> <math>P_L</math>  <b>B)</b> Probabilistic modification to Robertson &amp; Wride (1998) procedure as updated by Robertson (2009) from Ku et. al. (2012)  <u>Inputs:</u> CPT, PGA, <math>M_w</math>, GWT  <u>Outputs:</u> <math>P_L</math>  <b>C)</b> Moss et al. (2006) probabilistic liquefaction triggering procedure  <u>Inputs:</u> CPT, PGA, <math>M_w</math>, GWT  <u>Outputs:</u> <math>P_L</math></p>	<p>Level 3 methods and:  <b>A)</b> FLAC analyses with PM4Sand and PM4Silt  <b>B)</b> FLAC analyses with UBCSAND  <b>C)</b> PLAXIS analyses with PM4Sand  <b>D)</b> OpenSees analyses with multiple soil models</p>
<p style="text-align: center;"><b>Alternative Liquefaction Triggering Procedures and Model Inputs &amp; Outputs</b></p>	<p>No Alternatives Available or Considered</p>	<p><b>AA)</b> CA Earthquake Zones of Required Investigation Maps  <u>Inputs:</u> 1:24,000 scale map  <u>Outputs:</u> Delineates areas where liquefaction may occur converted to broad categories of effects</p>	<p><b>AA)</b> Kramer &amp; Mayfield (2007) PBEE  <u>Inputs:</u> Cetin et al. (2004) model coefficients, boring with <math>(N_1)_{60,cs}</math>, FC, <math>r_d</math>, PSHA  <u>Outputs:</u> <math>FS_L</math>, <math>N_{req}</math> hazard curves  <b>BB)</b> Franke et al. (2014) PBEE  <u>Inputs:</u> <math>r_d</math>, MSF, <math>K_\sigma</math> per Idriss &amp; Boulanger (2008), boring with <math>(N_1)_{60,cs}</math>, PSHA  <u>Outputs:</u> <math>FS_L</math>, <math>N_{req}</math> hazard curves</p>	<p>No Alternatives Available or Considered</p>

**Lateral Spreading**

<p style="text-align: center;"><b>Preferred Lateral Spreading Procedures and Model Inputs &amp; Outputs</b></p>	<p><b>A)</b> Zhu et al. (2017) coastal (&lt;20 km to coast and within coastal basin) and non-coastal models combined with Hazus methodology to estimate lateral spread displacement  <u>Inputs:</u> PGV, modeled <math>V_{s30}</math>, precip, <math>d_c</math>, <math>d_r</math>, <math>d_w</math>, modeled GWT  <u>Outputs:</u> Liquefaction susceptibility class converted to settlement estimate</p>	<p><b>A)</b> Youd &amp; Perkins (1978) and Witter et al. (2006) geologic based assessments used with HAZUS methodology to estimate lateral spread displacement  <u>Inputs:</u> Surficial Quaternary geologic maps, PGA, <math>M_w</math>, GWT  <u>Outputs:</u> Liquefaction susceptibility converted to lateral spread displacement  <b>B)</b> Proposed Bain &amp; Bray (2022) probabilistic lateral spread displacement procedure  <u>Inputs:</u> Surficial Quaternary geologic maps, PGA, <math>M_w</math>, GWT  <u>Outputs:</u> Probabilistic assessment of liquefaction triggering and lateral spread displacement</p>	<p><b>A)</b> Zhang et al. (2004)  <u>Inputs:</u> CPT, PGA, <math>M_w</math>, GWT, topographic slope or free-face ratio  <u>Outputs:</u> Estimate of lateral spread displacement  <b>AA)</b> Idriss &amp; Boulanger (2008) procedure for calculating maximum and limiting shear strains combined with Zhang et al. (2004) or Faris et al. (2006) procedure  <u>Inputs:</u> CPT or boring  <u>Outputs:</u> Estimate of lateral spreading displacement  <b>B)</b> Youd et al. (2002)  <u>Inputs:</u> Boring with <math>(N_1)_{60}</math>, <math>W</math>, <math>S</math>, <math>T_{15}</math>, <math>F_{15}</math>, <math>D50_{15}</math>  <u>Outputs:</u> Estimate of lateral spread displacement  <b>C)</b> Faris et al. (2006)  <u>Inputs:</u> CPT, PGA, <math>M_w</math>, GWT, topographic slope or free-face ratio  <u>Outputs:</u> Estimate of lateral spread displacement</p>	<p>Level 3 methods and:  <b>A)</b> FLAC analyses with PM4Sand and PM4Silt  <b>B)</b> FLAC analyses with UBCSAND  <b>C)</b> PLAXIS analyses with PM4Sand  <b>D)</b> OpenSees analyses with multiple soil models</p>
<p style="text-align: center;"><b>Alternative Lateral Spreading Procedures and Model Inputs &amp; Outputs</b></p>	<p>No Alternatives Available or Considered</p>	<p><b>AA)</b> CA Earthquake Zones of Required Investigation Maps  <u>Inputs:</u> 1:24,000 scale map  <u>Outputs:</u> Delineates areas where liquefaction and hence, lateral spreading, may occur if slightly sloping ground or adjacent to a free-face</p>	<p><b>AA)</b> Franke &amp; Kramer (2014) PBEE  <u>Inputs:</u> Youd et al. (2002) model coefficients, boring with <math>(N_1)_{60}</math>, <math>W</math>, <math>S</math>, <math>T_{15}</math>, <math>F_{15}</math>, <math>D50_{15}</math>, PSHA  <u>Outputs:</u> <math>D_H</math> hazard curve  <b>BB)</b> Coutu (2017) incorporation of Zhang et al. (2004) into PBEE  <u>Inputs:</u> CPT, PSHA  <u>Outputs:</u> Lateral spread displacement hazard curves</p>	<p>No Alternatives Available or Considered</p>

**Liquefaction-Induced Settlement**

<p align="center"><b>Preferred Liquefaction-Induced Settlement Procedures and Model Inputs &amp; Outputs</b></p>	<p><b>A)</b> Zhu et al. (2017) coastal (&lt;20 km to coast and within coastal basin) and non-coastal models combined with Hazus methodology to estimate liquefaction-induced settlement  <u>Inputs:</u> PGV, modeled <math>V_{S30}</math>, precip, <math>d_c</math>, <math>d_r</math>, <math>d_w</math>, modeled GWT  <u>Outputs:</u> Liquefaction Susceptibility Class Converted to Settlement Estimate</p>	<p><b>A)</b> Zhu et al. (2017) coastal (&lt;20 km to coast and within coastal basin) and non-coastal models combined with Hazus methodology to estimate liquefaction-induced settlement  <u>Inputs:</u> PGV, modeled <math>V_{S30}</math>, precip, <math>d_c</math>, <math>d_r</math>, <math>d_w</math>, GWT  <u>Outputs:</u> Liquefaction Susceptibility Class Converted to Settlement Estimate  <b>B)</b> Youd &amp; Perkins (1978) and Witter et al. (2006) geologic based assessments combined with Hazus methodology to estimate liquefaction-induced settlement  <u>Inputs:</u> Surficial Quaternary geologic maps, GWT  <u>Outputs:</u> Estimate of liquefaction-induced settlement according to liquefaction susceptibility category</p>	<p><b>A)</b> Cetin et al. (2009)  <u>Inputs:</u> Boring with SPT, PGA, <math>M_w</math>, GWT  <u>Outputs:</u> Estimate of free-field, level-ground settlement  <b>B)</b> Ishihara and Yoshimine (1992)  <u>Inputs:</u> Boring with SPT, PGA, <math>M_w</math>, GWT  <u>Outputs:</u> Estimate of free-field, level-ground settlement  <b>C)</b> Zhang et al. (2002)  <u>Inputs:</u> CPT, PGA, <math>M_w</math>, GWT  <u>Outputs:</u> Estimate of free-field, level-ground settlement</p>	<p>Level 3 methods and:  <b>A)</b> FLAC analyses with PM4Sand and PM4Silt  <b>B)</b> FLAC analyses with UBCSAND  <b>C)</b> PLAXIS analyses with PM4Sand  <b>D)</b> OpenSees analyses with multiple soil models</p>
<p align="center"><b>Alternative Liquefaction-Induced Settlement Procedures and Model Inputs &amp; Outputs</b></p>	<p>No Alternatives Available or Considered</p>	<p><b>AA)</b> CA Earthquake Zones of Required Investigation Maps  <u>Inputs:</u> 1:24,000 scale map  <u>Outputs:</u> Delineates areas where liquefaction and hence, liquefaction-induced settlement may occur</p>	<p><b>AA)</b> Peterson (2016) PBEE based on Cetin et al. (2009)  <u>Inputs:</u> Boring with <math>(N_1)_{60,cs}</math>, <math>N_{req}^{Cetin}</math>, <math>M_w</math>, <math>K_{md}</math>, <math>K_{Mw}</math>, <math>K_{\sigma}</math>, <math>D_R</math>, PSHA  <u>Outputs:</u> <math>\epsilon_v</math>, settlement hazard curves  <b>BB)</b> Peterson (2016) PBEE based on Ishihara and Yoshimine (1992)  <u>Inputs:</u> Boring with <math>(N_1)_{60,cs}</math> per Idriss and Boulanger (2008), <math>N_{req}^{B\&amp;I}</math>, <math>D_R</math>, PSHA  <u>Outputs:</u> <math>\epsilon_v</math>, settlement hazard curves  <b>CC)</b> Hatch (2017) PBEE based on probabilistic adaption of Ishihara &amp; Yoshimine (1992) from Juang et al. (2013)  <u>Inputs:</u> CPT, PGA, <math>M_w</math>, GWT  <u>Outputs:</u> Post-liquefaction free-field settlement hazard curves</p>	<p>No Alternatives Available or Considered</p>

**Seismic Slope Stability**

<p><b>Preferred Slope Stability/ Displacement Procedures and Model Inputs &amp; Outputs</b></p>	<p><b>A)</b> Infinite slope analysis using strength distributions developed from CGS database for generalized geologic units  <u>Inputs:</u> Statewide Geologic Map  <u>Outputs:</u> Estimate of Seismic Slope Displacement</p>	<p><b>A)</b> Grant et al. (2016) multimodal method for coseismic landslide hazard assessment  <u>Inputs:</u> DEM, <math>\phi</math>, <math>\gamma</math>, <math>c</math>, <math>c_r</math>, <math>S</math>, <math>h</math>, <math>H</math>, <math>\alpha</math>, <math>k_y</math>, <math>M_w</math>, <math>PGA</math>, <math>T_{PGA}</math>  <u>Outputs:</u> Model predicts the type of slope movement (rock-slope failures, disrupted soil slides, coherent rotational slides, and lateral spreads) and estimates seismic slope displacement distribution  <b>B)</b> Modified Bray &amp; Macedo (2019) &amp; Macedo et al. (2018) using <math>k_y</math> from Grant et al. (2016)  <u>Inputs:</u> <math>k_y</math>, <math>T_s</math> from slide depth estimate, <math>Sa(1.3T_s)</math>, <math>M_w</math>  <u>Outputs:</u> Seismic Slope Displacement Distribution</p>	<p><b>A)</b> Bray &amp; Macedo (2019)  <u>Inputs:</u> <math>k_y</math>, <math>T_s</math>, <math>Sa(1.3T_s)</math>, <math>M_w</math>, <math>PGV</math>  <u>Outputs:</u> Seismic Slope Displacement Distribution  <b>B)</b> Rathje &amp; Antonakos (2011)  <u>Inputs:</u> <math>k_y</math>, <math>PGA</math>, <math>T_s</math>, <math>T_m</math>, <math>PGV</math>  <u>Outputs:</u> Seismic Slope Displacement Distribution  <b>C)</b> Jibson (2007)  <u>Inputs:</u> <math>k_y</math>, <math>PGA</math>, <math>M_w</math>  <u>Outputs:</u> Seismic Slope Displacement Distribution  <b>D)</b> Macedo et al. (2018) PBEE  <u>Inputs:</u> <math>k_y</math>, <math>T_s</math>, <math>Sa(1.5T_s)</math>, <math>M_w</math>  <u>Outputs:</u> Seismic Slope Displacement Distribution  <b>E)</b> Block theory analyses  <u>Inputs:</u> Strike and dip measurements, rock mass properties, slope/block geometry  <u>Outputs:</u> FS rock slope failures converted to displacement estimate</p>	<p>Level 3 methods and:  <b>A)</b> FLAC analyses  <b>B)</b> PLAXIS analyses  <b>C)</b> OpenSees analyses</p>
<p><b>Alternative Slope Stability/ Displacement Procedures and Model Inputs &amp; Outputs</b></p>	<p><b>AA)</b> CGS Deep-Seated Landslide Susceptibility Map  <u>Inputs:</u> Statewide map  <u>Outputs:</u> Indicates the relative likelihood of deep-seated landsliding</p>	<p><b>AA)</b> Hazus methodology based on Wilson &amp; Keefer (1985)  <u>Inputs:</u> Surficial Quaternary geologic maps, <math>d_{wt}</math>, <math>M_w</math>, <math>\alpha_{is}</math>, slope angle  <u>Outputs:</u> Estimate of landslide displacement  <b>BB)</b> CA Earthquake Zones of Required Investigation Maps  <u>Inputs:</u> 1:24,000 scale map  <u>Outputs:</u> Delineates areas where earthquake-induced landsliding may occur  <b>CC)</b> CGS landslide inventory map  <u>Inputs:</u> GIS based inventory map  <u>Outputs:</u> Spatial extent, type, and age of known or suspected landslides</p>	<p>No Alternatives Available or Considered</p>	<p>No Alternatives Available or Considered</p>

**Transient Ground Strains**

<p style="text-align: center;"><b>Preferred Transient Ground Strain Procedures and Model Inputs &amp; Outputs</b></p>	<p><b>A) Newmark (1967)</b>  <u>Inputs:</u> PGV, modeled <math>V_s</math>, estimated <math>\gamma_{sr}</math>, modeled <math>C_R</math>  <u>Outputs:</u> <math>\epsilon_g</math>, which is assumed to be equal to <math>\epsilon_p</math> (no soil-pipe interface slippage)</p>	<p><b>A) Newmark (1967)</b>  <u>Inputs:</u> PGV, modeled <math>V_s</math>, estimated <math>\gamma_{sr}</math>, modeled <math>C_R</math>  <u>Outputs:</u> <math>\epsilon_g</math>, which is assumed to be equal to <math>\epsilon_p</math> (no soil-pipe interface slippage)  <b>B) Shinozuka &amp; Koike (1979)</b>  <u>Inputs:</u> A, E, <math>K_g</math>, <math>t</math>, modeled G, <math>\lambda</math>, estimated <math>t_u</math>, D, q, <math>\epsilon_g</math> from Newmark's Approach  <u>Outputs:</u> <math>\epsilon_p</math></p>	<p><b>A) Newmark (1967)</b>  <u>Inputs:</u> PGV, <math>V_s</math>, <math>\gamma_{sr}</math>, <math>C_R</math>  <u>Outputs:</u> <math>\epsilon_g</math>, which is assumed to be equal to <math>\epsilon_p</math> (no soil-pipe interface slippage)  <b>B) Shinozuka &amp; Koike (1979)</b>  <u>Inputs:</u> A, E, <math>K_g</math>, <math>t</math>, G, <math>\lambda</math>, <math>t_u</math>, D, q, <math>\epsilon_g</math> from Newmark's Approach  <u>Outputs:</u> <math>\epsilon_p</math>  <b>C) O'Rourke and El Hmadi (1988)</b>  <u>Inputs:</u> A, E, <math>K_g</math>, <math>t_u</math>, <math>U_g</math>, <math>U_{pr}</math>, <math>L_s</math>, H, D  <u>Outputs:</u> <math>\epsilon_g</math>, <math>\epsilon_p</math></p>	<p>Level 3 methods and:  <b>A) FLAC analyses</b>  <b>B) PLAXIS analyses</b>  <b>C) OpenSees analyses</b></p>
<p style="text-align: center;"><b>Alternative Transient Ground Strain Procedures and Model Inputs &amp; Outputs</b></p>	<p>No Alternatives Available or Considered</p>	<p>No Alternatives Available or Considered</p>	<p>No Alternatives Available or Considered</p>	<p>No Alternatives Available or Considered</p>

**Underground Pipeline Performance**

<p><b>Preferred Pipeline Performance Model Inputs &amp; Outputs</b></p>	<p><b>A)</b> O'Rourke (2020) response to transient ground strain  <u>Inputs:</u> Geomean PGV &amp; pipe type  <u>Outputs:</u> RR</p>	<p><b>A)</b> O'Rourke (2020) response to transient ground strain  <u>Inputs:</u> Geomean PGV &amp; pipe type  <u>Outputs:</u> RR  <b>B)</b> O'Rourke (2020) response to permanent ground deformation  <u>Inputs:</u> Ground deformation &amp; pipe type  <u>Outputs:</u> RR</p>	<p><b>A)</b> Soil-pipeline spring model  <u>Inputs:</u> Soil deformation magnitude and pattern, soil spring stiffness (Kg), and pipe material (D, t, E, and joints)  <u>Outputs:</u> <math>\epsilon_p</math></p>	<p><b>A)</b> FLAC SSI analyses  <b>B)</b> PLAXIS SSI analyses  <b>C)</b> OpenSees SSI analyses</p>
<p><b>Alternative Preferred Pipeline Performance Model Inputs &amp; Outputs</b></p>	<p>No Alternatives Available or Considered</p>	<p>No Alternatives Available or Considered</p>	<p>No Alternatives Available or Considered</p>	<p>No Alternatives Available or Considered</p>

## Abbreviations:

PGV	Peak ground velocity
$V_{S30}$	Time-averaged shear-wave velocity in upper 30 meters of subsurface
precip	Precipitation
$d_c$	Distance to nearest coast for use in Zhu et al. (2017)
$d_r$	Distance to nearest river for use in Zhu et al. (2017)
$d_w$	Distance to nearest water body for use in Zhu et al. (2017)
$P_L$	Probability of liquefaction triggering
GWT	Depth of the water table
FC	Fines content
PSHA	Probabilistic seismic hazard analysis
$FS_L$	Factor of safety against liquefaction triggering
$N_{req}$	Corrected SPT blow counts required to resist liquefaction triggering
MSF	Magnitude scaling factor. Procedure for computing MSF varies for different authors.
$K_\sigma$	Overburden correction factor
CPT	Cone penetration test
PGA	Peak ground acceleration
$M_w$	Moment magnitude
$\bar{V}_{s,12}$	Average shear wave velocity in upper 12 meters of subsurface profile
$P_{LAT}$	Probability of lateral spreading
DEM	Digital elevation model
$\phi$	Friction angle of soil or rock
$\gamma$	Unit weight of soil or rock
$c$	Cohesion of soil or rock
$c_r$	Root cohesion for Grant et al. (2016)
$S$	Ground slope angle
$h$	Vertical height of failure mass for Grant et al. (2016)
$H$	Local relief for Grant et al. (2016)
$\alpha$	Critical angle of slope for Grant et al. (2016)
$k_y$	Yield acceleration
$T_{PGA}$	PGA thresholds for liquefaction triggering used in Youd and Perkins (1978) and Witter et al. (2006) procedures
$W$	Free-face ratio
$T_{15}$	Cumulative thickness (in upper 20 meters) of all saturated soil layers susceptible to liquefaction initiation with $(N_1)_{60} > 15$ blows per 0.3 meters
$F_{15}$	Average fines content of the soil comprising $T_{15}$
$D50_{15}$	Average mean grain size comprising $T_{15}$
$D_H$	Lateral spread displacement
$T_s$	Natural period of sliding mass
$Sa(1.3T_s)$	Spectral acceleration at 1.3 times $T_s$
$T_m$	Mean period of earthquake motion
$Sa(1.5T_s)$	Spectral acceleration at 1.5 times $T_s$
$P_{LS}$	Probability of liquefaction-induced settlement
$K_{md}$	Correction factor to convert multidirectionally applied $CSR_{field}$ to unidirectionally applied $CSR_{lab}$
$K_{Mw}$	Magnitude correction factor
$K_\sigma$	Correction factor to account for nonlinear increase in cyclic resistance to shear stresses with increasing confining effective stresses
$D_R$	Relative density
$\epsilon_v$	Vertical strain

$V_s$	Shear wave velocity
$\gamma_s$	Angle between direction of wave propagation and orientation of pipeline
$C_R$	Propagation or phase velocity of the R-wave
$\epsilon_g$	Ground strain
$\epsilon_p$	Pipe strain
$A$	Cross-sectional area of pipeline
$E$	Young's modulus of pipeline
$D$	Pipeline diameter
$t$	Pipe wall thickness
$K_g$	Linear soil stiffness per unit length
$G$	Shear modulus of soil
$\lambda$	Wavelength
$t_u$	Maximal frictional resistance
$q$	Factor that ranges from 1 to $\pi/2$ and quantifies the degree of slippage at the pipe-soil interface
$\bar{a}_{is}$	Induced acceleration (equal to $a_{max}$ for rockslides or shallow, disrupted soil slides but less than $a_{max}$ for deep-seated, coherent slides)
RR	Repair rate (typically per km)

# Appendix B:

## *OpenSRA* Liquefaction and Slope Stability Displacement Models

---

### Level 1 Liquefaction Triggering Models

The Zhu et al. (2015) global model is presented as Equation (B.1).

$$X = a_1 + a_2 * \ln(PGA) + a_3 * CTI + a_4 * \ln(V_{S30}) \quad (B.1)$$

where  $X$  is an intermediate step to capture the probability,  $PGA$  is the peak ground acceleration (g),  $CTI$  is the compound topographic index (unitless),  $V_{S30}$  is the time-averaged shear wave velocity in the upper 30-meters of the subsurface in meters per second, and  $a_n$  are regression coefficients. Compound topographic index, sometimes called topographic wetness index, is a proxy for soil saturation and is calculated by taking the natural logarithm of the ratio of local upslope area draining through a point divided by the tangent of the slope of the point.

The Zhu et al. (2017) coastal model is presented as Equation (B.2).

$$X = a_1 + a_2 * \ln(PGV) + a_3 * \ln(V_{S30}) + a_4 * precip + a_5 * \sqrt{d_c} + a_6 * d_r + a_7 * (d_r * \sqrt{d_c}) \quad (B.2)$$

where  $PGV$  is the peak ground velocity in centimeters per second,  $precip$  is the mean annual precipitation in millimeters,  $d_c$  is the distance to the coast in kilometers,  $d_r$  is the distance to the nearest river in kilometers, and  $a_n$  are regression coefficients.

The Zhu et al. (2017) non-coastal model is presented as Equation (B.3).

$$X = a_1 + a_2 * \ln(PGV) + a_3 * \ln(V_{S30}) + a_4 * precip + a_5 * d_w + a_6 * wtd \quad (B.3)$$

where  $d_w$  is the distance to the nearest water body (river, lake, or coast) in kilometers and  $wtd$  is the modeled depth to the water table in meters.

The Zhu et al. (2015) and Zhu et al. (2017) model regression coefficients are defined in Table B.6.

**Table B.6: Zhu et al. (2015) and Zhu et al. (2017) Model Regression Coefficients**

Coefficient	Zhu et al. (2015)	Zhu et al. (2017) Model 1 (Coastal)	Zhu et al. (2017) Model 2 (Non-Coastal)
$a_1$	24.100	12.435	8.801
$a_2$	2.067	0.301	0.334
$a_3$	0.355	-2.615	-1.918
$a_4$	-4.784	$5.556 \times 10^{-4}$	$5.408 \times 10^{-4}$
$a_5$	-	-0.0287	-0.2054
$a_6$	-	0.0666	-0.0333
$a_7$	-	-0.0369	-

The Youd et al. (2001) MSF, which is used to scale the *PGA* data prior to analysis using the Zhu et al. (2015) procedure, is presented as Equation (B.4).

$$MSF = 10^{2.24} / M_w^{2.56} \quad (B.4)$$

The USGS implements the Zhu et al. (2017) models into their Prompt Assessment of Global Earthquakes for Response (PAGER) system and recommends a magnitude scaling factor (MSF), presented as Equation (B.5), that is multiplied by *PGV* before inserting the value of the ground motion parameter into the model (<https://earthquake.usgs.gov/data/ground-failure/background.php>).

$$MSF = \frac{1}{1 + e^{-2*(M_w-6)}} \quad (B.5)$$

Once the model inputs are determined and *X* has been calculated, the probability of liquefaction triggering is calculated using Equation (B.6).

$$Prob(Liq) = \begin{cases} \frac{1}{1 + e^{-X}}, & \text{If } PGV > 3 \frac{cm}{s} \text{ AND } PGA > 0.1 g \text{ AND } V_{S30} < 620 \frac{m}{s} \\ 0, & \text{Otherwise} \end{cases} \quad (B.6)$$

## Level 2 Liquefaction Triggering Models

Youd & Perkins (1978) maps relative liquefaction susceptibility using the geomorphic and age criterion presented in Table B.7.

**Table B.7: Relative Liquefaction Susceptibility of Various Types of Deposits Categorized by Age**

Type of Deposit	General Distribution of Cohesionless Sediments in Deposits	Likelihood that Cohesionless Sediments, when Saturated, would be Susceptible to Liquefaction (By Age of Deposit)			
		<500 yr	Holocene	Pleistocene	Pre-Pleistocene
<b>Continental Deposits</b>					
<b>River Channel</b>	Locally Variable	Very High	High	Low	Very Low
<b>Flood Plain</b>	Locally Variable	High	Moderate	Low	Very Low
<b>Alluvial Fan and Plain</b>	Widespread	Moderate	Low	Low	Very Low
<b>Marine Terraces and Plains</b>	Widespread	–	Low	Very Low	Very Low
<b>Delta and Fan-Delta</b>	Widespread	High	Moderate	Low	Very Low
<b>Lacustrine and Playa</b>	Variable	High	Moderate	Low	Very Low
<b>Colluvium</b>	Variable	High	Moderate	Low	Very Low
<b>Talus</b>	Widespread	Low	Low	Very Low	Very Low
<b>Dunes</b>	Widespread	Moderate	Low	Low	Very Low
<b>Loess</b>	Variable	High	High	High	Unknown
<b>Glacial Till</b>	Variable	Low	Low	Very Low	Very Low
<b>Tuff</b>	Rare	Low	Low	Very Low	Very Low
<b>Tephra</b>	Widespread	High	High	?	?
<b>Residual Soils</b>	Rare	Low	Low	Very Low	Very Low
<b>Sebka</b>	Locally Variable	High	Moderate	Low	Very Low
<b>Coastal Zone</b>					
<b>Delta</b>	Widespread	Very High	High	Low	Very Low
<b>Esturine</b>	Locally Variable	High	Moderate	Low	Very Low
<b>Beach – High Wave Energy</b>	Widespread	Moderate	Low	Very Low	Very Low
<b>Beach – Low Wave Energy</b>	Widespread	High	Moderate	Low	Very Low
<b>Lagoonal</b>	Locally Variable	High	Moderate	Low	Very Low
<b>Fore Shore</b>	Locally Variable	High	Moderate	Low	Very Low
<b>Artificial</b>					
<b>Uncompacted Fill</b>	Variable	Very High	–	–	–
<b>Compacted Fill</b>	Variable	Low	–	–	–

Table from Youd & Perkins (1978)

Hazus (FEMA, 2020) converts liquefaction susceptibility to the probability of liquefaction using Equation (B.7).

$$P(Liquefaction_{SC}) = \frac{P(Liquefaction_{SC} | PGA = a)}{K_M * K_W} * P_{ml} \quad (B.7)$$

where  $P(Liquefaction_{SC}|PGA = a)$  is the conditional probability of liquefaction given a susceptibility class and specified  $PGA$  level,  $K_M$  is the moment magnitude correction factor,  $K_W$  is the groundwater correction factor, and  $P_{ml}$  is the proportion of the map unit that is susceptible to liquefaction.  $P(Liquefaction_{SC}|PGA = a)$  is calculated using the formulas in Table B.8.

**Table B.8: Conditional Probability Relationships for Liquefaction Susceptibility Classes**

Susceptibility Class	$P(Liquefaction_{SC} PGA = a)$
Very High	$0 \leq 9.09 * a - 0.82 \leq 1.0$
High	$0 \leq 7.67 * a - 0.92 \leq 1.0$
Moderate	$0 \leq 6.67 * a - 1.0 \leq 1.0$
Low	$0 \leq 5.57 * a - 1.18 \leq 1.0$
Very Low	$0 \leq 4.16 * a - 1.08 \leq 1.0$
None	0.0

Table from Hazus (FEMA, 2020)

The moment magnitude correction factor,  $K_M$ , is calculated using Equation (B.8), and the groundwater correction factor is calculated using Equation (B.9).

$$K_M = 0.0027 * M_w^3 - 0.0267 * M_w^2 - 0.2055 * M_w + 2.9188 \quad (B.8)$$

$$K_W = 0.022 * d_w + 0.93 \quad (B.9)$$

where  $d_w$  is the depth to groundwater in feet. Lastly,  $P_{ml}$  is found using Table B.9.

**Table B.9: Proportion of Map Unit Susceptible to Liquefaction**

Susceptibility Class	Proportion of Map Unit
Very High	0.25
High	0.20
Moderate	0.10
Low	0.05
Very Low	0.02
None	0.00

Table from Hazus (FEMA, 2020)

### Level 3 Liquefaction Triggering Models

The Level 3 liquefaction triggering models for CPT based analyses are the Moss et al. (2006), Ku et al. (2012) probabilistic modification to the Robertson & Wride (1998) as updated by Robertson (2009), and the Boulanger & Idriss (2016) procedures. Each of the procedures assess the many aspects of performing liquefaction triggering analyses based on the simplified method such as the magnitude scaling factor, the depth reduction factor, and the fines content correction differently. For this reason, the readers are pointed to the referenced

documents for the necessary equations to evaluate liquefaction triggering using each of the procedures.

### Level 1 Liquefaction-Induced Lateral Spread Displacement and Vertical Settlement Models

At Level 1, Zhu et al. (2017) can be used to map liquefaction susceptibility by calculating either Equation (B.2) or Equation (B.3) but excluding the magnitude-scaled-PGV value from the calculation. The resulting value, termed the liquefaction susceptibility quantity, is correlated to liquefaction susceptibility classes in Table B.10.

**Table B.10: Liquefaction Susceptibility Quantity Classification**

Susceptibility Quantity (Unitless)	Liquefaction Susceptibility Class
-1.15 to 5.30	Very High
-1.95 to -1.15	High
-3.15 to -1.95	Moderate
-3.20 to -3.15	Low
-38.1 to -3.20	Very Low
less than -38.1	None

Table from Zhu et al. (2017)

The equation in Hazus (FEMA, 2020) for estimating lateral spread displacement is presented here as Equation (B.10).

$$D(\text{inches}) = K_{\Delta} * a \tag{B.10}$$

where  $a$  is calculated using Equation (B.11), and  $K_{\Delta}$  is a magnitude dependent displacement correction factor calculated using Equation (B.12).

$$a = \begin{cases} 12r - 12 & \text{for } 1 < r \leq 2 \\ 18r - 24 & \text{for } 2 < r \leq 3 \\ 70r - 180 & \text{for } 3 < r \leq 4 \end{cases} \text{ and } r = \frac{PGA}{T_{PGA}} \tag{B.11}$$

$$K_{\Delta} = 0.0086 * M_w^3 - 0.0914 * M_w^2 + 0.4698 * M_w - 0.9835 \tag{B.12}$$

where  $T_{PGA}$  is the threshold value for  $PGA$  necessary to trigger liquefaction, found using Table B.11. For this study, the procedure for calculating  $a$  is linearly extrapolated for  $r > 4$ .

**Table B.11: Threshold PGA Values for Liquefaction Triggering**

Susceptibility Class	$T_{PGA}$
Very High	0.09 g
High	0.12 g
Moderate	0.15 g
Low	0.21 g
Very Low	0.26 g
None	N/A

Table from Hazus (FEMA, 2020)

Table B.12 presents the liquefaction-induced settlement values from Hazus (FEMA, 2020), which has been modified by the authors such that sites with "very low" liquefaction susceptibility have non-zero settlement.

**Table B.12: Liquefaction Induced Settlement Corresponding to Liquefaction Susceptibility Classification**

Susceptibility Class	Settlement (in.)	Settlement (cm)
Very High	12	30
High	6	15
Moderate	2	5
Low	1	2.5
Very Low	0.5*	1*
None	0	0

\* Modified by authors from zero displacement  
Table from Hazus (FEMA, 2020)

## Level 2 Liquefaction-Induced Lateral Spread Displacement and Vertical Settlement Models

The proposed Level 2 liquefaction-induced lateral spread displacement model estimates a probability of LDI="0" and a distribution of non-zero LDI. The formula for LDI is presented as Equation (B.13). Note that LDI is not typically calculated with a depth weighting factor.

$$LDI = \int_0^{z_{max}} \gamma_{max} w(z) dz, \quad \text{where: } w(z) = 1 - \frac{z}{z_{max}} \quad (\text{B.13})$$

where  $w(z)$  is a linear the depth weighting factor and  $z_{max} = 15 \text{ m}$  for this study.

The relationship to estimate the probability of LDI="0" is presented as Equation (B.14).

$$Prob(LDI = "0") = 1 - \frac{1 + b_0 * GWT^{b_1}}{\left[1 + \exp\left[(b_2 + b_3 * GWT) * \left(\frac{PGA}{MSF} - (b_4 + GWT^{b_5})\right)\right]\right]^{b_6}} \quad (\text{B.14})$$

The relationship to estimate the mean, non-zero LN(LDI) is presented as Equation (B.15).

$$if, \frac{PGA}{MSF} \leq \left(\frac{PGA}{MSF}\right)_{min} \left\{ \begin{array}{l} LDI = 0 \\ else, LN(LDI) = \frac{[b_0 + b_1 * GWT] * \left[\frac{PGA}{MSF} - \left(\frac{PGA}{MSF}\right)_{min}\right]}{[b_2 + b_3 * GWT] + \left[\frac{PGA}{MSF} - \left(\frac{PGA}{MSF}\right)_{min}\right]} \pm \varepsilon\sigma \end{array} \right. \quad (\text{B.15})$$

where  $(PGA/MSF)_{min}$  is estimated using Equation (B.16).

$$\left(\frac{PGA}{MSF}\right)_{min} = 0.012 * GWT + 0.06 \quad (\text{B.16})$$

Equation (B.16) was estimated by finding a relationship to the minimum value of PGA/MSF where the average value of LN(LDI) is greater than 3 for each GWT depth for each of the

assessed geologic units and is used to control the minimum value of LN(LDI) in Equation (B.15).

Lastly, the Magnitude Scaling Factor,  $MSF$ , comes from Boulanger & Idriss (2008), presented as Equation (B.17).

$$MSF = 6.9 * \exp\left(\frac{-M_w}{4}\right) - 0.058 \quad \text{for } 6.0 \leq M_w \leq 8.0 \quad (\text{B.17})$$

The model coefficients for the assessed units in the San Francisco Bay area are presented in Table B.13.

**Table B.13: Model Coefficients for Surficial Geologic Units in San Francisco Bay Area**

Surficial Geologic Deposit	Probability of LDI="0" Models						
	Parameter						
	$b_0$	$b_1$	$b_2$	$b_3$	$b_4$	$b_5$	$b_6$
afem	-0.060	1.128	-28.317	2.179	-0.987	0.012	17.028
Qhly	-0.041	1.222	-25.300	1.112	-0.975	0.013	15.973
Alluvial Fan	-0.217	0.575	-14.216	0.758	-1.039	0.019	21.216
Surficial Geologic Deposit	Mean Non-Zero LN(LDI) Models						
	Parameter						
	$b_0$	$b_1$	$b_2$	$b_3$	$\sigma$		
afem	4.144	-0.226	0.021	-0.001	0.789		
Qhly	4.112	-0.086	0.024	0.001	0.895		
Alluvial Fan	3.356	-0.150	0.014	0.003	0.862		

After estimating a distribution of LDI, the Zhang et al. (2004) topographic correlations are used to convert LDI to a distribution of lateral spread displacement. The Zhang et al. (2004) correlation of LDI to lateral spread displacement for sloping ground without a free face is presented as Equation (B.18).

$$\frac{LD}{LDI} = S + 0.2 \quad (\text{for } 0.1\% < S < 5.0\%) \quad (\text{B.18})$$

The correlation of LDI to displacement for sites with a free-face is presented as Equation (B.19).

$$\frac{LD}{LDI} = 6 * \left(\frac{L}{H}\right)^{-0.8} \quad (\text{for } 4 < L/H < 50) \quad (\text{B.19})$$

### Level 3 Liquefaction-Induced Lateral Spread Displacement and Vertical Settlement Models

With CPT data, lateral spread displacement is assessed using the Zhang et al. (2004) models, presented as Equation (B.18) and Equation (B.19), and post-liquefaction vertical settlement is estimated using the Zhang et al. (2002) model, presented as Equation (B.20).

$$S = \int_0^{z_{max}} \varepsilon_v dz \quad (B.20)$$

where  $\varepsilon_v$  is the post-liquefaction volumetric strain for the  $dz$  increment of soil, which is a function of normalized, clean sand equivalent CPT tip resistance and the factor of safety against liquefaction triggering.

With SPT data, lateral spread displacement is assessed using the Youd et al. (2002) models, presented in Equation (B.21) through Equation (B.23). Equation (B.21) estimates the lateral spread displacement for gently sloping sites.

$$\log D_H = -16.213 + 1.532 * M_w - 1.406 * \log R^* - 0.012 * R + 0.338 * \log S + 0.540 * \log T_{15} + 3.413 * \log(100 - F_{15}) - 0.795 * \log(D50_{15} + 0.1 \text{ mm}) \quad (B.21)$$

where  $D_H$  is the estimated lateral spread displacement in meters,  $R$  is the horizontal distance from the site to the nearest bound of the seismic energy source in kilometers,  $S$  is the ground slope in percent,  $T_{15}$  is the cumulative thickness of saturated granular layers with corrected blow counts,  $(N_1)_{60}$  less than 15,  $F_{15}$  is the average fines content for granular materials included within  $T_{15}$  in percent,  $D50_{15}$  is the average mean grain size for granular materials within  $T_{15}$  in millimeters, and  $R^*$  is defined by Equation (B.22).

$$R^* = R + 10^{(0.89 * M_w - 5.64)} \quad (B.22)$$

Equation (B.23) estimates the lateral spread displacement for sites with a free face.

$$\log D_H = -16.713 + 1.532 * M_w - 1.406 * \log R^* - 0.012 * R + 0.592 * W + 0.540 * \log T_{15} + 3.413 * \log(100 - F_{15}) - 0.795 * \log(D50_{15} + 0.1 \text{ mm}) \quad (B.23)$$

where  $W$  is the free-face ratio.

With SPT data, liquefaction-induced vertical settlement is estimated using the Cetin et al. (2009) procedure. The Cetin et al. (2009) procedure probabilistically assesses the volumetric strain potential of saturated, cohesionless soil using the closed-form solution presented in Equation (B.24).

$$\ln(\varepsilon_v) = \ln \left[ 1.879 * \ln \left[ \frac{780.416 * \ln(CSR_{SS,20,1D,1 atm}) - N_{1,60,CS} + 2442.465}{636.613 * N_{1,60,CS} + 306.732} \right] + 5.583 \right] + \varepsilon \sigma \quad (B.24)$$

$$\text{lim: } 5 \leq N_{1,60,CS} \leq 40, \quad 0.05 \leq CSR_{SS,20,1D,1 atm} \leq 0.60$$

where  $\varepsilon_v$  is the volumetric strain potential of the soil,  $\varepsilon$  represents the number of standard deviations from the mean, the model standard deviation  $\sigma = 0.689$ .  $CSR_{field}$  is converted to  $CSR_{SS,20,1D,1 atm}$  using Equation (B.25).

$$CSR_{SS,20,1D,1 atm} = \frac{CSR_{field}}{K_{md} * K_{M_w} * K_{\sigma}} \quad (B.25)$$

where  $K_{md}$  is a multidirectional shaking effects correction factor found using Equation (B.26).

$$K_{md} = 0.361 * \ln(D_R) - 0.579 \quad (B.26)$$

$K_{M_w}$  is a magnitude correction factor found using Equation (B.27).

$$K_{M_w} = \frac{87.1}{M_w^{2.217}} \quad (B.27)$$

The confining effective stress correction factor is found using Equation (B.28).

$$K_{\sigma} = \left( \frac{\sigma'_{v,0}}{P_a} \right)^{f-1}, \quad f = 1 - 0.005 * D_R \quad (B.28)$$

Additionally, a linear depth weighting factor to 18 m, presented in Equation (B.29), is multiplied to the value calculated in Equation (B.24).

$$DF_i = 1 - \frac{d_i}{18 m} \quad (B.29)$$

Therefore, the estimated volumetric strain of each sublayer of saturated, cohesionless soil is presented as Equation (B.30).

$$\varepsilon_{v,eqv} = \frac{\sum \varepsilon_{v,i} t_i DF_i}{\sum t_i DF_i} \quad (B.30)$$

The estimated settlement at the ground surface is presented as Equation (B.31).

$$s_{estimated} = \varepsilon_{v,eqv} * \sum t_i \quad (B.31)$$

Equation (B.24) through Equation (B.31) present a theoretical framework for assessing liquefaction induced ground settlements in the free field. This model is then calibrated against the case history database to assess its performance and uncertainty. The final, calibrated model to assess liquefaction induced ground settlement is presented as Equation (B.32).

$$\ln(s_{estimated}) = \ln(1.15 * s_{estimated}) + \varepsilon\sigma \quad (B.32)$$

where  $\sigma = 0.64$ .

### Level 1 Seismic Slope Stability and Slope Displacement Models

The equation to estimate the static factor of safety for infinite slope type failures from Grant et al. (2016) is presented as Equation (B.33).

$$FS = \frac{c + c_r}{\gamma * t * \sin(\beta)} + \frac{\tan(\phi)}{\tan(\beta)} \quad (B.33)$$

where  $c$  is cohesion,  $c_r$  is root cohesion from vegetation,  $\gamma$  is the unit weight of the sliding mass,  $t$  is the thickness of the sliding mass,  $\phi$  is the friction angle of the sliding mass, and  $\beta$  is

the topographic slope in degrees. Estimates for root cohesion vary significantly for different vegetation types and even within individual landslides and range from 0 kPa in unvegetated slopes to over 100 kPa in old growth forests (Schmidt et al. 2001). Given the uncertainty and near impossibility of accurately estimating root cohesion at the statewide level, it is ignored at Level 1, which introduces a slight conservative bias. Seismically induced disrupted soil slides are typically shallow, usually 1 – 3 m thick (Grant et al., 2016) and can be reasonably modeled as a rigid Newmark (1965) sliding block.

Newmark (1965) estimates the yield coefficient as presented in Equation (B.34).

$$k_y = (FS - 1) * \sin(\beta) \quad (B.34)$$

The yield coefficient can also be estimated using Equation (B.35), which comes from Bray (2007).

$$k_y = \tan(\Phi - \beta) + \frac{c}{\gamma t \cos^2 \beta (1 + \tan(\Phi) \tan(\beta))} \quad (B.35)$$

where  $\Phi$  is the friction angle of the sliding mass,  $c$  is cohesion of the sliding mass,  $\gamma$  is unit weight of the sliding mass,  $t$  is the thickness of the sliding mass, and  $\beta$  is the topographic slope.

For rigid sliding masses (i.e., the fundamental period of the sliding mass is  $T_s = 0.00$  s), Bray & Macedo (2019) present Equation (B.36) to estimate the probability of “zero displacement” (i.e., displacement less than 0.5 cm).

$$P(D = "0") = 1 - \Phi \left( -2.46 - 2.98 \ln(k_y) - 0.12(\ln(k_y))^2 + 2.76 * \ln(PGA) \right) \quad (B.36)$$

“Non-zero” displacement for a rigid sliding block is estimated using Equation (B.37).

$$\ln(D) = -4.684 - 2.482 * \ln(k_y) - 0.244(\ln(k_y))^2 + 0.344 * \ln(k_y) * \ln(PGA) + 2.649 * \ln(PGA) - 0.090 * (\ln(PGA))^2 + 0.603 * M_w + \varepsilon * \sigma \quad (B.37)$$

where  $\sigma = 0.72$  for Equation (B.37). Equation (B.36) is combined with Equation (B.37) using a mixed-random variable model to estimate the non-zero slope displacement distribution.

The equation from Jibson (2007) to estimate seismic slope displacement that does not consider earthquake magnitude is presented as Equation (B.38).

$$\log(D_N) = 0.215 + \log \left[ \left( 1 - \frac{k_y}{PGA/g} \right)^{2.341} * \left( \frac{k_y}{PGA/g} \right)^{-1.438} \right] \pm 0.510 \quad (B.38)$$

where  $D_N$  is seismic slope displacement in centimeters and the model standard deviation equals 0.510. The equation from Jibson (2007) that does consider earthquake magnitude is presented as Equation (B.39).

$$\log(D_N) = -2.710 + \log \left[ \left( 1 - \frac{k_y}{PGA/g} \right)^{2.335} * \left( \frac{k_y}{PGA/g} \right)^{-1.478} \right] + 0.424 * M_w \pm 0.454 \quad (B.39)$$

where the terms are as previously described, and the model standard deviation equals 0.454. Equation (B.39) is applicable for the magnitude range  $5.3 \leq M_w \leq 7.6$ . The Jibson (2007) equations apply only to rigid sliding masses, such as shallow infinite slope type failures. They are stand-alone equations and do not require an estimate for the probability of zero displacement to be made.

The Level 1 geologic map comes from Wills et al. (2015). A description of the 17 map units is provided in Table B.14.

**Table B.14: Mapped Units in Statewide Geologic Map from Wills et al. (2015)**

<b>Unit</b>	<b>Description</b>
<b>adf</b>	Artificial dam fill (Latest Holocene)
<b>Qi</b>	Intertidal mud, including mud around the San Francisco Bay and similar mud around the Sacramento/San Joaquin delta and Humboldt Bay (Quaternary)
<b>af/Qi</b>	Artificial fill over intertidal mud around the San Francisco Bay and similar areas (Latest Holocene over Quaternary)
<b>Qa1</b>	Quaternary (Holocene) alluvium in areas of very low slopes (less than 0.5%)
<b>Qa2</b>	Quaternary (Holocene) alluvium in areas of moderate slopes (0.5 – 2.0%)
<b>Qa3</b>	Quaternary (Holocene) alluvium in areas of steep slopes (>2%)
<b>Qoa</b>	Quaternary (Pleistocene) alluvium
<b>Qs</b>	Quaternary (Pleistocene) sand deposits, such as the Merritt Sand in the Oakland area
<b>QT</b>	Quaternary to Tertiary (Pleistocene to Pliocene) alluvial deposits, such as the Saugus Formation of Southern California, the Paso Robles Formation of the central Coast Ranges, and the Santa Clara Formation of the San Francisco Bay area
<b>Tsh</b>	Tertiary shale and siltstone units, such as the Repetto, Fernando, Puente, and Modelo Formations of the Los Angeles area
<b>Tss</b>	Tertiary shale and siltstone units, such as the Topanga Formation in the Los Angeles area and the Butano Formation in the San Francisco area
<b>Tv</b>	Tertiary volcanic units including the Conejo Volcanics in the Santa Monica Mountains and the Leona Rhyolite in the East Bay Hills
<b>sp</b>	Serpentinite
<b>Kss</b>	Cretaceous sandstone of the Great Valley Sequence in the central Coast Ranges
<b>KJf</b>	Franciscan complex rocks, including mélangé, sandstone, shale, chert, and greenstone
<b>crystalline</b>	Crystalline rocks, including Cretaceous granitic rocks, Jurassic metamorphic rocks, schist, and Precambrian gneiss
<b>crystalline2</b>	Crystalline rocks including granites, granodiorites, and diorites in the Sierra Nevada

The estimated mean, median, and standard deviation for the friction angle and cohesion for each of the map units is provided in Table B.15.

**Table B.15: Level 1 Engineering Properties for Statewide Geologic Map**

Unit (MS48)	Subunits	Count	Mean $\phi'$ (°)	Median $\phi'$ (°)	STDEV $\phi'$ (°)	Mean $c'$ (psf)	Median $c'$ (psf)	STDEV $c'$ (psf)
<b>adf</b>	N/A	N/A	N/A	N/A	N/A	N/A	N/A	N/A
<b>Qi</b>	Qhym	11	17	19	9	329	250	172
<b>af/Qi</b>	N/A	N/A	N/A	N/A	N/A	N/A	N/A	N/A
<b>Qal1, Qal2, Qal3</b>	Qha	142	23	23	11	678	500	559
	Qal	18						
	Qhy	12						
<b>Qoa</b>	Qoa	67	29	30	11	692	500	733
	Qpa	258						
<b>Qs</b>	Qs	134	36	37	5	221	100	376
<b>QT</b>	Qts	348	26	26	11	905	750	713
<b>Tsh, Tss</b>	Tes	49	27	27	11	852	625	998
	Tmoes	2						
	Tmos	45						
	Tms	120						
	Tpas	2						
	Tpms	7						
	Toes	47						
<b>Tv</b>	Tmov	8	30	29	14	534	575	344
	Tpmv	4						
<b>sp</b>	Jsp	111	28	26	12	1006	750	972
<b>Kss</b>	KJs	103	24	24	10	762	600	652
	Ks	119						
<b>KJf</b>	fsr	20	26	25	10	903	610	1022
	Kfs	77						
	Kfv	3						
	KJf	43						
	KJfc	25						
	KJfm	103						
	KJfs	34						
	KJfv	12						
<b>Crystalline</b>	Ji	30	26	26	9	379	350	314
<b>Crystalline2</b>	N/A	N/A	40*	40*	10*	500*	500*	500*

\*Estimated values without data

**Level 2 Seismic Slope Stability and Slope Displacement Models**

At Level 2, the seismic slope stability and slope displacement models are the same as at Level 1. The difference between Level 1 and Level 2 slope stability and slope displacement models is the quality of the input geology and rock/soil strength data.

### Level 3 Seismic Slope Stability and Slope Displacement Models

Many pipelines are located in geologic materials that can be assessed using the CPT. CPT tip resistance and sleeve friction can be correlated to soil strength parameters to evaluate seismic slope stability and potential displacements. To evaluate the strength of clayey soils, it is useful to estimate the undrained shear strength ratio ( $s_u/\sigma'_{v0}$ ), which is directly related to the overconsolidation ratio (OCR). Equation (B.40) is used to estimate the undrained shear strength ratio for normally consolidated clays from the CPT.

$$(s_u/\sigma'_{v0})_{NC} = \left[ \frac{q_t - \sigma_{v0}}{\sigma'_{v0}} \right] * (1/N_{kt}) = (Q_t/N_{kt}) \quad (B.40)$$

where  $N_{kt}$  ranges from approximately 10 to 18, with a mean value of 14.

Assuming that sleeve friction,  $f_s$ , is a direct measurement of the remolded undrained shear strength, the undrained shear strength ratio is presented as Equation (B.41).

$$(s_{u-remolded}/\sigma'_{v0}) = (f_s/\sigma'_{v0}) = \left[ \frac{F * Q_t}{100} \right] \quad (B.41)$$

For mechanically overconsolidated soils, the undrained shear strength ratio is calculated using Equation (B.42).

$$(s_u/\sigma'_{v0})_{OC} = (s_u/\sigma'_{v0})_{NC} * (OCR)^{0.8} \quad (B.42)$$

where  $OCR$  can be calculated using Equation (B.43) from Robertson (2009) or Equation (B.44) from Kulhawy & Mayne (1990).

$$OCR = 0.25 * (Q_t)^{1.25} \quad (B.43)$$

$$OCR = k * \left[ \frac{q_t - \sigma_{v0}}{\sigma'_{v0}} \right] = k * Q_t \quad (B.44)$$

Where  $k$  ranges from 0.2 to 0.5, with a mean value of 0.33. According to Robertson & Cabal, (2015), values in the higher end of the range are expected for aged, heavily overconsolidated clays.

Several relationships have been proposed to evaluate the friction angle of sandy soil. To estimate the peak friction angle for clean, rounded, uncemented quartz sands, Kulhawy & Mayne (1990) suggest Equation (B.45) based on high quality field data and Robertson & Campanella (1983) suggest Equation (B.46) based on calibration chamber tests.

$$\phi' = 17.6 + 11 * \log(Q_{tn}) \quad (B.45)$$

$$\tan(\phi') = \frac{1}{2.68} * \left[ \log\left(\frac{q_c}{\sigma'_{v0}}\right) + 0.29 \right] \quad (B.46)$$

Alternatively, Been & Jefferies (2006) present a relationship, presented here as Equation (B.47), to estimate the peak friction angle by relating the critical state friction angle of the soil, which is influenced by mineralogy, to the normalized, clean sand equivalent CPT tip resistance.

$$\phi' = \phi'_{cs} + 15.84 * \log(Q_{tn,cs}) - 26.88 \quad (\text{B.47})$$

According to Robertson & Cabal (2015), Equation (B.47) is the best relationship for estimating the peak friction angle in predominantly non-quartz sands.

## **Appendix C:** ***OpenSRA* Geospatial Datasets**

---

**Figure C.1: Statewide 30 m Digital Elevation Model (DEM)**



**Figure C.2: Statewide 30 m Digital Elevation Model (DEM) Slope**

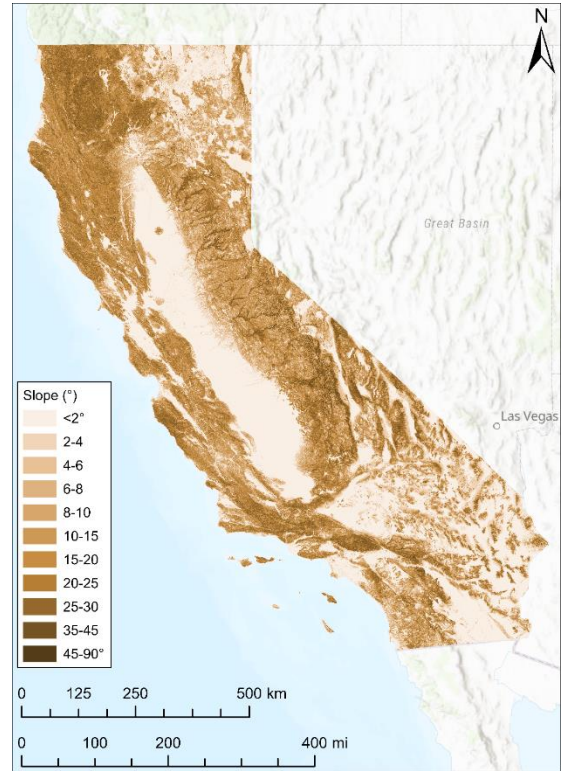


**Figure C.3: Statewide Geologic Map from Wills et al. (2015)**

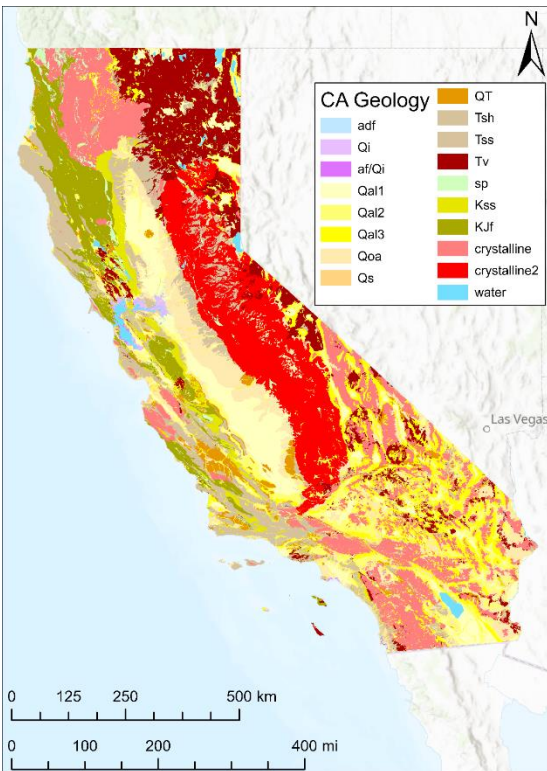


**Figure C.4: ESRI USA Detailed Streams GIS Layer (ESRI, 2019)**

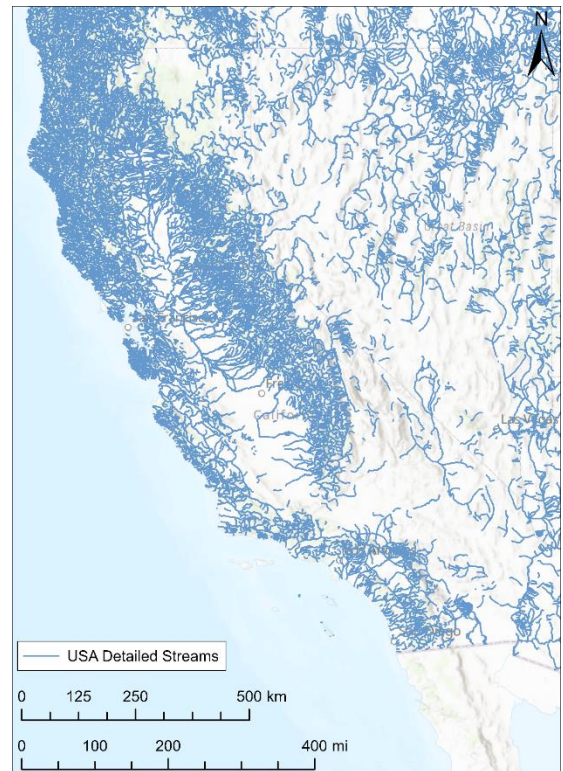


**Figure C.5: Distance to River (30 m Resolution) for Zhu et al. (2017) Procedure**

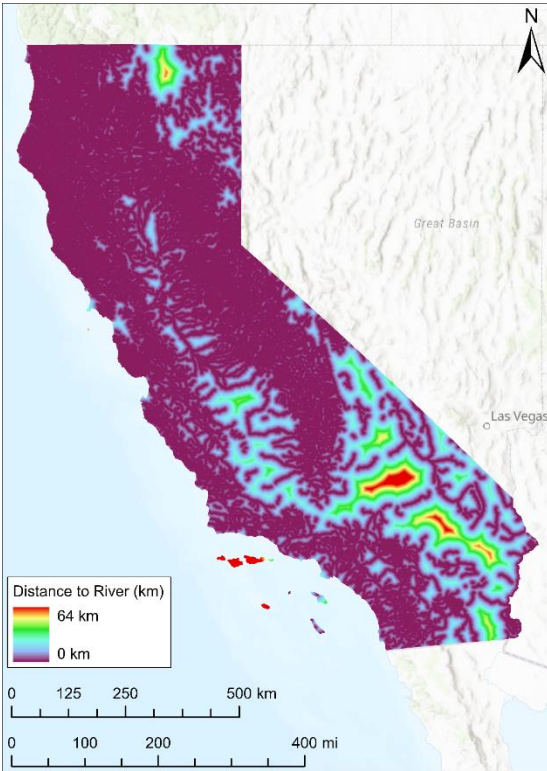


**Figure C.6: Distance to Coast (30 m Resolution) for Zhu et al. (2017) Procedure**

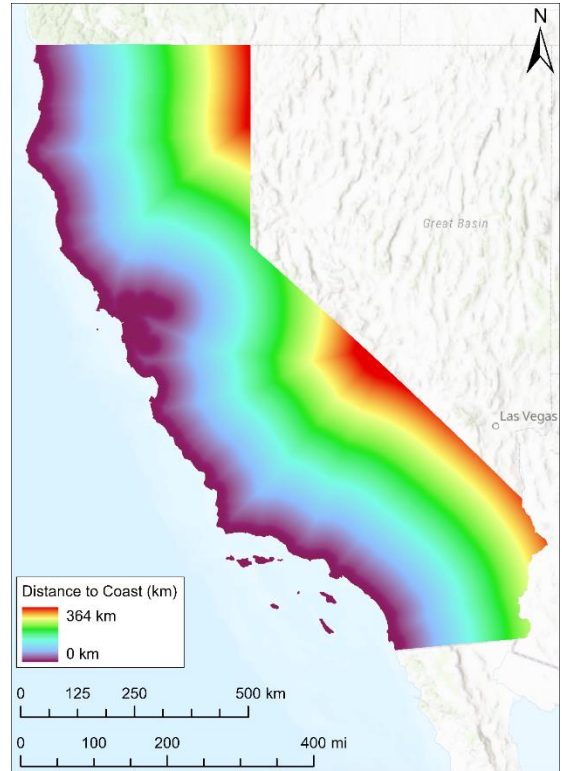


**Figure C.7: Distance to Coast or River (30 m Resolution) for Zhu et al. (2017) Procedure**

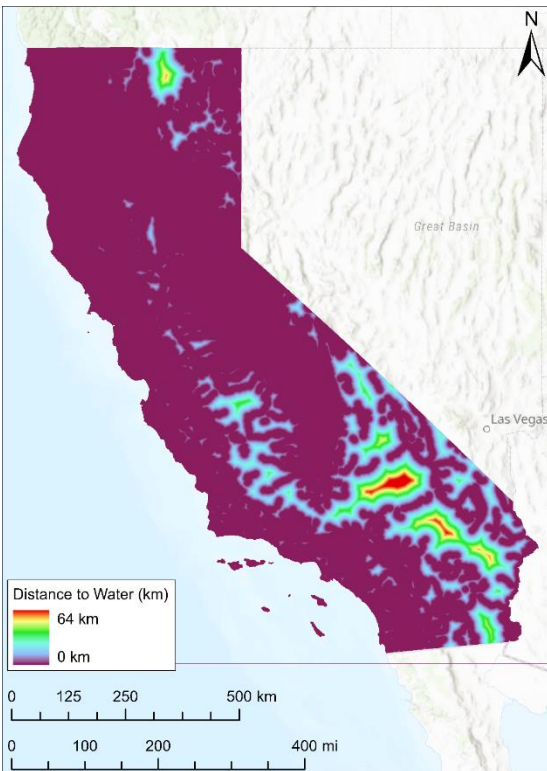


**Figure C.8: Statewide Precipitation Map for Zhu et al. (2017) Procedure**

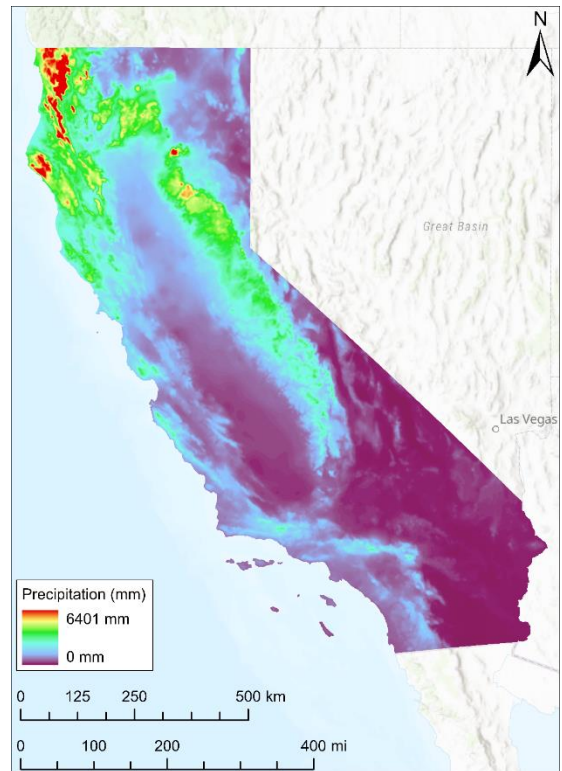


**Figure C.9: Modeled Groundwater Table (250 m) Described in Fan & Miguez-Macho (2010)**

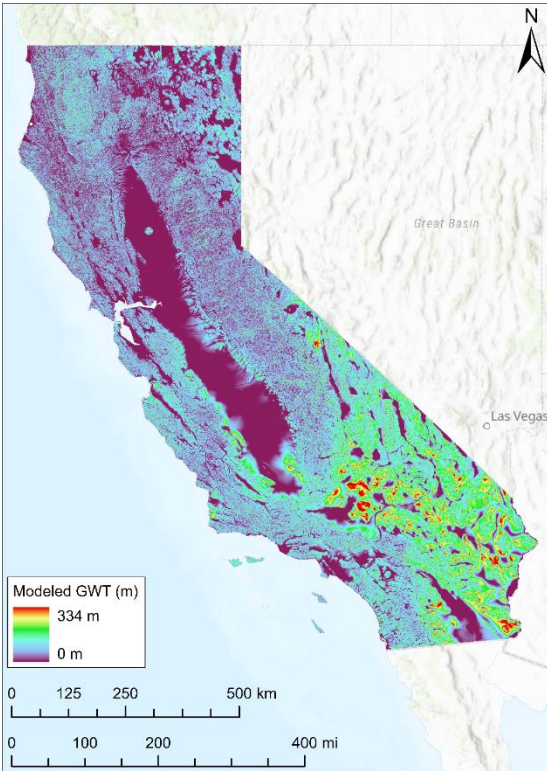


**Figure C.10: Statewide  $V_{s30}$  Model from Wills et al. (2015)**

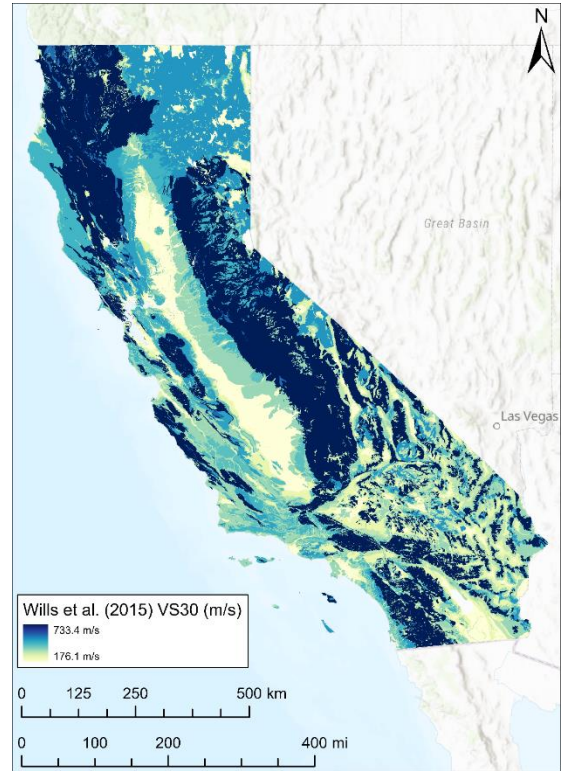
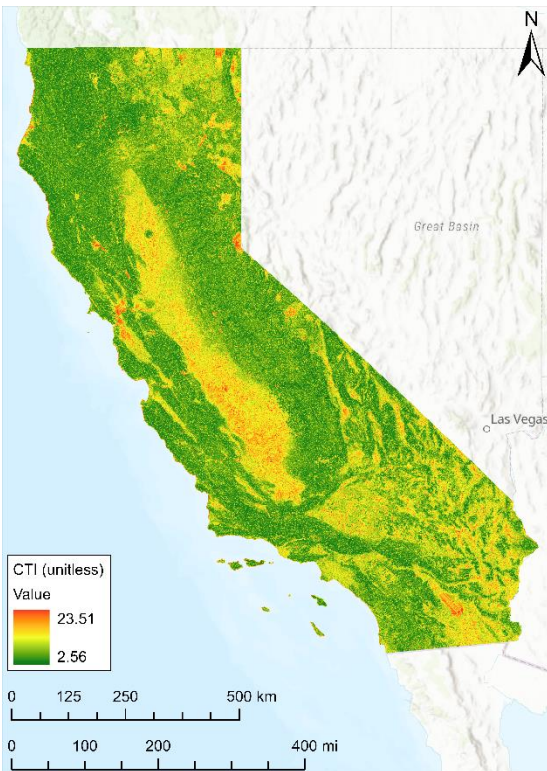


**Figure C.11: Statewide CTI Map (90 m Resolution) for Zhu et al. (2015) Procedure**



# **Appendix D: Fragility Models**

---

## Tensile Damage State Fragility Functions

For continuous steel pipelines with high-quality, overmatched girth welds subjected to tensile strain caused by permanent ground deformation (PGD), the 1984 ASCE *Guidelines for the Seismic Design of Oil and Gas Pipeline Systems* permit longitudinal strains in the 3–5% range while the ALA (2001) guidelines recommend a tensile strain limit of 2% to maintain normal operability of the pipeline and 4% to maintain pressure integrity. Similarly, the 2004 PRCI *Guidelines for Gas and Liquid Hydrocarbon Pipelines* (Honegger & Nyman, 2004) suggest tensile strain limits of 1–2% for normal operability and 2–4% to maintain pressure integrity. For a natural gas pipeline risk assessment project in British Columbia, Canada, Wijewickreme et al. (2005) use 7% tensile strain as the median value to maintain pressure integrity, with the 90 and 10% probability of exceedance tensile strains assumed to be 3% and 10%, respectively. Wijewickreme et al. (2005) developed these values with the goal of not being overly conservative after a review of pipeline rupture criterion available at the time, including the ASCE (1984) guidelines.

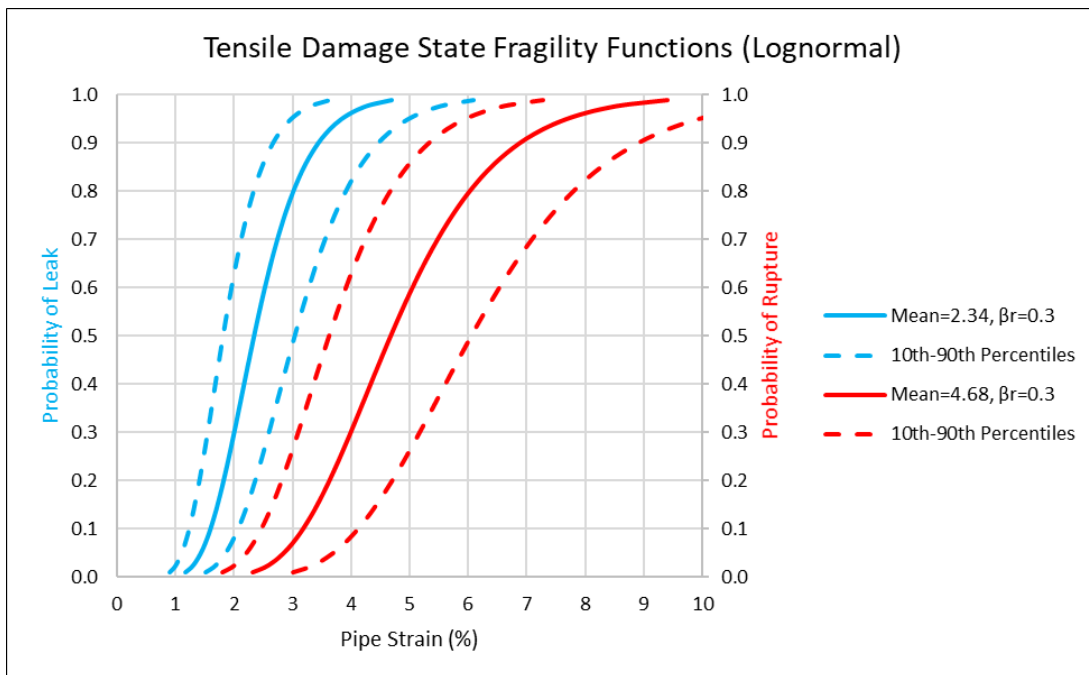
To develop realistic (not overly conservative) tensile damage state fragility functions, this study assumes that the 2% pipe strain criterion suggested by ALA (2001) and Honegger & Nyman (2004) to maintain normal operability corresponds to a 30% probability of minor, nuisance leakage and the 4% pipe strain criterion to maintain pressure integrity corresponds to a 30% probability of pipeline rupture. The typical recommended pipe strain limits of 2 to 4% likely correspond to a small probability of leakage or rupture as would be appropriate for regulatory guidelines. However, because the exact probability of leakage or rupture at 2 or 4% pipe strain is unknown, leakage and rupture were estimated to have 30% probability of occurrence at 2 and 4% pipe strain, respectively, on the basis of expert judgement. The tensile leakage damage state fragility function is presented as Equation (D.1) and the tensile rupture damage state fragility function is presented as Equation (D.2).

$$Prob(Tensile Leakage) = 1 - \Phi \left( \frac{-\ln(\varepsilon_p) + \ln(2.34)}{0.3} \right) \quad (D.1)$$

$$Prob(Tensile Rupture) = 1 - \Phi \left( \frac{-\ln(\varepsilon_p) + \ln(4.68)}{0.3} \right) \quad (D.1)$$

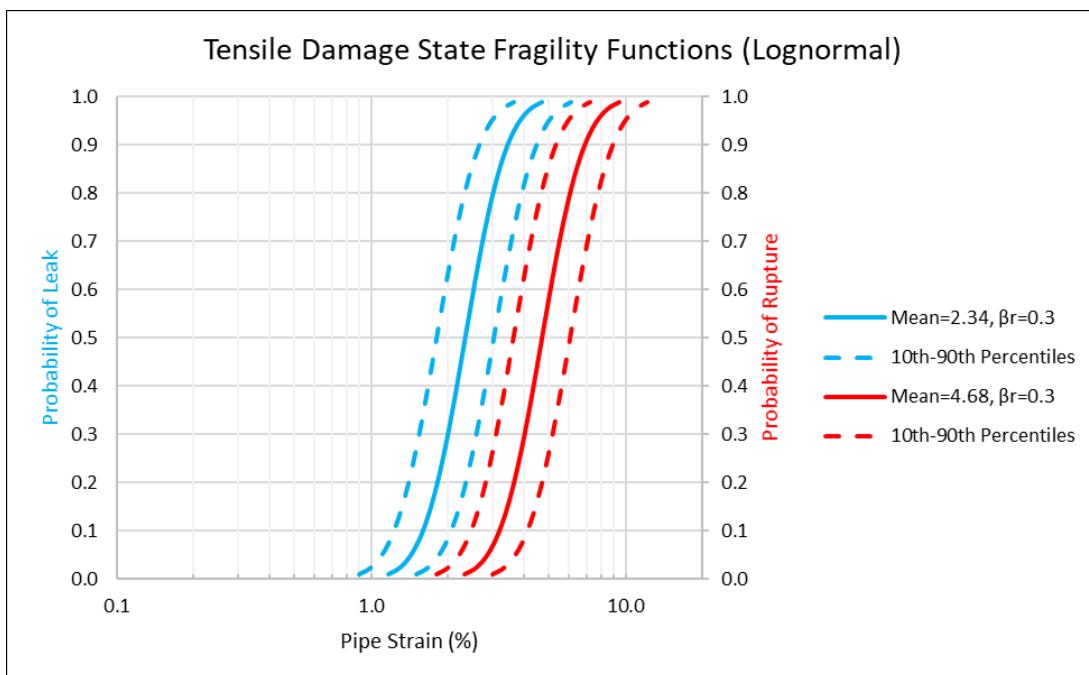
Figure D.1 and Figure D.2 present plots of Equation (D.1) and Equation (D.2). 10<sup>th</sup> and 90<sup>th</sup> percentiles are presented for the fragility functions assuming  $\beta_u=0.20$ , a common assumption for structural systems.  $\beta_r$  represents the aleatory variability in the fragility models due to inherent randomness in the loading conditions (e.g., eccentricities in the pipe alignment, nonuniform backfill soil conditions) and pipe properties (e.g., post-yield stress-strain behavior, weld quality, corrosion).  $\beta_u$  represents the epistemic uncertainty in the mean or median value (i.e., uncertainty that the suggested models are the correct models).

**Figure D.1: Lognormal Pipe Leakage and Rupture Fragility Functions (Arithmetic Scale)**



Fragility functions corresponding to the probability of leakage or rupture given tensile pipe strain from permanent ground deformation (arithmetic scale)

**Figure D.2: Lognormal Pipe Leakage and Rupture Fragility Functions (Log Scale)**

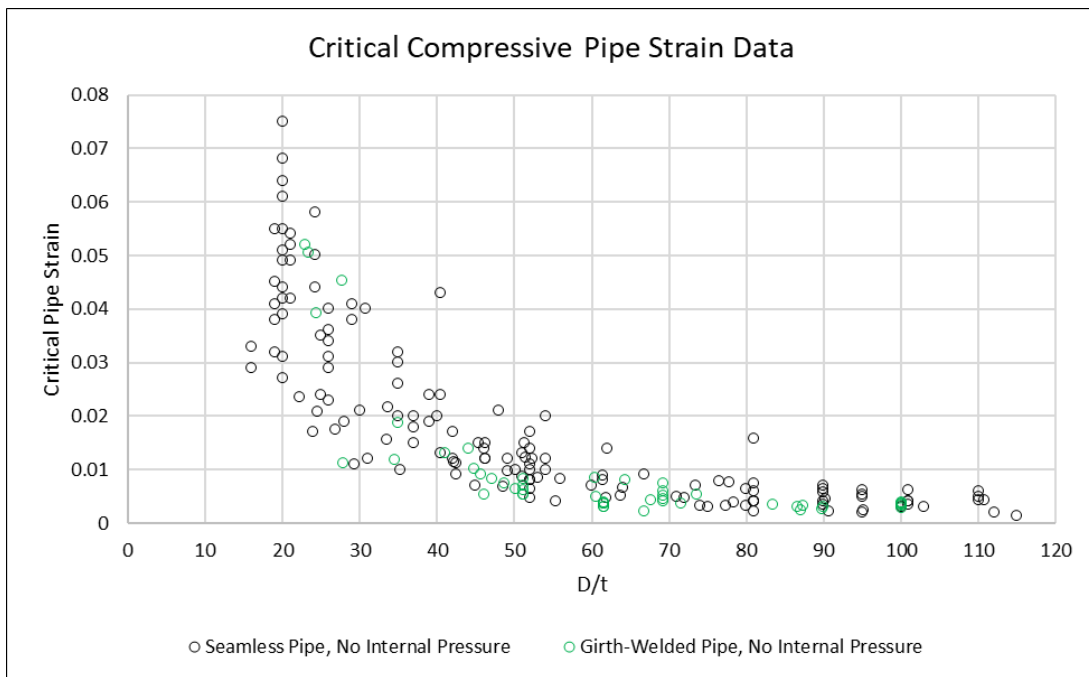


Fragility functions corresponding to the probability of leakage or rupture given tensile pipe strain from permanent ground deformation (log scale)

## Compressive Damage State Fragility Functions

For continuous steel pipelines with high-quality, overmatched girth welds subjected to compressive strain caused by permanent ground deformation (PGD), leakage and rupture are often not differentiated. As stated in Wijewickreme et al. (2005), "The pipe wall response following the onset of compressive wrinkling is complex and it is not well understood in terms of specifying pressure integrity strain limits". Buckling itself is therefore taken as the critical damage state because tearing of the pipe wall can occur during buckling and any further straining in the pipe that occurs from permanent ground deformation tends to concentrate at the buckle, dramatically increasing the likelihood of pipe wall tearing or rupture. Mohr (2003) collected the results of published laboratory compressive pipe tests. These are the same data presented by O'Rourke & Liu (2012). The results of the tests, which are plotted as the critical compressive pipe strain versus the pipe diameter to pipe wall thickness ( $D/t$ ) ratio, are presented in Figure D.3. These data correspond to the longitudinal pipe strain at the maximum compressive stress. According to Harris et al. (1957), buckling occurs at or just before the maximum load the pipe can resist.

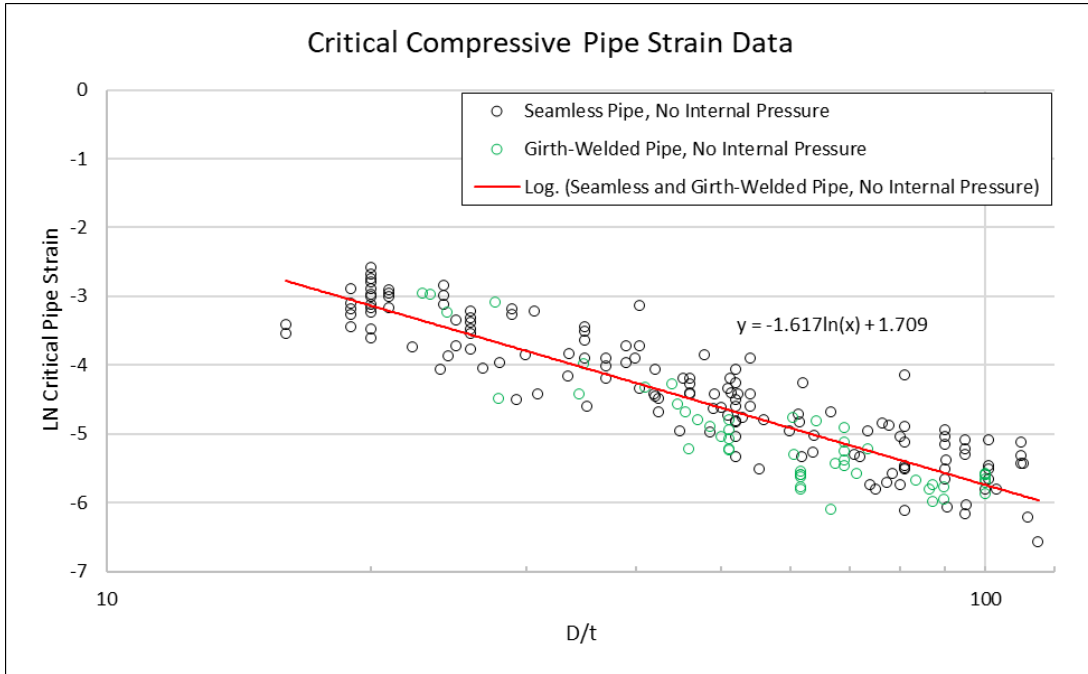
**Figure D.3: Critical Compressive Pipe Strain Test Data**



**Test data compiled by Mohr (2003)**

The strain data in Figure D.3 are transformed using the natural logarithm and found to be linear in natural log space. Figure D.4 presents the strain data transformed by the natural logarithm and presented in log scale.

**Figure D.4: Natural Logarithm of Critical Compressive Pipe Strain Test Data**



**Test data compiled by Mohr (2003) and transformed using the natural logarithm**

Equation (D.3) presents the regression to the compressive pipe strain test data.

$$\ln(\varepsilon_p) = -1.617 * \ln\left(\frac{D}{t}\right) + 1.709 + \varepsilon\sigma \quad (D.3)$$

where  $\varepsilon_p$  is the critical pipe strain in percent,  $\frac{D}{t}$  is the pipe diameter to wall thickness ratio,  $\varepsilon$  represents the number of standard deviations from the mean, and  $\sigma = 0.407$ , where  $\sigma$  is the standard deviation of the residuals in natural log space. The residuals are approximately normally distributed in natural log space.

The data presented in Figure D.3 and Figure D.4 are for pipes without internal pressure. In tension, the effect of internal pressure on the performance of the pipeline is small and it is reasonable to ignore it; however, in compression, the stabilizing effect of internal pressure should be accounted for. Mohr (2003) recommends a correction factor to convert a pipe strain estimate to a zero-pressure-equivalent pipe strain, presented here as Equation (D.4).

$$\varepsilon_{p-eq} = \frac{\varepsilon_p}{1 + \sigma_h/\sigma_y} \quad (D.4)$$

where  $\varepsilon_{p-eq}$  is the zero-pressure-equivalent compressive longitudinal pipe strain,  $\varepsilon_p$  is the estimated compressive longitudinal pipe strain,  $\sigma_h$  is the pipe hoop stress, and  $\sigma_y$  is the pipe yield stress.

The data presented in Figure D.3 and Figure D.4 come from controlled laboratory experiments that would have less uncertainty than that of field conditions. To account for the greater uncertainty associated with field conditions,  $\beta_r$  is increased from 0.407 to 0.500. The resulting

probability of compressive buckling or pipe wall wrinkling fragility function is presented as Equation (D.5).

$$Prob(\text{Compressive Buckling}) = 1 - \Phi \left( \frac{-\ln(\varepsilon_{p-eq}) - 1.617 * \ln\left(\frac{D}{t}\right) + 1.709}{0.500} \right) \quad (D.5)$$

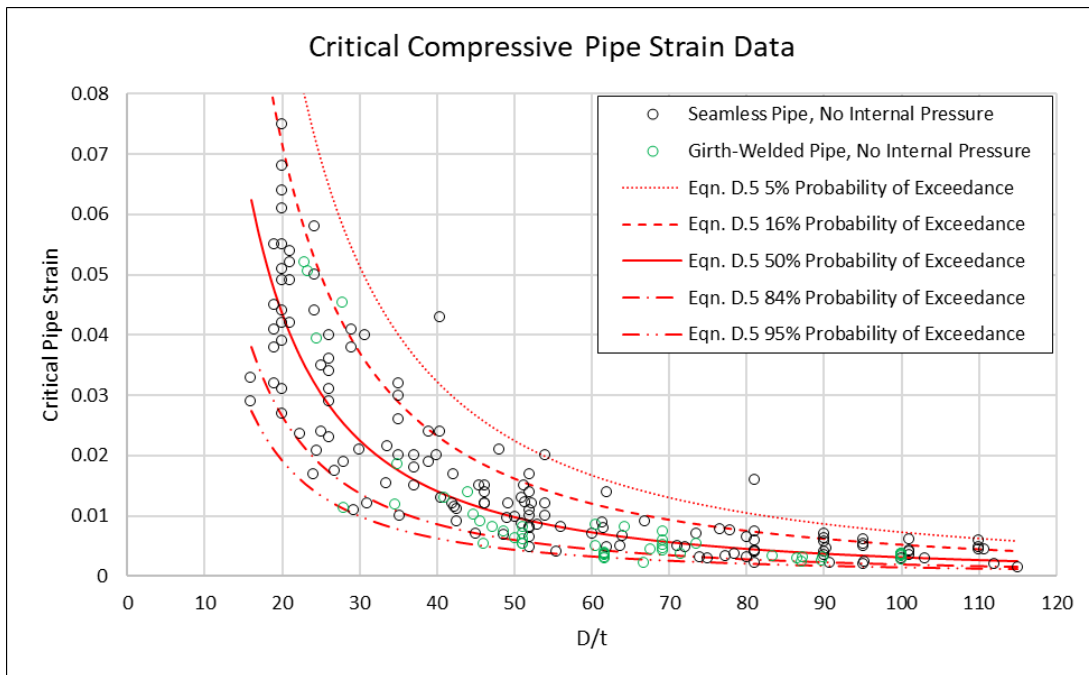
where  $\Phi$  is the standard normal cumulative distribution,  $\varepsilon_{p-eq}$  is the estimated zero-pressure-equivalent longitudinal pipe strain caused by permanent ground deformation,  $\frac{D}{t}$  is the pipe diameter to wall thickness ratio, and  $\beta_r=0.500$ .

Pipelines can often sustain more axial strain after buckling or pipe wall wrinkling has occurred prior to the pipe wall tearing or rupturing. To convert Equation (D.3) to a probability of pipe rupture fragility function, the 50% probability of exceedance values are shifted up to the 20% probability of exceedance level. The resulting probability of compressive rupture fragility function is presented as Equation (D.6).

$$Prob(\text{Compressive Rupture}) = 1 - \Phi \left( \frac{-\ln(\varepsilon_{p-eq}) - 1.617 * \ln\left(\frac{D}{t}\right) + 2.130}{0.500} \right) \quad (D.6)$$

Equation (D.5) and the 95%, 84%, 50%, 16%, and 5% probability of exceedance percentiles of Equation (D.5) are plotted over the regressed range of D/t values in Figure D.5. Figure D.5 also shows the critical pipe strain data from Mohr (2003).

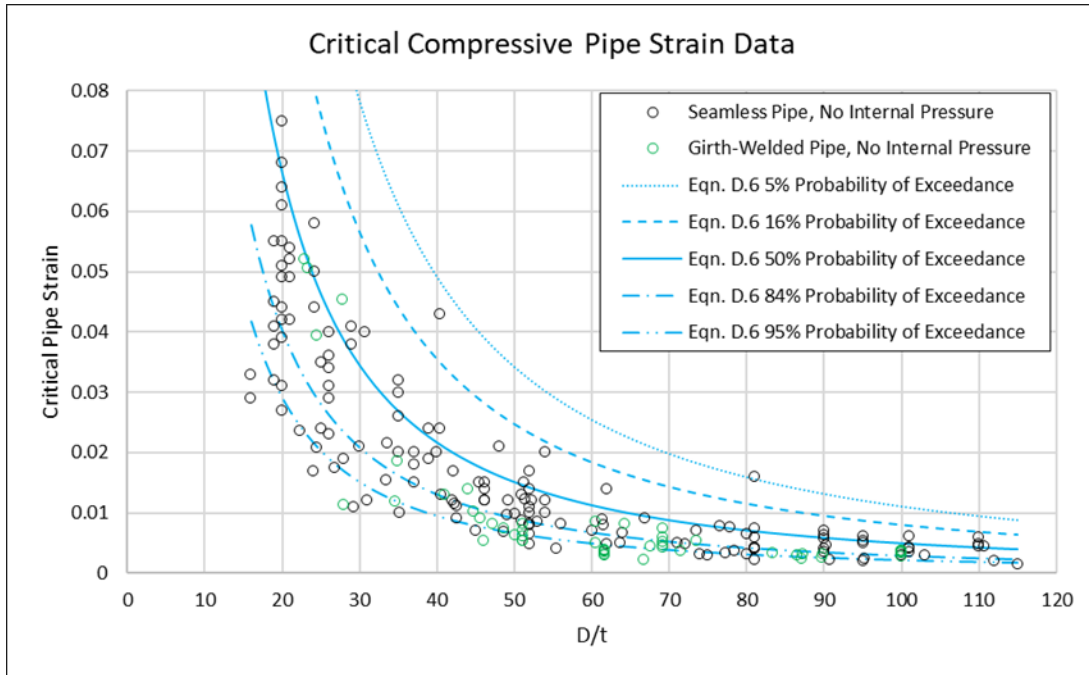
**Figure D.5: Compressive Buckling or Pipe Wall Wrinkling Fragility Function**



**Probability of compressive buckling or pipe wall wrinkling fragility function (Equation D.5) with probability of exceedance percentiles assuming  $\beta_r=0.5$**

Equation (D.6) and the 95%, 84%, 50%, 16%, and 5% probability of exceedance percentiles of Equation (D.6) are plotted over the regressed range of D/t values in Figure D.6. Figure D.6 shows the probability of rupture percentiles shift upwards allowing for more strain relative to the probability of compressive buckling or pipe wall wrinkling percentiles presented in Figure D.5.

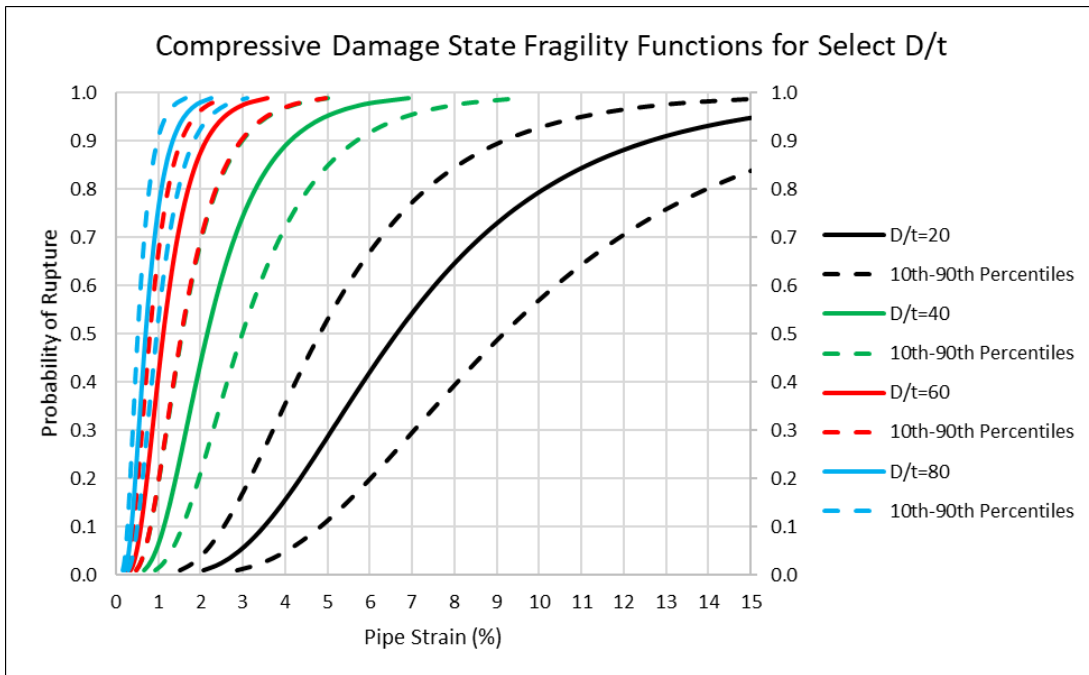
**Figure D.6: Compressive Pipe Rupture Fragility Function**



**Probability of compressive rupture fragility function (Equation D.6) with probability of exceedance percentiles assuming  $\beta_r=0.5$**

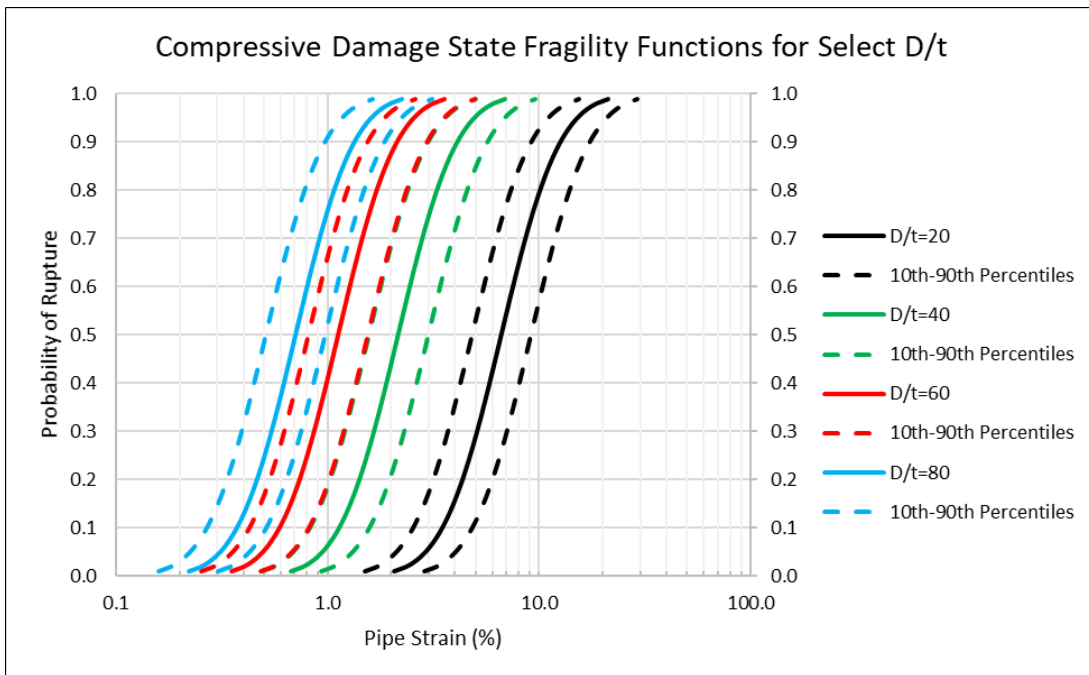
The epistemic uncertainty in the mean can be estimated as the standard error of the intercept in Equation (D.3) (intercept = 1.709); from the regression statistics, the standard error of the intercept equals 0.22. In structural systems,  $\beta_u$  is commonly assumed to be 0.20 to 0.25. Given the limitations of the dataset,  $\beta_u$  is taken as 0.25. Figure D.7 and Figure D.8 display the compressive probability of rupture CDFs (Equation E.4) for pipes with D/t ratios of 20, 40, 60, and 80 along with the 10<sup>th</sup> and 90<sup>th</sup> percentiles assuming  $\beta_u=0.25$ .

**Figure D.7: Probability of Compressive Rupture for Select D/t Ratios (Arithmetic Scale)**



Compressive rupture fragility function (Equation D.6) plotted for select D/t ratios (arithmetic scale)

**Figure D.8: Probability of Compressive Rupture for Select D/t Ratios (Log Scale)**



Compressive rupture fragility function (Equation D.6) plotted for select D/t ratios (log scale)